# Regularities, Resurgence and R-Matrices in Chern Simons Theory

Thesis by
Angus Fred Wilkinson Gruen

In Partial Fulfillment of the Requirements for the
Degree of
Doctor of Philosophy in Mathematics


CALIFORNIA INSTITUTE OF TECHNOLOGY
Pasadena, California

2023
Defended May 16, 2023

Angus Fred Wilkinson Gruen
ORCID: 0000-0003-0284-009X

# ACKNOWLEDGEMENTS

*If you want to go fast, go alone. If you want to go far, go together.*

– African Proverb

First and foremost, I would like to thank my advisor Sergei Gukov. It was an absolute pleasure being your graduate student, and I am deeply grateful for all the assistance, advice and encouragement you have given me.

Despite the outward impression we cultivate, mathematical research is rarely an individual pursuit, and I am indebted to all of my collaborators: Ovidiu Costin, Gerald Dunne, Tobias Ekholm, Piotr Kucharski, Piotr Sułkowski, Marko Stošić and Sunghyuk Park. This thesis would not have been possible without everything I learnt from you all. I was also lucky to have the opportunity to pass on some of my knowledge: to Alberto Oriol and Lara San Martín Suárez it was a pleasure mentoring you, I hope you enjoyed your time at Caltech and wish you the very best for everything to come. I would also like to thank Tobias Ekholm, Matilde Marcolli and Yi Ni for being part of my thesis committee.

Throughout my PhD, whenever I was stuck on a problem, my first and most successful strategy always involved exercise. To that end I'd to thank everyone involved with my Woden Valley soccer team as well the Caltech alpine and triathlon clubs. From the two seasons of soccer we managed to sneak in during COVID, to all the crazy weekend running and biking adventures which culminated in a half Ironman, I have had an absolute ball and look forward to many more adventures to come.

I would also like to thank my roommates, Adam Shaw, Danny Ebanks and Daniel Van Beveren among others, for putting up with my peculiar Australian ways and Tobias Köhne for every movie night. I look forward to seeing you all in my corner of the world some day. Thanks is also due to Damon Binder and Aidan Zellner, whose enduring friendship proves that even oceans of distance cannot weaken strong bonds.

Of course, a heartfelt thank you to my sisters, Jessica and Emma. It is an absolute joy watching you forge your own paths in life, and I always look forward to returning to Australia and spending time with you. And I will be eternally grateful to my Mum and Dad, who inspired my passion for mathematics, have always provided unconditional love and support and welcomed me back home during those strange months of lockdowns. Finally, I dedicate my thesis to Katrina for patiently listening to my mathematical ramblings far longer than I deserved. It has been a long five years stuck in different countries and timezones, but we will be together again soon.

# ABSTRACT

This thesis aims to address two related but distinct problems in Chern Simons theory:

- In 2019, Gukov and Manolescu observed that for fixed a knot $K$, the family of coloured Jones polynomials $J_k(K;q)$ display regularity in colour $k$ and conjectured that this could be captured by a 2 variable series $F_K(x,q)$. Over the subsequent few years, Park proved that, for a large family of knots, $F_K(x,q)$ could be computed using the $R$-matrix for a particular Verma module.

  We will show that it is possible to extend the work of Park to compute the 2 variable series $F_K^N(x,q)$ associated to other lie groups, $\mathfrak{sl}_N$, which capture a similar regularity in the quantum invariants $\mathcal{P}_k^N(K;q)$. Following on from this we will further show that in many cases these series $F_K^N(x,q)$ themselves display a regularity in $N$, reminiscent of the HOMFLY-PT polynomial, allowing the construction of a 3 variable series $F_K(x,a,q)$ interpolating $F_K^N(x,q)$ for all $N$.

- Complex Chern Simons theory is a rare example of Quantum field theory with both interesting non-perturbative behaviour and whose perturbative expansion can be computed to high order. For a nice class of 3-manifolds, namely surgeries on knot complements, we will show how to predict aspects of the non-perturbative behaviour first semi-classically and then, using resurgence, through studying just the perturbative expansion around the trivial flat connection. Finally, we show that contrary to expectation, these families of 3-manifolds display regularity in the surgery coefficient.

# PUBLISHED CONTENT AND CONTRIBUTIONS

[1] Ovidiu Costin, Gerald Dunne, Angus Gruen, and Sergei Gukov. Going to the Other Side via the Resurgent Bridge, 2023. To Appear.

[2] Tobias Ekholm, Angus Gruen, Sergei Gukov, Piotr Kucharski, Sunghyuk Park, Marko Stošić, and Piotr Sułkowski. Branches, quivers, and ideals for knot complements. *Journal of Geometry and Physics*, 177:104520, 2022. ISSN 0393-0440. DOI: 10.1016/j.geomphys.2022.104520.

[3] Tobias Ekholm, Angus Gruen, Sergei Gukov, Piotr Kucharski, Sunghyuk Park, and Piotr Sułkowski. $\widehat{Z}$ at large $n$: from curve counts to quantum modularity. *Communications in Mathematical Physics*, 396, 08 2022. DOI: 10.1007/s00220-022-04469-9.

[4] Angus Gruen. The $\mathfrak{sl}_N$ Symmetrically Large Coloured $R$ Matrix. 12 2022. arXiv:2212.05222.

*Angus Fred Wilkinson Gruen participated in the conception, research, and authoring of all projects listed above."*

# TABLE OF CONTENTS

Acknowledgements . . . iii
Abstract . . . iv
Published Content and Contributions . . . v
Table of Contents . . . v
Chapter 1: Introduction . . . 1
Chapter 2: Background . . . 6
2.1 Quantum Groups . . . 7
2.2 Quantum Knot Invariants . . . 13
2.3 Chern Simons Theory . . . 16
2.4 $F_K$ invariants . . . 21
2.5 The A-Polynomial . . . 27
Chapter 3: The $\mathfrak{sl}_N$ Symmetrically Large Coloured R-Matrix . . . 30
3.1 The Symmetric Large Colour Limit . . . 30
3.2 Positive Braid Knots . . . 37
3.3 The Inverted State Sum Technique . . . 47
Chapter 4: A-Deformed $F_K$ . . . 53
4.1 Explicit $F_K$ Formula for $(2, 2p + 1)$ Torus Knots . . . 53
4.2 Computing $F_K$ from $A$-Polynomial Recursion . . . 57
4.3 Different Branches of $F_K$ . . . 63
4.4 The Knots-Quivers Correspondence . . . 69
4.5 The $B$-Polynomial and Holomorphic Lagrangian . . . 77
Chapter 5: Resurgent Analysis in Chern Simons Theory . . . 82
5.1 Borel Plane Predictions from Knot Polynomials . . . 82
5.2 Resurgent Analysis for Surgeries . . . 105
5.3 Generic Small Surgeries . . . 117
Bibliography . . . 120

*Chapter 1*

# INTRODUCTION

The interface of high energy theoretical physics and knot theory (and, more generally, low dimensional topology) is interesting from several points of view. Physically, it gives a playground in which non-perturbative aspects of quantum field theories can be somewhat rigorously explored. Mathematically, this area draws widely from disparate fields including but not limited to representation theory, number theory and analysis which it combines to generate new invariants of knots and three manifolds.

Intuitively, a knot is a piece of string which you tangle before gluing the ends together to form a loop, see Figure 1.1. The key question at the heart of knot theory is, given 2 knots, are they the same? For example, in Figure 1.1, each knot on the bottom row is simply a further tangled version of one of the knots on the top row. Determining the correspondence between the top and bottom rows is left as an exercise to the inclined reader.

The mathematical study of knots originated in the 19th century with the Gauss linking integral

$$\mathrm{lk}(\gamma_1, \gamma_2) = \frac{1}{4\pi} \oint_{\gamma_1} \oint_{\gamma_2} \frac{\mathbf{r}_1 - \mathbf{r}_2}{|\mathbf{r}_1 - \mathbf{r}_2|^3} \cdot (d\mathbf{r}_1 \times d\mathbf{r}_2). \tag{1.0.1}$$

Given a link composed of two knots, this measures to what extent they are intertwined. Following this, knots were briefly applied in physics by Tait and Thomson as a possible model for atoms, but this was abandoned after the Michelson Morley

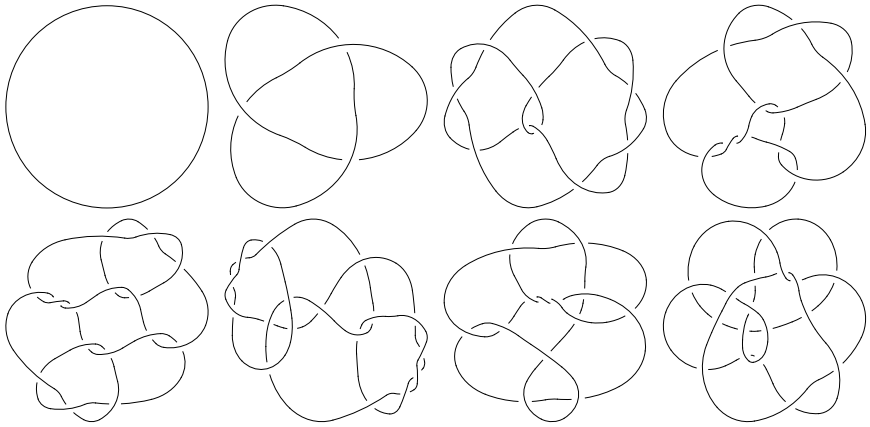

Figure 1.1: Some example Knots

experiment. Mathematical interest in knots picked up again in the early 20th century following the invention of topology. The work of Dehn, Alexander and Reidemeister (among others) laid the foundations of knot theory introducing the Reidemeister moves (which describe how projections of the same knot can differ), the Alexander polynomial (the first polynomial knot invariant) and Dehn surgery (which uses knots as a tool to construct 3-manifolds). Knot theory also began to be applied in low dimensional topology which was kick-started by the famous theorem of Lickorish and Wallace which states that any 3-manifold can be transformed into any other 3-manifold by Dehn surgery on an appropriate link.

Modern knot theory originates in the 1980s with the discovery of the Jones polynomial [Jon85]. Soon after its discovery, the Jones polynomial was generalised to the HOMFLY-PT polynomial [HOMFLY85, PT87] and, a couple of years later, was further generalised [Wit89, RT90] into a large family of so-called quantum invariants. Whilst the Jones polynomial was initially only defined for knots, quantum invariants lead not only to invariants of knots but also 3-manifold invariants known as Witten-Reshetikhin-Turaev (WRT) invariants [Wit89, RT90].

Physically, quantum invariants come from the study of a gauge theory called Chern Simons Theory [Wit89]. When the gauge group $G$ is compact (e.g. $G = \mathrm{SU}(2)$), the space of states $\mathcal{H}(\Sigma)$ in Chern Simons theory is finite dimensional and so the theory admits a non-perturbative [Wit89] and mathematically rigorous [RT90] formulation as a TQFT. This allows for exact computations via cutting-and-gluing of 3-manifolds. On the other hand, when $G$ is complex, (e.g. $G = \mathrm{SL}(2,\mathbb{C})$), the spaces $\mathcal{H}(\Sigma)$ become infinite-dimensional, as in most QFTs of physical interest.

Detailed computations in complex Chern Simons theory started in [Guk05], where they were used to explain and generalize the volume conjecture and the analogues of the Melvin-Morton-Rozansky (MMR) expansion around complex $SL(2,\mathbb{C})$ flat connections. This led to a variety of perturbative techniques allowing computations of perturbative expansions (see (2.3.4)) at all loops, and even to non-perturbative calculations for cusped 3-manifolds. However, the quantitative non-perturbative formulation of the theory that extends to arbitrary closed 3-manifolds remained elusive until recently. A candidate for non-perturbative complex Chern Simons was proposed in [GPV17, GPPV20] and associates to a closed 3-manifold $M^3$, a collection of $q$-series of the form

$$\widehat{Z}_b(M^3,q) = q^{\Delta_b}\left(c_0^{(b)} + c_1^{(b)}q + c_2^{(b)}q^2 + \dots\right) \in q^{\Delta_b}\mathbb{Z}[[q]] \tag{1.0.2}$$

indexed by Spin$^c$ structures $b$ on $M^3$. Unlike the formal perturbative series one gets from the standard saddle-point expansion of a quantum field theory, (1.0.2) is conjectured to be an actual function, well-defined inside the unit disk $|q| < 1$. This variable $q$ is related to the coupling constant via

$$q = e^{\hbar} = e^{\frac{2\pi i}{k}}. \tag{1.0.3}$$

These $\hat{Z}$ invariants were generalised by Gukov and Manolescu in [GM21] to knot complements, where they take the form

$$\begin{aligned} F_K(x,q) &:= \widehat{Z}_b(S^3\backslash K, x, q) \\ &= \frac{1}{2}\sum_{m\geq 1, odd} f_m(q)(x^{\frac{m}{2}} - x^{-\frac{m}{2}}) \end{aligned} \tag{1.0.4}$$

with $f_m \in q^{\Delta_m}\mathbb{Z}[[q]]$ again expected to be a well-defined function for $|q| < 1$. This $F_K$ can be reinterpreted as an analytic continuation of coloured Jones polynomials [GM21]. Following this interpretation, in [Par20b, Par21] Park showed that $F_K$ can be computed for a large class of knots using Verma modules over quantum groups.

This thesis will primarily focus on three distinct but interconnected problems[1].

Ch. 3: ([Gru22]) Can we generalise the methods developed by Park in [Par20b, Par21] to compute $F_K^{\mathfrak{g}}$ for other lie algebras $\mathfrak{g}$?

For a lie algebra $\mathfrak{g}$ of rank $n$, $F_K^{\mathfrak{g}}$ should be a series in the $n+1$ variables, $x_1, \cdots, x_n$ and $q$, [Par20a]. This quickly becomes unwieldy and so to simplify matters let us make 2 choices. Assume first that $\mathfrak{g} = \mathfrak{sl}_N$ and, instead of considering $F_K^{\mathfrak{sl}_N}$ in full generality, consider

$$F_K^N(x,q) = F_K^{\mathfrak{sl}_N, sym}(x,q) = F_K^{\mathfrak{sl}_N}(x_1 = x, x_2 = q, \cdots, x_{N-1} = q, q)$$

which is the series associated to just the symmetric representations. Using a large colour $R$-matrix, we are able to construct $F_K^N$ for an infinite family of knots.

**Theorem 1.0.5.** *Fix a positive (or negative) braid knot and a positive integer $N$. Then the knot invariant $F_K^N$ is well-defined.*

Additionally, we provide compelling evidence for a more general conjecture.

[1] In what follows we give a somewhat intuitive overview of the objects, theorems and conjectures which will appear in this thesis. Everything will be made more precise in the corresponding chapters.

**Conjecture 1.0.6** (Inverted State Sum)**.** *The previous theorem extends to all homogeneous braid knots and more generally all links admitting a signed braid diagram (as in Theorem 2 of [Par21]).*

Ch. 4: ([EGGKPS22, EGGKPSS22]) Coloured Jones polynomials admit a one parameter refinement known as coloured HOMFLY-PT polynomials which interpolate the quantum invariants associated to a fixed representation with varying lie group $\mathfrak{sl}_N$. It is natural then to conjecture the existence of a similar refinement $F_K(x, a, q)$ of $F_K(x, q)$.

We show that, for a certain class of knots, $F_K(x, a, q)$ exists.

**Theorem 1.0.7.** *There is an explicit formula for $F_K(x, a, q)$ for $(2, 2p + 1)$ torus knots.*

Additionally, for a larger class of knots, we can compute a natural $F_K(x, a, q)$ candidate using the quantum $A$-polynomial.

**Theorem 1.0.8.** *If the abelian branch of the quantum a-deformed A-polynomial of a given knot is non-degenerate, the solution of the corresponding q-difference equation is unique and exhibits properties (2.4.12-2.4.15) of Conjecture 2.4.10.*

This refined series, $F_K(x, a, q)$ interacts in interesting ways with the knots-quivers correspondence [KRSS17, KRSS19]. On the one hand, we can use this correspondence as a computational tool, applying to a quiver a "Fourier transform" which relates the HOMFLY-PT generating functions to a particular branch of $F_K$ (see Section 4.3). At the same time, the $R$-matrix method we discuss in Chapter 3 allows us to produce knot complement quiver forms [Kuc20] for $F_K^N$ for a large class of knots:

**Theorem 1.0.9.** *Assuming conjecture 1.0.6, for any positive braid knot $K$, there is an algorithm to produce a quiver form of $F_K^N(x, q)$ from the $R$-matrix state sum.*

Finally, we introduce the quantum $B$-polynomial, an analogue of the quantum $A$-polynomial for rank instead of colour. This naturally leads us to considering the holomorphic Lagrangian, a higher structure which unifies the $A$ and $B$-polynomials.

Ch. 5: ([CDGG23]) Given the perturbative expansion of the WRT invariant (2.3.4) for a manifold $M^3$, what non-perturbative information can be extracted. Chapter 5 focuses on investigating this question when $M^3 = S^3_{\frac{p}{r}}(K)$ is a surgery on a knot complement using $S^3_{\pm\frac{1}{2}}(4_1)$ and $S^3_{\pm\frac{1}{2}}(5_2)$ as examples. We first focus on computing the Chern Simons values and torsions algebraically. For the Chern Simons values we broadly follow [KK90] though we highlight some subtleties. The torsion computations on the other hand are more novel and rely on the following lemma:

**Lemma 1.0.10.** *Let $x$ and $y$ denote eigenvalues of $\rho(m)$ and $\rho(l)$ viewed in the standard representation corresponding to a common eigenvector. Then*

$$\tau^{adj}_{S^3_{\frac{p}{r}}(K)}(\rho) = \frac{\left(p\frac{y}{x}\frac{dx}{dy} + r\right)\tau^{adj}_{S^3\setminus K,[l]}(\rho)}{2 - y^2 - y^{-2}}.$$

Simple observations from the complete set of invariants for these manifolds already leads to a collection of interesting conjectures (see Section 5.1.4).

We then describe how to compute the perturbative expansion (2.3.4), to a high loop order, and how these Chern Simons values and torsions appear in the Borel plane as the locations of poles and the associated residues. Using some singularity elimination methods, we can locate poles to high accuracy and excitingly observe the existence of "Phantom Saddles" 2.3.14, saddles that could exist in the Borel plane but appear not to for currently unknown reasons.

Finally, we show that invariants of families of surgeries $S^3_{\frac{p}{r}}(K)$ are surprisingly regular in $\frac{p}{r}$. We find that we can make universal predictions for many Chern Simons values including, for $\left|\frac{p}{r}\right|$ small, the minimal Chern Simons value.

**Conjecture 1.0.11.** *Fix a knot $K$ and a root $x^*$ of $\Delta_K(x^2)$. Then for any $n \in \mathbb{Z}$, for small enough $\frac{p}{r} \in \mathbb{Q}$, the manifold $S^3_{\frac{p}{r}}(K)$ has a Chern Simons value approximately equal to*

$$\frac{(\log(x^*) + n\pi i)^2}{4\pi^2}\frac{p}{r} + O(\frac{p}{r})^2 \tag{1.0.12}$$

*If additionally, $x^*$ is chosen to minimise $|\log(x^*)|$ then, the above estimate at $n = 0$ will correspond to the smallest non 0 Chern Simons value of $S^3_{\frac{p}{r}}(K)$.*

*Chapter 2*

# BACKGROUND

To describe knots mathematically, we need to add some rigour to the intuitive description given earlier.

**Definition 2.0.1.** *A knot is a smooth embedding $K : S^1 \to S^3$.*

Slightly more generally, an $n$-component link is a smooth embedding of $n$ disjoint copies of $S^1$ into $S^3$.

**Definition 2.0.2.** *Two knots $K_1$ and $K_2$ are equivalent ($K_1 \equiv K_2$) if they are equivalent up to ambient isotopy.*

It is possible (and interesting) to study knots inside other 3-manifolds, but we will mostly ignore that here, except for the following general definition about Dehn Surgery.

**Definition 2.0.3** (Dehn Surgery)**.** *Let $M$ be a manifold, $L \subset M$ an $n$-component link and $\frac{\mathbf{p}}{\mathbf{r}} = (\frac{p_i}{r_i})_{1\leq i\leq n} \in (\mathbb{Q} \cup \infty)^n$ a collection of rational numbers indexed by components of $L$. Then the manifold $S_{\frac{\mathbf{p}}{\mathbf{r}}}(M; L)$ is constructed from $M$ in the following way.*

1. *Remove an open tubular neighbourhood of $L$ from $M$. This leaves a manifold with $n$ torus boundary components $T_1 \cdots T_n$. Choose two simple closed curves $m_i, l_i$ on each boundary torus with $m_i$ a meridian and $l_i$ a longitude.*
2. *Glue a solid torus to each boundary component with homomorphism $f$ which maps the meridian of the solid torus to a curve homotopic to $[r_i l_i + p_i m_i]$.*

Note that if the slope is $\infty$ this corresponds to doing nothing, we glue back the torus identically to how it was removed. When $M = S^3$ is the three sphere, and $L = K$ is a knot, we define the collection of manifolds

$$S^3_{\frac{p}{r}}(K) = S_{\frac{\mathbf{p}}{\mathbf{r}}}(S^3; K). \tag{2.0.4}$$

One of the main methods for studying knots, is to study invariants which to each knot assign some algebraic object (e.g. a number, a polynomial, homology groups...).

## 2.1 Quantum Groups

The key observation behind the quantum group approach is that knot invariants can be constructed from solutions to the Yang Baxter Equation, [Tur88],

$$\widetilde{R}_{23}\widetilde{R}_{12}\widetilde{R}_{23} = \widetilde{R}_{12}\widetilde{R}_{23}\widetilde{R}_{12}. \tag{2.1.1}$$

This is due to the fact that solutions give rise to representations of the braid group. Quantum groups appear in this story as they are a large family of quasi-triangular Hopf algebras constructed from deforming the universal enveloping algebra of Lie algebras. Being quasi-triangular precisely means that their representation category possess an $R$-matrix which gives a solution to (2.1.1). On top of this $R$-matrix, quantum groups have a ribbon structure, which allows a knot invariant to be constructed from the induced Braid group representation [RT90].

We start with some algebraic preliminaries.

### 2.1.1 Lie Groups and the Polynomial Representation

Every complex simple Lie algebra is essentially a collection of interacting copies of $\mathfrak{sl}_2$.

**Definition 2.1.2.** *The Lie algebra $\mathfrak{sl}_2$ is the 3-dimensional algebra spanned by $E, F, H$ with Lie bracket*

$$[E, F] = H, \quad [H, E] = 2E, \quad [H, F] = -2F$$

Thus to describe a more complicated Lie algebra, it suffices to describe the interactions which can be done using a Cartan matrix. For example, the Cartan matrix for $\mathfrak{sl}_N$ is the $(N-1)\times(N-1)$ square matrix

$$A_{\mathfrak{sl}_N} = \begin{pmatrix} 2 & -1 & 0 & 0 & \cdots \\ -1 & 2 & -1 & 0 & \cdots \\ & & \ddots & & \\ \cdots & 0 & -1 & 2 & -1 \\ \cdots & 0 & 0 & -1 & 2 \end{pmatrix} \tag{2.1.3}$$

From this matrix we read off a generating set for $\mathfrak{sl}_N$ as $(N-1)$ $\mathfrak{sl}_2$ triples $(E_i, F_i, H_i)$ which satisfy the usual internal $\mathfrak{sl}_2$ relations as well as

$$[X_i, Y_j] = 0 \quad \forall X, Y \in \{E, F, H\},\ |i-j| > 1$$
$$[H_i, E_{i\pm1}] = A_{i,i\pm1}E_{i\pm1} = -E_{i\pm1}$$

$$[H_i, F_{i\pm1}] = -A_{i,i\pm1}F_{i\pm1} = F_{i\pm1}$$
$$[E_i, F_{i\pm1}] = [H_i, H_{i\pm1}] = 0$$
$$[E_i, [E_i, E_{i\pm1}]] = [F_i, [F_i, F_{i\pm1}]] = 0.$$

From these relations, it can be easily checked that the map

$$E_i \mapsto z_i \frac{\partial}{\partial z_{i+1}} \qquad F_i \mapsto z_{i+1} \frac{\partial}{\partial z_i}$$
$$H_i \mapsto z_i \frac{\partial}{\partial z_i} - z_{i+1} \frac{\partial}{\partial z_{i+1}}$$

gives an action of $\mathfrak{sl}_N$ on $\mathbb{C}[z_1, \cdots, z_N]$. As the action fixes the degree of monomials, the polynomial representation decomposes as

$$\mathbb{C}[z_1, \cdots, z_N] = \bigoplus_{k=0}^{\infty} V_{N,k},$$

where $V_{N,k}$ is the subrepresentation of homogeneous polynomials of degree $k$.

**Lemma 2.1.4.** *The representation $V_{N,k}$ is exactly the $k'$th symmetric representation of $\mathfrak{sl}_N$.*

*Proof.* It can be easily checked that the representation $V_{N,k}$ is finite, irreducible and that the highest weight is $(k, 0, \cdots, 0)$. □

The action of $E, F, H$ triples corresponding to non-simple positive roots can be derived using the adjoint action. Recall that the positive roots of $\mathfrak{sl}_N$ are indexed by pairs $1 \leq i \leq j \leq N-1$ with $\alpha_{i,j} = \alpha_i + \alpha_{i+1} + \cdots + \alpha_j$. Then we define

$$\begin{aligned}
E_{i,j} &= [E_i, [E_{i+1}, [\cdots, [E_{j-1}, E_j]] \cdots] \\
&= ad_{E_i}(ad_{E_{i+1}}(\cdots ad_{E_{j-1}}(E_j)) \cdots) \mapsto z_i \frac{\partial}{\partial z_{j+1}} \\
F_{i,j} &= [F_j, [F_{j-1}, [\cdots, [F_{i+1}, F_i]] \cdots] \\
&= ad_{F_j}(ad_{F_{j-1}}(\cdots ad_{F_{i+1}}(F_i)) \cdots) \mapsto z_{j+1} \frac{\partial}{\partial z_i} \\
H_{i,j} &= H_i + H_{i+1} + \cdots + H_j \mapsto z_i \frac{\partial}{\partial z_i} - z_{j+1} \frac{\partial}{\partial z_{j+1}}.
\end{aligned}$$

In each case the final arrow gives the action in the polynomial representation.

Finally, to any lie algebra $\mathfrak{g}$ we can associate the universal enveloping algebra $U(\mathfrak{g})$:

**Definition 2.1.5.** *Given* $\mathfrak{g}$*, let* $T(\mathfrak{g}) = \mathbb{C} \oplus \mathfrak{g} \oplus (\mathfrak{g} \otimes \mathfrak{g}) \cdots$ *denote the tensor algebra. Then the universal enveloping algebra* $U(\mathfrak{g})$ *is given by:*

$$U(\mathfrak{g}) = T(\mathfrak{g})/\sim$$

*with* $\sim$ *the relation* $[A, B] = A \otimes B - B \otimes A$ *for all* $A, B \in \mathfrak{g}$*.*

Algebraically, $U(\mathfrak{g})$ and $\mathfrak{g}$ are close to identical. In particular, the representation categories of $\mathfrak{g}$ as a Lie algebra and $U(\mathfrak{g})$ as a regular algebra are isomorphic. This is the starting point for describing the quantum analogue of, $\mathfrak{g}$ which will be a one parameter deformation of $U(\mathfrak{g})$.

### 2.1.2 Quantum Analogues

The basic idea of a quantum analogue (q-analogue) involves introducing a $q$ parameter to an equation such that the limit as $q \to 1$ recovers the original expression. Chosen carefully, these added $q$ parameters have interesting combinatorial and topological interpretations. We start by defining the quantum integers[1] as

$$[n]_q = \frac{q^{\frac{n}{2}} - q^{-\frac{n}{2}}}{q^{\frac{1}{2}} - q^{-\frac{1}{2}}}.$$

Using this, we define the quantum factorial and derivative as

$$[n]_q! = \prod_{i=1}^{n} [i]_q \quad \text{and} \quad \left(\frac{\partial f}{\partial z}\right)_q = \frac{f(q^{\frac{1}{2}}z) - f(q^{-\frac{1}{2}}z)}{q^{\frac{1}{2}}z - q^{-\frac{1}{2}}z}.$$

The derivative is defined such that, analogously to the classical case,

$$\left(\frac{\partial z^n}{\partial z}\right)_q = [n]_q z^{n-1}.$$

We also take a moment to introduce the $q$-Pochhammer symbol which depends on an integer $n$ or an integer vector $\mathbf{r}$.

$$(x)_n = (x;q)_n = \prod_{i=0}^{n-1} (1 - q^i x) \qquad (q)_{\mathbf{r}} = \prod_i (q;q)_{r_i}.$$

This symbol is closely related to the quantum factorial as

$$[n]_q = q^{-\frac{n-1}{2}} \frac{1-q^n}{1-q} \implies [n]_q! = q^{-\frac{n(n-1)}{4}} \frac{(q;q)_n}{(1-q)^n}.$$

[1] Unfortunately, there are a litany of competing conventions in the literature. This definition will be most natural for us.

Due to this there are 2 natural definitions for the quantum binomial which differ by an overall factor of $q$,

$$\binom{n}{m}_q = \frac{(q;q)_n}{(q;q)_{m-n}(q;q)_m} \qquad \begin{bmatrix} n \\ m \end{bmatrix}_q = \frac{[n]_q!}{[n-m]_q![m]_q!}.$$

We will primarily use the first one.

### 2.1.3 The Quantum Group $U_q(\mathfrak{sl}_N)$

Following the Drinfeld Jimbo prescription, we use the above definitions to construct a quantum deformation $U_q(\mathfrak{sl}_N)$ of $U(\mathfrak{sl}_N)$. The quantum group $U_q(\mathfrak{sl}_N)$ is the unital associative algebra generated by $N-1$ tuples[2] $(E_i, F_i, K_i, K_i^{-1})$ which satisfy

$$\begin{aligned}
K_0 &= 1 \\
K_i K_j &= K_j K_i \\
K_j E_i K_j^{-1} &= q^{A_{ij}} E_i \\
K_j F_i K_j^{-1} &= q^{-A_{ij}} F_i \\
[E_i, F_j] &= \delta_{ij} \frac{K_i - K_i^{-1}}{q^{\frac{1}{2}} - q^{-\frac{1}{2}}} \\
\sum_{n=0}^{1-A_{ij}} (-1)^n \begin{bmatrix} 1-A_{ij} \\ n \end{bmatrix}_q E_i^n \, E_j \, E_i^{1-A_{ij}-n} &= 0 \\
\sum_{n=0}^{1-A_{ij}} (-1)^n \begin{bmatrix} 1-A_{ij} \\ n \end{bmatrix}_q F_i^n \, F_j \, F_i^{1-A_{ij}-n} &= 0.
\end{aligned}$$

Here, $A$ denotes the Cartan matrix given earlier (2.1.3).

The polynomial representation described above admits an almost trivial quantization.

**Proposition 2.1.6.** *The maps*

$$\begin{aligned}
E_i &\mapsto z_i \left( \frac{\partial}{\partial z_{i+1}} \right)_q & F_i &\mapsto z_{i+1} \left( \frac{\partial}{\partial z_i} \right)_q \\
H_i &\mapsto z_i \frac{\partial}{\partial z_i} - z_{i+1} \frac{\partial}{\partial z_{i+1}} & K_i &= q^{\frac{H_i}{2}}
\end{aligned}$$

*give a well-defined representation of* $U_q(\mathfrak{sl}_N)$ *on* $\mathbb{C}(q^{\frac{1}{2}})[z_1, \cdots, z_N]$.

[2] Implicitly we are identifying $K_i$ with $K_{\omega_i}$, where $\omega_i$ is the fundamental weight dual to the $i$'th simple root.

Verifying that this representation is well-defined is easy but tedious so we skip it here. It mostly boils down to the following pair of relations for quantum integers,

$$[b+1]_q[a]_q - [b]_q[a+1]_q = [a-b]_q$$
$$[a+2]_q - [2]_q[a+1]_q + [a]_q = 0.$$

Identically to the classical case, each generator fixes the overall degree of monomials and so this representation decomposes as a direct sum

$$\mathbb{C}(q^{\frac{1}{2}})[z_1, \cdots, z_N] = \bigoplus_{k=0}^{\infty} V_{N,k}^q$$

with $V_{N,k}^q$ the irreducible subrepresentation of homogeneous polynomials of degree $k$. It will be useful to introduce a specific basis $\{v_{\mathbf{a}}\}$ of $V_{N,k}^q$. Here $\mathbf{a}$ will denote an $N-1$ tuple of integers $k \geq a_1 \geq \cdots \geq a_{N-1} \geq 0$ related to the natural polynomial basis by

$$v_{\mathbf{a}} = |a_0 = k, a_1, \cdots, a_{N-1}, a_N = 0\rangle = z_1^{a_0 - a_1} \cdots z_N^{a_{N-1} - a_N}.$$

With respect to this basis, our actions become

$$\begin{aligned} E_i \cdot v_{\mathbf{a}} &= [a_i - a_{i+1}]_q v_{\mathbf{a}-e_i} \\ F_i \cdot v_{\mathbf{a}} &= [a_{i-1} - a_i]_q v_{\mathbf{a}+e_i} \\ K_i \cdot v_{\mathbf{a}} &= q^{\frac{a_{i-1}+a_{i+1}-2a_i}{2}} v_{\mathbf{a}}. \end{aligned} \tag{2.1.7}$$

To find the actions for elements $E_\alpha, F_\alpha, K_\alpha$ corresponding to other positive roots we replace the adjoint action with its quantized version [Bur90] given by

$$ad_{X_\alpha}^q(X_\beta) = \begin{cases} q^{\frac{(\alpha,\beta)}{4}} X_\alpha X_\beta - q^{-\frac{(\alpha,\beta)}{4}} X_\beta X_\alpha & \text{if} \quad \alpha < \beta \\ -ad_{X_\beta}^q(X_\alpha) & \text{if} \quad \alpha > \beta \\ 0 & \text{if} \quad \alpha = \beta. \end{cases}$$

Here $X_\alpha, X_\beta$ are either both $E$'s or both $F$'s, the ordering[3] is the reverse dictionary order $\alpha_{i,j} < \alpha_{i',j'}$ if $j < j'$ or $j = j'$ and $i < i'$ and the inner product is given by

$$(\alpha_{i,j}, \alpha_{i',j'}) = \begin{cases} 2 & (i,j) = (i',j') \\ 1 & i = i' \text{ or } j = j' \text{ but not both} \\ -1 & i = j'+1 \text{ or } i' = j+1 \\ 0 & else. \end{cases}$$

[3]We use a slightly different but equivalent ordering to [Bur90]. Calling the ordering in [Bur90] $<_B$, the orderings are equivalent in the sense that $\alpha < \beta$ if and only if $\alpha <_B \beta$ or $(\alpha, \beta) = 0$.

Note that if $(\alpha, \beta) = 0$ then $ad^q_{X_\alpha}(Y_\beta)$ is also 0. Hence, the elements $E_\alpha, F_\alpha, K_\alpha$ are

$$\begin{aligned} E_{i,j} &= ad^q_{E_i}(ad^q_{E_{i+1}}(\cdots ad^q_{E_{j-1}}(E_j))\cdots) \\ F_{i,j} &= ad^q_{F_j}(ad^q_{F_{j-1}}(\cdots ad^q_{F_{i+1}}(F_i))\cdots) \\ K_{i,j} &= K_\alpha = K_i K_{i+1}\cdots K_j. \end{aligned}$$

Specialising to our representation, we find that there are some extra factors of $q$ have appeared on top of the expected quantisation of the classical action

$$\begin{aligned} E_{i,j}\cdot v_{\mathbf{a}} &= q^{\frac{j-i}{4}+\frac{a_j-a_i}{2}}[a_{j+1}-a_j]_q v_{\mathbf{a}-e_i-e_{i+1}-\cdots-e_j} \\ F_{i,j}\cdot v_{\mathbf{a}} &= q^{-\frac{j-i}{4}-\frac{a_j-a_i}{2}}[a_i-a_{i-1}]_q v_{\mathbf{a}+e_i+e_{i+1}-\cdots+e_j} \\ K_{i,j}\cdot v_{\mathbf{a}} &= q^{\frac{(a_j+a_i-a_{j+1}-a_{i-1})}{2}} v_{\mathbf{a}}. \end{aligned}$$

### 2.1.4 The quantum trace

When we quantize the underlying algebra to $U_q(\mathfrak{sl}_N)$, this also quantizes the evaluation and co-evaluation[4] maps:

$$\overrightarrow{ev}^q_{N,k} : V^q_{N,k}\otimes (V^q_{N,k})^* \to \mathbb{C}(q^{\frac{1}{2}}), \qquad v_{\mathbf{i}}\otimes v^*_{\mathbf{j}} \mapsto \left(\prod_{\alpha\in\Phi^+} K_{\alpha,\mathbf{i}}\right)\delta_{\mathbf{i},\mathbf{j}} \tag{2.1.8}$$

$$\overleftarrow{coev}^q_{N,k} : \mathbb{C}(q^{\frac{1}{2}}) \to V^q_{N,k}\otimes (V^q_{N,k})^*, \qquad 1 \mapsto \sum_{\mathbf{i}} v_{\mathbf{i}}\otimes v^*_{\mathbf{i}}. \tag{2.1.9}$$

Here by $K_{\alpha,\mathbf{i}}$ we mean the eigenvalue satisfying $K_\alpha\cdot v_{\mathbf{i}} = K_{\alpha,\mathbf{i}} v_{\mathbf{i}}$. On $V^q_{k,N}$ this factor is

$$\left(\prod_{\alpha\in\Phi^+} K_{\alpha,\mathbf{i}}\right) = q^{\frac{N-1}{2}k-|\mathbf{i}|},$$

where $|\mathbf{i}| = i_1+\cdots+i_{N-1}$ is the sum of the entries of $\mathbf{i}$. Using these maps, we can take the quantum trace of a function $f : V^q_{N,k}\to V^q_{N,k}$, denoted $\mathrm{Tr}^q_{N,k}(f)\in\mathbb{C}(q^{\frac{1}{2}})$ by

$$\overrightarrow{ev}^q_{N,k}\circ(f\otimes 1)\circ\overleftarrow{coev}^q_{N,k} : \mathbb{C}(q^{\frac{1}{2}})\to\mathbb{C}(q^{\frac{1}{2}}), \qquad 1\mapsto \mathrm{Tr}^q_{N,k}(f).$$

We can easily generalise this definition of a trace to functions on tensor products $f : (V^q_{N,k})^{\otimes i}\to(V^q_{N,k})^{\otimes i}$ by composing $i$ copies of $\overrightarrow{ev}^q_{N,k}$ and $\overrightarrow{coev}^q_{N,k}$. For an immediate application of this, let us compute the quantum dimension of $V^q_{N,k}$ given by the trace of the identity.

$$\dim_q(V^q_{N,k}) = \mathrm{Tr}^q_{N,k}(\mathbf{1}) = q^{\frac{N-1}{2}k}\sum_{k\geq i_1\geq\cdots\geq i_{N-1}\geq 0} q^{-|\mathbf{i}|} = q^{-\frac{N-1}{2}k}\frac{(q^{k+1};q)_{N-1}}{(q;q)_{N-1}}.$$

[4] There are also $\overleftarrow{ev}^q_{N,k}$, $\overrightarrow{coev}^q_{N,k}$ maps, but we ignore them here.

Setting $a = q^N$, we recover (with a little manipulation) the HOMFLY-PT polynomial for the unknot from [FGS13]. If we additionally set $x = q^k$, we recover the fully unreduced $F_{0_1}(x, a, q)$ (see Section 2.4.3). The appearance of the unknot comes from the fact that the unknot is the closure of the trivial braid.

### 2.1.5 The $U_q(\mathfrak{sl}_N)$ $R$-matrix

As indicated earlier, the reason for this construction is that $U_q(\mathfrak{sl}_N)$ has an $R$-matrix which produces interesting solutions to (2.1.1). The general form for $R_{\mathfrak{sl}_N}$ is given in [Bur90]:

$$R_{\mathfrak{sl}_N} = q^{\frac{f(\mathbf{H})}{2}} \prod_{\alpha\in\Phi^+}^{<} \mathrm{Exp}_{q^{-1}}((1-q^{-1})K_\alpha^{\frac{1}{2}} E_\alpha \otimes K_\alpha^{-\frac{1}{2}} F_\alpha) \tag{2.1.10}$$

$$\mathrm{Exp}_q(x) = \sum_{r=0}^{\infty} \frac{q^{\frac{r(r-1)}{4}} x^r}{[r]_q!}$$

$$f(\mathbf{H}) = \sum_{i,j} a_{ij}^{-1} H_i \otimes H_j.$$

Note that in comparing the above to [Bur90] we have slightly differing conventions, which lead to the slightly unnatural definition for $\mathrm{Exp}_q$. To compute the product, we need to use the ordering for the roots which we defined a moment ago and looks like

$$\alpha_1 < \alpha_{1,2} < \alpha_2 < \alpha_{1,3} < \alpha_{2,3} < \alpha_3 < \alpha_{1,4} \cdots$$

A nice feature of this choice of ordering is that we have a natural recursive formulation for this matrix:

$$R_{\mathfrak{sl}_N} = q^{\frac{f_N(\mathbf{H}) - f_{N-1}(\mathbf{H})}{2}} R_{\mathfrak{sl}_{N-1}} \times \prod_{i=1}^{N-1} \mathrm{Exp}_{q^{-1}}((1-q^{-1})K_{\alpha_{i,N}}^{\frac{1}{2}} E_{\alpha_{i,N}} K_{\alpha_{i,N}}^{-\frac{1}{2}} F_{\alpha_{i,N}}).$$

This might appear still quite abstract but, if we fix a representation $V$, it is relatively straightforward to compute the individual matrix elements of $R_{\mathfrak{sl}_N} : V \otimes V \longrightarrow V \otimes V$ using a computer algebra system. Next, given some large tensor product $V^{\otimes n}$, let $R_{ij}$, denote the $R$ acting on $i$'th and $j$'th components and define $\widetilde{R} = PR$ to be the $R$-matrix followed by the swap operator $P : v_{\mathbf{i}} \otimes v_{\mathbf{j}} = v_{\mathbf{j}} \otimes v_{\mathbf{i}}$.

**Lemma 2.1.11.** *For any finite representation $V$, $\widetilde{R}_{\mathfrak{sl}_N}$ solves the Yang-Baxter equation (2.1.1).*

## 2.2 Quantum Knot Invariants

Fixing a finite dimensional representation $V$ of $U_q(\mathfrak{sl}_N)$, as discussed earlier, $V^{\otimes n}$ naturally carries a representation of the $n$-strand braid group $B_n$ given by $\sigma_i \mapsto \widetilde{R}_{i,i+1}$.

For a knot $K$, let $\beta_K$ be a braid whose right closure is $K$. The simplest examples of this are the Unknot, Trefoil and Figure Eight, shown in Figure 2.1.

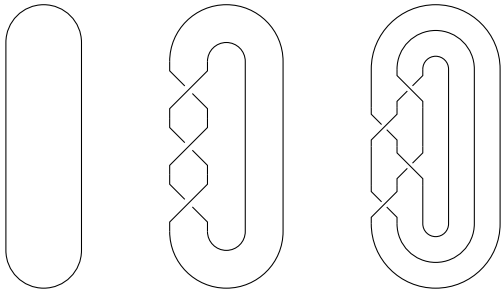

Figure 2.1: Braid Closure diagrams for the Unknot $\beta_{0_1} = \mathbf{1}$, Trefoil $\beta_{3_1} = \sigma_1^3$ and Figure Eight $\beta_{4_1} = \sigma_1\sigma_2^{-1}\sigma_1\sigma_2^{-1}$ knots.

Using our Braid group representation, we map $\beta_K$ to an automorphism of $V^{\otimes n}$ and take quantum trace using the evaluation and co-evaluation maps to get an element of $\mathbb{C}[q]$. For the braids in Figure 2.1 we get

$$\overline{\mathcal{P}}_V(\beta_{0_1}) = \mathrm{Tr}_V^q(\mathbf{1}), \quad \overline{\mathcal{P}}_V(\beta_{3_1}) = \mathrm{Tr}_{V^{\otimes 2}}^q(\widetilde{R}_{12}^3), \quad \overline{\mathcal{P}}_V(\beta_{4_1}) = \mathrm{Tr}_{V^{\otimes 3}}^q(\widetilde{R}_{12}\widetilde{R}_{23}^{-1}\widetilde{R}_{12}\widetilde{R}_{23}^{-1}).$$

**Lemma 2.2.1.** *For any finite dimensional representation $V$ of $U_q(\mathfrak{sl}_N)$ over $\mathbb{C}(q)$, the map*

$$K \mapsto \overline{\mathcal{P}}_V(\beta_K)$$

*is a framed*[5] *knot invariant.*

It remains to slightly adjust these definitions to remove the dependence on framing. First define the writhe of a braid as

$$\omega(\beta) = |\beta_+| - |\beta_-|.$$

Here $|\beta_\pm|$ denotes the number of positive/negative crossings in $\beta$. Then, in all cases we will consider[6], we can find a constant factor $f_V(q)$ such that for any two braids $\beta_1, \beta_2$, whose closures represent the same knot,

$$f_V(q)^{\omega(\beta_2)}\overline{\mathcal{P}}_V(\beta_1) = f_V(q)^{\omega(\beta_1)}\overline{\mathcal{P}}_V(\beta_2).$$

Using this factor, we get the full knot invariant:

$$\widetilde{\mathcal{P}}_V(K) = f_V(q)^{-\omega(\beta_K)}\overline{\mathcal{P}}_V(\beta_K),$$

[5] Meaning a ribbon invariant, which obeys only the Reidemeister 2, 3 moves.

[6] This occurs whenever the map corresponding to a Reidemeister 1 move is central meaning it has the form $f_V(q)\mathbf{1}$.

where $\beta_K$ is any braid representative of $K$. Setting $V = V^q_{2,1}$ this is exactly the celebrated unreduced Jones polynomial [Jon85]. In practice, it is usually simpler to compute the reduced version of these invariants which, algebraically, corresponds to dividing the unreduced invariant by the value of the invariant on the unknot. From the quantum group perspective, these reduced invariants come from the observation that, if we leave the left most strand open as in Figure 2.2, braids become maps $V \longrightarrow V$. If this map is central[7], it is given by $v \mapsto C_\beta v$ for some $C_\beta$ and so we can define the reduced trace $\widetilde{\mathrm{Tr}}^q_V(\beta) := C_\beta$.

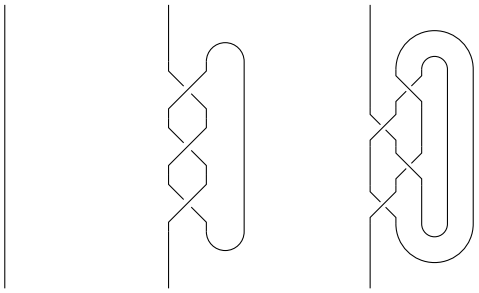

Figure 2.2: Reduced Braid Closure diagrams for the Unknot $\beta_{0_1} = \mathbf{1}$, Trefoil $\beta_{3_1} = \sigma_1^3$ and Figure Eight $\beta_{4_1} = \sigma_1\sigma_2^{-1}\sigma_1\sigma_2^{-1}$ knots.

This finally leads us to the definition of the reduced invariant

$$\mathcal{P}_V(K) = f_V(q)^{-\omega(\beta_K)}\widetilde{\mathrm{Tr}^q_V}(\beta_K) = \frac{\widetilde{\mathcal{P}}_V(K)}{\widetilde{\mathcal{P}}_V(0_1)}.$$

To simplify notation, we define the symmetric $\mathfrak{sl}_N$ quantum invariants and coloured Jones polynomials by

$$\mathcal{P}^N_k(K;q) = \mathcal{P}_{V^q_{N,k}}(K) \quad \text{and} \quad J_k(K;q) = \mathcal{P}^2_k(K;q) = \mathcal{P}_{V^q_{2,k}}(K).$$

### 2.2.1 Coloured HOMFLY-PT Polynomials

One of the early surprises of these invariants was a regularity in $N$. Indeed, for every knot $K$ and colour $k$, there exists a finite polynomial $P_k(K;a,q)$ which interpolates the $\mathcal{P}^N_k(K;q)$ in the sense that

$$\mathcal{P}^N_k(K;q) = P_k(K;a=q^N,q).$$

When $k = 2$, $P_k$ is known as the HOMFLY-PT polynomial [HOMFLY85, PT87] and more generally these are referred to as coloured HOMFLY-PT Polynomials.

[7] Which it will be for the braids and representations we consider.

## 2.3 Chern Simons Theory

Chern Simons theories are some of the simplest examples of quantum field theories (and in particular gauge theories) with interesting non-perturbative behaviour. To define them, we start by fixing a 3-manifold $M^3$ and a Lie group $G$ with Lie algebra $\mathfrak{g}$. Then let $A$ be a $\mathfrak{g}$ valued one form, a map

$$\begin{aligned} A : M^3 &\to \mathfrak{g} \otimes T^*M^3 \\ p &\mapsto A(p)_\mu dx(p)_\mu = A_\mu dx_\mu. \end{aligned}$$

In [CS74], Chern and Simons introduced the 3- form $\mathrm{Tr}\left(A \wedge dA + \frac{2}{3} A \wedge A \wedge A\right)$ with Tr denoting the trace in the defining representation. As this is a 3-form, we can integrate it over $M^3$ to define[8]

$$CS[A] = \frac{1}{8\pi^2} \int_{M^3} \mathrm{Tr}\left(A \wedge dA + \frac{2}{3} A \wedge A \wedge A\right). \tag{2.3.1}$$

Observe that this action is topological, as it has no dependence on a metric or other geometric data of $M^3$. The bundle $\mathfrak{g} \otimes T^*M^3$ carries a gauge action, given a map $g : M^3 \to G$, we define

$$(g \cdot A)_\mu = g A_\mu g^{-1} + g^{-1} \partial_\mu g.$$

It can be checked that $CS[g \cdot A] = CS[A] + \omega(g)$ where $\omega(g) \in \mathbb{Z}$ is the winding number of the map $g$. Hence, $e^{2\pi i k CS[A]}$ is invariant under this gauge action for any integer $k$. This allows us to define the Chern Simons theory partition function, [Wit89],

$$\mathcal{Z}(M^3; k) = \int_{\mathcal{A}} \mathcal{D}A \, e^{-\frac{4\pi^2}{\hbar} CS(A)}, \tag{2.3.2}$$

with $\hbar = \frac{2\pi i}{k}$ and $\mathcal{A}$ denoting the space of $\mathfrak{g}$ connections on $M^3$ modulo gauge equivalence. There are a couple of subtleties to this definition, in particular that $k$ acquires an integer shift depending on $G$ and a minor normalisation difference between $\mathcal{Z}(M^3; k)$ and the WRT partition function but we ignore these here.

### 2.3.1 Perturbative Expansion and Resurgence

Given any quantum field theory, we can expand the partition function as trans series summation of the perturbative contributions from different saddle points

$$\mathcal{Z}(\hbar) = \sum_\alpha n_\alpha e^{\frac{1}{\hbar} S_\alpha} \mathcal{Z}_\alpha^{\mathrm{pert}}(\hbar). \tag{2.3.3}$$

[8] We chose the normalization constant $\frac{1}{8\pi^2}$ so that given a gauge equivalent class of flat connections $[A]$, $CS[A]$ is valued in $\mathbb{R}/\mathbb{Z}$.

The coefficients $n_\alpha$ are called transseries parameters and are constant away from Stokes rays, where their values may experience a jump [BH90, BH91]. The contributions $\mathcal{Z}_\alpha^{\text{pert}}$ are (formal) power series in the small "coupling constant" parameter $\hbar$:

$$\mathcal{Z}_\alpha^{\text{pert}}(\hbar) \;=\; \sum_{n=0}^{\infty} a_n^\alpha \hbar^{n+c_\alpha}. \tag{2.3.4}$$

One of the surprises of resurgence analysis is that if you can compute sufficiently many perturbative coefficients $a_n^\alpha$, then you can extract detailed quantitative information about other saddle points $\beta \neq \alpha$. In other words, it provides an opportunity to understand the non-perturbative structure (and, hopefully, one day can lead to a mathematical definition) of the Feynman path integral. In general, computing these $a_n^\alpha$ involves summing over Feynman diagrams and becomes exponentially more difficult as $n$ rises. Indeed, these sorts of loop computations are rarely attempted past $n \sim 10$. However, due to its close connection with topology, for Chern Simons theories it is possible to compute perturbative coefficients $a_n^\alpha$ to much higher loop order, $n \sim 200$, with relatively little work. This makes these theories a good model for testing resurgent analysis.

The saddle points $\alpha$, are critical points of the action functional $CS(A)$, (2.3.1) which occurs when $A$ satisfies

$$dA + A \wedge A = 0 \tag{2.3.5}$$

meaning it is a $G$ flat connection. Note however that the integration domain $\mathcal{A}$ in (2.3.2) is not simply-connected. It consists of gauge connections on $M^3$ modulo gauge equivalence, and the latter quotient is responsible for a non-trivial $\pi_1(\mathcal{A}) \cong \mathbb{Z}$. If we work with the universal cover of $\mathcal{A}$, gauge equivalent connections can have different actions, so it is important to differentiate between an element

$$\mathbb{a} \in \pi_0(\mathcal{M}_{\text{flat}}(M^3, G)) \times \mathbb{Z}$$

and its gauge equivalence class

$$\alpha \in \pi_0(\mathcal{M}_{\text{flat}}(M^3, G)).$$

With this notation,

$$\mathbb{a} = (\alpha, CS(\mathbb{a})), \qquad CS(\mathbb{a}) \in \mathbb{Z} + CS(\alpha) \tag{2.3.6}$$

remembers the exact Chern Simons value in $\mathbb{R}$ whereas $\alpha$ remembers it in $\mathbb{R}/\mathbb{Z}$.

In section 5.1.2 we establish a new explicit relation between the perturbative $\hbar$-series (2.3.4) for surgeries on a knot $K$ and the twisted Alexander polynomial of $K$. In a nutshell, the relation comes from a closer look at the perturbative $\hbar$-series (2.3.4) which, for a general complex flat connection $\alpha$, is conjectured to take the following form [Guk05, GM08]:

$$e^{-\frac{1}{\hbar}S_\alpha}\mathcal{Z}^{\text{pert}}_\alpha(\hbar) \;=\; e^{-\frac{4\pi^2}{\hbar}CS(\alpha)}\sqrt{\tau^{adj}_{M^3}(\alpha)}\;\hbar^{\delta^{(\alpha)}/2}\left(1+\sum_{n=1}^{\infty}a^\alpha_n\,\hbar^n\right). \tag{2.3.7}$$

Here, $\tau^{adj}_{M^3}(\alpha)$ sometimes abbreviated as $\tau(\alpha)$ is the adjoint torsion twisted by $\alpha$, and $\delta^{(\alpha)} = h^1 - h^0$ is a simple cohomological invariant of a complex flat connection that depends on its stabilizer, $\text{Stab}_G(\alpha) \subseteq G$. When $G = \text{SL}(2,\mathbb{C})$, $\delta^{(\alpha)} = 0$ if the connection $\alpha$ is irreducible, $\delta^{(\alpha)} = 1$ if $\alpha$ is abelian, and $\delta^{(\alpha)} = 3$ if $\alpha$ is central [GM08]. As we explain in section 5.1.2, for 3-manifolds given by surgeries knots, (2.0.4), $\tau^{adj}_{M^3}(\alpha)$ is determined by the twisted Alexander polynomial of $K$. Besides potential applications to topology, this has important direct applications to resurgence that we discuss next.

### 2.3.2 Vanishing theorem for the Stokes data

In resurgence, one of the most important pieces of data is that of the Stokes coefficients, which we denote by $\mathcal{S}^{\beta}_{\alpha}$. Specifically, starting with a perturbative expansion near a saddle point $\alpha$ (a lift of $\alpha$ to the universal cover in the space of fields described around (2.3.6)), we expect to see other critical values $S_\beta$ as singularities of $B_\alpha(\xi)$, the analytic continuation of the Borel transform[9] $B\mathcal{Z}^{\text{pert}}_\alpha(\xi)$. Generically, near $\xi = -S_\beta = -4\pi^2 CS(\beta)$ we expect

$$B_\alpha(\xi) \;=\; \frac{\mathcal{S}^{\beta}_{\alpha}}{\xi + 4\pi^2 CS(\beta)} + \text{less singular terms}. \tag{2.3.8}$$

In Chapter 5 we will verify the following conjecture that follows directly from the structure of (2.3.7).

**Conjecture 2.3.9.**

$$\mathcal{S}^{\beta}_{\alpha} \;\in\; \frac{1}{2\pi i}\sqrt{\frac{\tau(\beta)}{\tau(\alpha)}}\,\mathbb{Z} \tag{2.3.10}$$

Based on this, we can define

$$m^{\beta}_{\alpha} \;:=\; 2\pi i\,\mathcal{S}^{\beta}_{\alpha}\sqrt{\frac{\tau(\alpha)}{\tau(\beta)}} \tag{2.3.11}$$

[9] For a series $\sum_{n=0}^{\infty} a_n\hbar^{n+c}$ the Borel transform is defined as $\sum_{n=1}^{\infty}\frac{a_n}{\Gamma(n+c)}\xi^{n+c-1}$.

which is expected to be an integer.

Unlike the standard Picard-Lefschetz theory—where Stokes coefficients can be interpreted as intersection numbers between Lefschetz thimbles and, therefore, are (skew) symmetric—this is no longer the case in gauge theory. In particular,

**Theorem 2.3.12** ([GMP16])**.** *In complex Chern Simons theory the Stokes coefficients in general are asymmetric in* $\mathfrak{a}$ *and* $\mathfrak{b}$*; in particular,*

$$\mathcal{S}_{\mathfrak{a}}^{\mathfrak{b}} = 0 \quad \textit{whenever} \quad \dim \mathit{Stab}_G(\mathfrak{a}) < \dim \mathit{Stab}_G(\mathfrak{a}) \tag{2.3.13}$$

*while* $\mathcal{S}_{\mathfrak{b}}^{\mathfrak{a}}$ *does not need to vanish.*

This general vanishing theorem does not prevent non-degenerate (Gaussian) saddles from appearing as trans-series in the Borel resummation of a degenerate (non-Gaussian) saddles. (It says the converse can not happen.) Therefore, in fairly generic examples, like the ones considered here, one might expect all non-degenerate saddles to behave similarly and, in particular, "light up" as singularities on the Borel plane for a degenerate saddle.[10] When this does not happen, it draws our attention to such special instances, and so we give them a name.

**Definition 2.3.14** (phantom saddles)**.** *We call a saddle* $\mathfrak{b}$ *a phantom saddle (relative to* $\mathfrak{a}$*) when* $\mathcal{S}_{\mathfrak{a}}^{\mathfrak{b}} = 0$ *that is not enforced by the Theorem 2.3.12.*

In other words, phantom saddles are true saddles of the path integral (2.3.2) that do not show up on the Borel plane.

Curiously, we find strong (numerical) evidence for such saddles already in the simplest members of the family (2.0.4). It would be interesting to uncover the precise condition that trigger this phenomenon; clearly, it must be more subtle than (2.3.13). We do not address this question in the present paper, but expect that such phantom saddles can be explained by an extra grading ("height") assigned to saddle points that is not directly visible in the path integral formulation (2.3.2). Then, $\mathcal{S}_{\mathfrak{a}}^{\mathfrak{b}} = 0$ would be a consequence of a strict inequality between the gradings of $\mathfrak{a}$ and $\mathfrak{b}$, much as in (2.3.13). This should lead to a new vanishing theorem, a refinement of Theorem 2.3.12.

[10] In the context of $SL(2,\mathbb{C})$ Chern Simons theory on $S^3_{\frac{p}{r}}(K)$ with $|p| = 1$, the only degenerate saddle is the trivial flat connection, usually denoted $\alpha = 0$. In gauge theory literature, it is also sometimes denoted $\alpha = \theta$.

### 2.3.3 Knot and 3 Manifold Invariants

Stepping back from this resurgence discussion, we turn to a slightly different aspect of Chern Simons theory which makes a connection with the quantum invariants introduced in Section 2.2. Consider what the natural space of observables in Chern Simons Theory will be. To maintain the topological nature of this theory, it makes sense to consider Wilson loops:

$$W_V(\gamma) = \mathrm{Tr}_V\left(\mathrm{PExp}\left(\int_\gamma A\right)\right).$$

Here $\gamma$ is an embedded loop in $M^3$, $V$ a representation of $\mathfrak{g}$ and PExp denotes the path ordered exponential which computes the holonomy of $A$ around $\gamma$. Given an observable, we should immediately ask what its expectation value computes:

$$\langle W_V(\gamma)\rangle := \frac{\int_{\mathcal{A}} DA\, W_V(\gamma) e^{-\frac{1}{\hbar}S[A]}}{\int_{\mathcal{A}} DA\, e^{-\frac{1}{\hbar}S[A]}}.$$

As realised in [Wit89], for $M^3 = S^3$, these expectation values turn out to be well-known knot invariants. In the simplest case $G = U(1), V = \mathbb{C}$, this computes the self linking number and $\langle W_V(\gamma_1)W_V(\gamma_2)\rangle$ reproduces the Gauss Linking integral (1.0.1). The next simplest case is $G = \mathrm{SU}(2), V = V_{2,1}$ where the expectation value is exactly the unreduced Jones polynomial [Jon85] evaluated at $q = e^{\hbar}$,

$$\widetilde{J}(K; q = e^{\hbar}) = \langle W_{V_{2,1}}(\gamma_K)\rangle.$$

Here $\gamma_K$ is any embedded loop with knot type equal to $K$. More generally, with $G = \mathrm{SU}(N), R = V_{N,k}$, this setup produces the unreduced invariants as we defined in Section 2.2:

$$\widetilde{\mathcal{P}}_k^N(K; q = e^{\hbar}) = \langle W_{V_{N,k}}(\gamma_K)\rangle.$$

This construction gives a natural correspondence between the Jones polynomial and WRT invariants. Due to this, given any property which the Jones polynomial satisfies, we should investigate if that property has a 3-manifold analogue. For example, thanks to the work of Khovanov [Kho00], it is known that the Jones polynomial admits a categorification. Thus, we are directed to ask:

**Question 2.3.15.** *Does WRT invariant admit a categorification?*

At a simplified level, the idea of categorification is to take an integer invariant and replace it with a collection of homology groups. For example, the homology of a

manifold is a categorification of its Euler characteristic. This immediately highlights a problem, unlike the Jones polynomial, the WRT invariant is not naturally an integer invariant. Early progress on this problem as made by Lawrence and Zagier [LZ99] and later by Hikami [Hik04] who showed that for various Seifert manifolds, all WRT invariants can be realised as the limit of a power series with integer coefficients.

Later, in the study of 3d $\mathcal{N} = 2$ theories $T[M^3]$, Gukov, Putrov and Vafa in [GPV17] and in a follow-up paper with Pei [GPPV20] conjectured the existence of the 3-manifold invariants $\widehat{Z}_a(M^3)$.

**Conjecture 2.3.16** ([GPV17, GPPV20, GM21])**.** *Let $M^3$ be a closed 3-manifold with $b_1(M^3) = 0$. Let $Spin^c(M^3)$ denote the set of $Spin^c$ structures on $M^3$ with the action of $\mathbb{Z}_2$ by conjugation. Set*

$$T = Spin^c(M^3)/\mathbb{Z}_2.$$

*Then for every $a \in T$, there exist invariants*

$$\Delta_a \in \mathbb{Q}, \quad c \in \mathbb{Z}_+, \quad \hat{Z}_a(q) \in 2^{-c} q^{\Delta_a} \mathbb{Z}[[q]]$$

*with $\widehat{Z}_a(q)$ converging for $q < 1$ such that, for infinitely many $k$, the radial limits as $q \to e^{\frac{2\pi i}{k}}$ exist and can be used to recover the WRT invariant as:*

$$\mathcal{Z}(M^3; k) = \frac{1}{i\sqrt{2k}} \sum_{a,b \in T} e^{2\pi i k \cdot lk(a,a)} S_{ab} \widehat{Z}_b(q)\big|_{q \to e^{\frac{2\pi i}{k}}}.$$

*For this formula, the linking numbers $lk$ are the standard linking numbers on $H_1(M^3, \mathbb{Z})$ which can be applied to elements of $Spin^c(M^3)$ using a $\mathbb{Z}_2$-equivariant identification and*

$$S_{ab} \frac{e^{2\pi i k \cdot lk(a,b)} + e^{-2\pi i k \cdot lk(a,b)}}{|\mathcal{W}_a||\mathcal{W}_b|\sqrt{|H_1(M^3, \mathbb{Z})|}}.$$

*where $\mathcal{W}_a = Stab_{\mathbb{Z}_2}(x)$ is $\mathbb{Z}_2$ if $x = \bar{x}$ and 1 otherwise.*

These invariants exhibit peculiar modular properties, the exploration of which was initiated in [BMM20a, CCFGH19, BMM20b, CFS20].

## 2.4 $F_K$ invariants

More recently, Gukov and Manolescu [GM21] studied what happens when, instead of being closed, the manifold $M^3$ is a knot complement[11] $S^3 \backslash K$ and introduced

[11] Sometimes in the literature it is also denoted as $S^3 \setminus N(K)$ or $S^3 \setminus \nu K$, where $N(K)$ or $\nu K$ denotes the tubular neighbourhood of $K$. Of these different notations, we choose the most compact one.

$F_K = \widehat{Z}(S^3 \setminus K)$. The motivation behind this was to study $\widehat{Z}$ more systematically using Dehn surgery. This $F_K$ invariant is conjectured to be closely related to coloured Jones Polynomials and function as a type of "Analytic Continuation".

To make this explicit, first recall the Melvin Morton Rozansky (MMR) expansion [MM95, BNG96, Roz96, Roz98] of the coloured Jones polynomials:

$$J_k(K;q) \xrightarrow[x=e^{k\hbar}]{q=e^{\hbar}} \sum_{j\geq 0} \frac{P_j(K;x)}{\Delta_K(x)^{2j+1}} \frac{\hbar^j}{j!},$$

where $\Delta_K(x)$ is the Alexander polynomial of $K$, $P_j(K;x) \in \mathbb{Z}[x,x^{-1}]$ and $P_0(K;x) = 1$. This equality holds $k \in \mathbb{N}$ and small $\hbar$.

**Conjecture 2.4.1** ([GM21], Conjecture 1.5)**.** *For every knot $K \subset S^3$, there exists a two-variable series* [12]

$$F_K(x,q) = x^p \sum_{m=0}^{\infty} f_m(q) x^m, \qquad f_m(q) \in \mathbb{Z}[q^{-1},q]] \tag{2.4.2}$$

*such that the asymptotic expansion agrees with the MMR expansion:*

$$F_K(x, q=e^{\hbar}) \xrightarrow{resurgence} \sum_{j\geq 0} \frac{p_j(x)}{\Delta_K(x)^{2j+1}} \frac{\hbar^j}{j!}. \tag{2.4.3}$$

*Moreover, this series is annihilated by the quantum A-polynomial* [13]*:*

$$\hat{A}_K(\hat{x},\hat{y},q) F_K(x,q) = 0.$$

By resurgence, we mean that to realise this equality, one has to repackage the perturbative invariants using Borel resummation or other similar techniques. Whilst initially defined via negative definite plumbings [GM21], the work of Park [Par20b, Par21] showed that $F_K$ can be computed using the $R$-matrix associated to a particular Verma module of $U_q(\mathfrak{sl}_2)$. We discuss this further in Chapter 3. Simple surgery formula relate $F_K(x,q)$ and $\widehat{Z}_b(S^3_{\frac{p}{r}}(K),q)$for a large family of $\frac{p}{r}$ depending on $K$.

**Conjecture 2.4.4** ([GM21], Conjecture 1.7)**.** *Let $K \subset S^3$ be a knot and $S^3_{\frac{p}{r}}(K)$ the manifold given by $\frac{p}{r}$ Dehn surgery on $K$. Then there exists $\epsilon \in \pm 1$ and $d \in \mathbb{Q}$ such that*

$$\widehat{Z}_a(S^3_{\frac{p}{r}}(K)) = \epsilon q^d \mathcal{L}^{(a)}_{\frac{p}{r}} \left( (x^{\frac{1}{2r}} - x^{-\frac{1}{2r}} F_K(x,q) \right) \tag{2.4.5}$$

*provided the right-hand side is well-defined.*

[12] This looks slightly different to the conjecture given in [GM21] due to differing conventions. See Section 2.4.3

[13] See Section 2.5 for the definition of $\hat{A}$.

Here, $\mathcal{L}^{(a)}_{\frac{p}{r}}$ is a type of Laplace transform defined as

$$\mathcal{L}^{(a)}_{\frac{p}{r}}(q^i x^j) = \begin{cases} q^{i-j^2\frac{r}{p}} & rj - a \in p\mathbb{Z} \\ 0 & \text{otherwise.} \end{cases} \tag{2.4.6}$$

There are mild generalisation of Conjecture 2.4.4 given in [Par21] which, in certain cases, show how to regularise the right-hand side of Equation 2.4.5.

### 2.4.1 $F_K$ invariants for other Lie groups

Conjecture 2.4.1 concerns $\mathfrak{g} = \mathfrak{sl}_2$. An extension to arbitrary $\mathfrak{g}$ was studied in [Par20a]. In particular, the existence of a $\mathfrak{sl}_N$ generalisation of $F_K$, denoted $F_K^{\mathfrak{sl}_N}$, was conjectured which is a series in $(x_1, \cdots, x_{N-1}, q)$. Specialising $x_i \mapsto q$ for $i > 1$, reduces us back to a 2 variable series which is expected to correspond to the analytic continuation of the quantum invariants corresponding to the symmetric representations of $\mathfrak{sl}_N$ and so we denote it $F_K^{\mathfrak{sl}_N,sym} = F_K^N$.

**Conjecture 2.4.7** ($F_K$ for $\mathfrak{sl}_N$)**.** *For any knot $K$ there exists a two variable series $F_K^N$ of similar form to $F_K$ which satisfies*

$$F_K^N(x, q = e^{\hbar}) = \frac{1}{\Delta_K(x)^{N-1}} + \sum_{j=1}^{\infty} \frac{R_j(x, N)}{\Delta^{N+2j-1}(x)} \hbar^j, \tag{2.4.8}$$

$$\hat{A}_K(\hat{x}, \hat{y}, q^N, q) F_K^N(x, q) = 0, \tag{2.4.9}$$

where $\hat{A}_K(\hat{x}, \hat{y}, a, q)$ is the quantum super $A$-polynomial.

One of the beautiful features of the $\mathfrak{sl}_N$ quantum invariants is their regularity in $N$ which, as described earlier, is captured by the coloured HOMFLY-PT polynomial $P_k(K; a, q)$. From this structure, it is natural to predict the existence of a HOMFLY-PT version of $F_K$:

**Conjecture 2.4.10** ($a$-deformed $F_K$)**.** *For every knot $K \subset S^3$, there exists a three-variable function $F_K(x, a, q)$ interpolating all the $F_K^N$ in the following sense:*

$$F_K(x, a = q^N, q) = F_K^N(x, q), \tag{2.4.11}$$

$$\hat{A}_K(\hat{x}, \hat{y}, a, q) F_K(x, a, q) = 0. \tag{2.4.12}$$

*Moreover, it has the following properties:* [14]

$$F_K(x,1,q) = \Delta_K(x), \tag{2.4.13}$$

$$F_K(x,q,q) = 1, \tag{2.4.14}$$

$$\lim_{q\to 1} F_K(x,q^N,q) = \frac{1}{\Delta_K(x)^{N-1}}. \tag{2.4.15}$$

*Its asymptotic expansion should agree with that of the coloured HOMFLY-PT polynomials. That is,*

$$\log F_K(e^{k\hbar},a,e^{\hbar}) = \log P_k(K;a,e^{\hbar}) \tag{2.4.16}$$

*as $\hbar$-series.*

### 2.4.2 Knots-Quivers Correspondence

A quiver $Q$ is an oriented graph, in other words, a pair $(Q_0,Q_1)$ where $Q_0$ is a finite set of $m$ vertices and $Q_1$ is a finite set of arrows between them. We can fully capture the information contained in $Q_1$ by way of an adjacency matrix $C$ where $C_{ij}$ is the number of arrows from $i$ to $j$. A symmetric quiver is a quiver whose adjacency matrix is symmetric.

A quiver representation with dimension vector $\boldsymbol{d} = (d_1,\ldots,d_m)$ consists of an assignment of a vector space of dimension $d_i$ to the node $i \in Q_0$ and, for each arrow $i \to j \in Q_1$, a linear map $\gamma_{ij} : \mathbb{C}^{d_i} \to \mathbb{C}^{d_j}$. Quiver representation theory studies moduli spaces of quiver representations. While explicit expressions for invariants describing those spaces are difficult to find in general, they are well understood in the case of symmetric quivers [KS08, KS10, Efi11, MR14, FR18]. Indeed, many invariants can be encoded into the motivic generating series:

$$P_Q(\boldsymbol{x},q) = \sum_{\boldsymbol{d}\geq 0} (-q^{\frac{1}{2}})^{\boldsymbol{d}\cdot\boldsymbol{C}\cdot\boldsymbol{d}} \frac{\boldsymbol{x}^{\boldsymbol{d}}}{(q;q)_{\boldsymbol{d}}} = \sum_{d_1,\ldots,d_m\geq 0} (-q^{\frac{1}{2}})^{\sum_{i,j} C_{ij}d_id_j} \prod_{i=1}^{m} \frac{x_i^{d_i}}{(q;q)_{d_i}}.$$

Similarly, given a knot $K$ we can combine the polynomials $P_k(K;a,q)$ into the HOMFLY-PT generating series:

$$P_K(y,a,q) = \sum_{k=0}^{\infty} \frac{P_k(K;a,q).}{(q)_k} y^k.$$

[14] Here we are using the *reduced* normalisation. For the *unreduced* normalisation, we should have, for instance,

$$\lim_{q\to 1} F_K(x,q^N,q) = \left(\frac{x^{\frac{1}{2}} - x^{-\frac{1}{2}}}{\Delta_K(x)}\right)^{N-1}.$$

The knots-quivers correspondence is the idea that, for each knot, we can associate a quiver whose motivic generating series is equal (after specialisations) to the HOMFLY-PT generating series.

**Conjecture 2.4.17.** *For every knot $K$ there exists a symmetric quiver $Q$ (with adjacency matrix $C$), vector $\boldsymbol{n} = (n_1, \dots, n_m)$ with integer entries, and vectors $\boldsymbol{a} = (a_1, \dots, a_m)$, $\boldsymbol{l} = (l_1, \dots, l_m)$ with half-integer entries such that*

$$P_K(y, a, q) = \sum_{\boldsymbol{d} \geq 0} (-q^{\frac{1}{2}})^{\boldsymbol{d} \cdot \boldsymbol{C} \cdot \boldsymbol{d}} \frac{y^{\boldsymbol{n} \cdot \boldsymbol{d}} a^{\boldsymbol{a} \cdot \boldsymbol{d}} q^{\boldsymbol{l} \cdot \boldsymbol{d}}}{(q)_{\boldsymbol{d}}} = P_Q(\boldsymbol{x}, q)\big|_{x_i = y^{n_i} a^{a_i} q^{l_i}} .$$

This conjecture was proven for all 2-bridge knots in [SW17] and for all arborescent knots in [SW21]. Some exotic cases with $n_i > 1$ (the simplest examples are $\mathbf{9}_{42}$ and $\mathbf{10}_{132}$) require a generalisation of the correspondence, for more details see [EKL21].

This correspondence can be refined and extended to knot complements ($F_K$) [Kuc20].

**Conjecture 2.4.18.** *For every knot $K$ there exists a symmetric quiver $Q$ (with adjacency matrix $C$), vector $\boldsymbol{n} = (n_1, \dots, n_m)$ with integer entries, and vectors $\boldsymbol{a} = (a_1, \dots, a_m)$, $\boldsymbol{l} = (l_1, \dots, l_m)$ with half-integer entries such that*

$$F_K(x, a, q) = \sum_{\boldsymbol{d} \geq 0} (-q^{\frac{1}{2}})^{\boldsymbol{d} \cdot \boldsymbol{C} \cdot \boldsymbol{d}} \frac{x^{\boldsymbol{n} \cdot \boldsymbol{d}} a^{\boldsymbol{a} \cdot \boldsymbol{d}} q^{\boldsymbol{l} \cdot \boldsymbol{d}}}{(q)_{\boldsymbol{d}}} = P_Q(\boldsymbol{x}, q)\big|_{x_i = x^{n_i} a^{a_i} q^{l_i}} . \tag{2.4.19}$$

Note that these correspondences are very far from being bijections [KRSS19, JKLNS21]. Indeed, given a quiver, there are a collection of quiver transformations that preserve the motivic generating function [EKL20a, EKL20b]. Due to the still-experimental nature of $F_K(x, a, q)$ this conjecture has only been proven in a couple of cases [Kuc20]. Instead, it can be used in the opposite direction as a way to construct the $a$ deformed $F_K$, as we discuss in Section 4.4. Also note that there is a family of similar but weaker conjectures to Conjecture 2.4.18 where instead of a quiver for $F_K(x, a, q)$ we are looking for a quiver for $F_K^N$.

### 2.4.3 Normalisation and Conventions

Before continuing, we make a few remarks on different conventions involving $F_K$ and $\mathcal{P}_k^N$.

- In [GM21] and Conjecture 2.4.1, $F_K$ is presented in the *balanced* expansion which involves a summation over both positive and negative powers of $x$ with

Weyl symmetry being manifest. However, for our purposes it will be more natural to work with the *positive* expansion where we express $F_K$ as a power series in $x$ expanded around 0. There is a closely related *negative* expansion coming from expanding around $x = \infty$ or by applying Weyl symmetry to the positive expansion.

$$F_K(x^{-1}, a, q) = F_K(a^{-1}x, a, q).$$

The balanced expansion can be recovered by averaging the positive and negative expansions.

- When working with quiver forms (Sections 2.4.2 and 4.4), we often treat $F_K$ as an integer power series starting with 1, see e.g. Equation (2.4.19). We stress that this is only correct up to an overall prefactor

$$\exp\left(\frac{p(\log x, \log a)}{\hbar}\right),$$

where $p$ is a polynomial of degree at most 2. These prefactors are important for some properties of $F_K$ and can be derived from the quantum $A$ and $B$-polynomials.

- In the literature there are a collection of different normalisations in which $F_K$ and $\mathcal{P}_k^N$ are presented. The three possibilities correspond to the different values which can be assigned to the unknot invariant.

  – The *reduced* normalisation corresponds to normalizing away the unknot,

  $$\mathcal{P}_k^N(\mathbf{0}_1, q) = 1 = F_{\mathbf{0}_1}(x, a, q).$$

  This is the convention most present in the literature on HOMFLY-PT, superpolynomials, and $A$-polynomials, e.g. [DGR05, FGSA12, FGS13, FGSS12, NRZS12]. This is also the convention we use throughout this thesis.

  – The *unreduced* normalisation corresponds to normalizing away the denominator of the full unknot factor,

  $$\mathcal{P}_k^{N,unreduced}(\mathbf{0}_1, q) = \frac{(xq;q)_\infty}{(xa;q)_\infty} = F_{\mathbf{0}_1}^{unreduced}(x, a, q).$$

  This convention is common in the growing literature on $F_K$ invariants, e.g. [GM21, Par20a, Par20b, GHNPPS21], but we do not use this normalisation in this thesis.

– The *fully unreduced* normalisation corresponds to leaving the full unknot factor intact,

$$\begin{aligned}\widetilde{\mathcal{P}}_k^N(\mathbf{0}_1, q) &= e^{\frac{-\log(x)\log(a)}{2\hbar}} x^{\frac{1}{2}} \frac{(a;q)_\infty (xq;q)_\infty}{(xa;q)_\infty (q;q)_\infty} \\ &= F_{\mathbf{0}_1}^{fully\ unreduced}(x, a, q).\end{aligned}$$

This normalisation is natural in the context of enumerative invariants and can be found in [OV00, AENV14, EN20, EKL20a, EKL20b, ES19, DE20]. In the literature this normalisation is usually called just "unreduced" and we will also refer to it this way outside this section.

## 2.5 The A-Polynomial

Given a flat connection $A$ on $M^3$, the holonomy of the connection around loops in $M^3$ gives a representation

$$Hol_A : \pi_1(M^3) \to G.$$

If we act on $A$ by a gauge transformation, the representation changes by conjugation and so if we quotient by this action, we find that

$$\alpha \mapsto Hol_\alpha$$

is a bijection between gauge equivalence classes of flat connections and representations up to conjugation. Fix a knot complement $S^3\backslash K$ with fundamental group $\pi_1(K)$ and let $R(K)$ denote the variety of representations $\rho : \pi(K) \to SL_2(\mathbb{C})$. As $S^3\backslash K$ has torus boundary, the inclusion map induces a map between fundamental groups

$$i_* : \pi_1(T^2) \to \pi_1(K),$$

where $\pi_1(T^2)$ is the free abelian group generated by a chosen pair of longitude and meridian curves, $l, m$. Hence, any representation $\rho$ restricts to a representation

$$\rho \circ i_* : \mathbb{Z}_l \oplus \mathbb{Z}_m \to \mathrm{SL}_2(\mathbb{C})$$

which, by conjugation[15], we can assume has the following form:

$$l \mapsto \begin{bmatrix} y & * \\ 0 & y^{-1} \end{bmatrix} \qquad m \mapsto \begin{bmatrix} x & * \\ 0 & x^{-1} \end{bmatrix}.$$

[15] If $x, y \neq \pm 1$, we can do even better and make the corresponding matrix diagonal.

This gives a map from $R(K)$ to an affine variety[16] $\mathcal{A}_K \subset (\mathbb{C}^*)^2$ which is the zero locus of a polynomial called the classical $A$-polynomial, [CCGLS94],

$$\mathcal{A}_K = \{(x, y) \in (\mathbb{C}^*)^2 \mid A_K(x, y) = 0\}. \tag{2.5.1}$$

### 2.5.1 The Quantum A Polynomial

Thanks to the correspondence between representations and the holonomy, of flat connections, $\mathcal{A}_K$ should be identified with the classical space of solutions for Chern Simons theory on a knot complement. Quantization replaces the algebraic equation $A = 0$ with operator equations, $\hat{A}\mathcal{Z} = 0$ which means that we should expect a quantization of the $A$-polynomial to annihilate $\mathrm{SL}(2, \mathbb{C})$ partition functions. We have actually already come across 2 such partition functions, the coloured Jones polynomials $J_k$ and $F_K$. This led to the following conjecture which arose concurrently in the physical [Guk05] and mathematical [Gar04] literature[17].

**Conjecture 2.5.2** (The Quantum A Polynomial)**.** *For any knot $K$, there exists a polynomial $\hat{A}_K(\hat{x}, \hat{y}, q)$ which satisfies:*

$$\hat{A}_K(\hat{x}, \hat{y}, q) J_*(K; q) = 0,$$

*where*

$$\hat{x} J_k(K; q) = q^k J_k(K; q), \qquad \hat{y} J_k(K; q) = J_{k+1}(K; q),$$

*with $\hat{y}\hat{x} = q\hat{x}\hat{y}$. This polynomial is a quantization of the usual A-polynomial in the sense that*

$$\lim_{q \to 1} \hat{A}_K(\hat{x}, \hat{y}, 1)$$

*contains $A(x, y)$ as a factor*[18]*.*

Given how $F_K$ relates to $J_k$, we immediately see that this conjecture implies

$$\hat{A}_K(\hat{x}, \hat{y}, q) F_K(x, q) = 0,$$

where, $\hat{x}$ and $\hat{y}$ act by

$$\hat{x} F_K(x, q) = x F_K, \qquad \hat{y} F_K(x, q) = F_K(qx, q).$$

[16] Technically speaking this map lands in $(\mathbb{C}^*)^2/(x, y) \sim (x^{-1}, y^{-1})$ but following [CCGLS94, Guk05] we suppress this quotient.

[17] Note that the conjecture is purely that $\hat{A}$ is a quantization of $A$. The existence of a q-deformation relation for Jones polynomials was proven in [GL05].

[18] In general $\lim_{q \to 1} \hat{A}_K(\hat{x}, \hat{y}, 1)$ contains a couple of other factors of the form $(1 \pm x^n)$.

Conjecture 2.5.2 was generalized to coloured HOMFLY-PT polynomials [AV12] in which case the polynomial becomes $a$-dependent. In particular, the asymptotics of coloured HOMFLY-PT $P_k(K;a,q)$ for large $k$ is captured by an algebraic curve called the *super-A-polynomial*, defined by the equation $A_K(x,y,a) = 0$ where $A_K(x,y,1)$ has $A_K(x,y)$ as a factor. The quantisation of the super-$A$-polynomial gives rise to quantum super-$A$-polynomial $\hat{A}_K(\hat{x},\hat{y},a,q)$, which is a $q$-difference operator that encodes the recurrence relations for the coloured HOMFLY-PT:

$$\hat{A}_K(\hat{x},\hat{y},a,q)P_*(K;a,q) = 0.$$

A universal framework that enables us to determine a quantum $A$-polynomial from an underlying classical curve $A(x,y) = 0$ was proposed in [GS12] (irrespective of extra parameters these curves depend on, and also beyond examples related to knots).

### 2.5.2 Twisted Super Potential

The twisted superpotential is the leading genus-0 contribution to the generating function of enumerative invariants and is given by the double-scaling limit that combines large-colour and semiclassical limits of the HOMFLY-PT polynomials [FGS13, FGSS12]:

$$P_k(K;a,q) \underset{\hbar\to 0}{\overset{k\to\infty}{\longrightarrow}} \int \prod_i \frac{dz_i}{z_i} \exp\left[\frac{1}{\hbar}\widetilde{\mathcal{W}}(z_i,x,a) + O(\hbar^0)\right], \tag{2.5.3}$$

with $x = q^k$ kept fixed. Encoded in this superpotential is the structure of the 3d $\mathcal{N} = 2$ theory $T[S^3\backslash K]$. If we integrate out the dynamical fields (whose VEVs are given by $\log z_i$) using the saddle point approximation we obtain the effective twisted superpotential:

$$\widetilde{\mathcal{W}}_{\text{eff}}(x,a) = \frac{\partial\widetilde{\mathcal{W}}(z_i,x,a)}{\partial \log z_i}. \tag{2.5.4}$$

Introducing the dual variable $y$ (the effective Fayet-Iliopoulos parameter), we arrive back at the super-$A$-polynomial:

$$\log y = \frac{\partial\widetilde{\mathcal{W}}_{\text{eff}}(x,a)}{\partial \log x} \qquad \Leftrightarrow \qquad A_K(x,y,a) = 0. \tag{2.5.5}$$

*Chapter 3*

# THE $\mathfrak{sl}_N$ SYMMETRICALLY LARGE COLOURED R-MATRIX

In [Par20b, Par21] Park constructed a Verma module for $U_q(\mathfrak{sl}_2)$ such that, when put through the usual quantum invariant machinery, the knot invariant produced was (Provided the infinite summations converged) $F_K$. It was left as an open problem if the same approach could work for other quantum groups. The goal of this chapter is to investigate Conjecture 2.4.7 and extend Park's work to $U_q(\mathfrak{sl}_N)$. We prove Theorem 1.0.5 and provide methods to compute $F_K^N$ in wider generality.

## 3.1 The Symmetric Large Colour Limit

### 3.1.1 An Infinite Verma Module for $U_q(\mathfrak{sl}_N)$

In the $U_q(\mathfrak{sl}_2)$ case, every irreducible representation can be thought of as a one dimensional lattice with nodes corresponding to $K$ eigenspaces of dimension 1. Acting on an eigenspace by $E$ or $F$ has the effect of moving one step either up or down this lattice. This picture extends to the irreducible symmetric representations of $U_q(\mathfrak{sl}_N)$ but, as might be expected, the lattice is no longer 1 dimensional. For example, when $N = 3$ we get the 2 dimensional lattice illustrated in Figure 3.1. The triangular structure of this lattice comes simply from our choice of basis and note that for the $k$'th symmetric representation, the right-hand boundary of this lattice are the eigenspaces $V_{k,i}$.

The key algebraic feature of our choice of basis is that the actions of $E_i, F_i, K_i$, given in Equation (2.1.7), are mostly independent of the colour $k$. Indeed, $k$ appears only in the actions of $F_1, K_1$ as $q^{\pm\frac{k}{2}}$. Thus, replacing $q^k$ by $x$ and extending the lattice in Figure 3.1 to infinity, we get a lowest weight Verma module $V_N^x$ of $\mathfrak{sl}_N$ over the field $\mathbb{C}(q^{\frac{1}{2}}, x^{\frac{1}{2}})$.

This module has basis

$$v_{\mathbf{a}} = |a_1, \cdots, a_{n-1}, a_n = 0\rangle$$

with $a_1 \geq \cdots \geq a_{n-1} \geq 0$ with actions given by:

$$E_i \cdot v_{\mathbf{a}} = [a_i - a_{i+1}]_q v_{\mathbf{a}-e_i}$$

$$F_1 \cdot v_{\mathbf{a}} = \frac{x^{\frac{1}{2}} q^{-\frac{a_1}{2}} - x^{-\frac{1}{2}} q^{\frac{a_1}{2}}}{q^{\frac{1}{2}} - q^{-\frac{1}{2}}} v_{\mathbf{a}+e_1} \qquad F_i \cdot v_{\mathbf{a}} = [a_{i-1} - a_i]_q v_{\mathbf{a}+e_i}$$

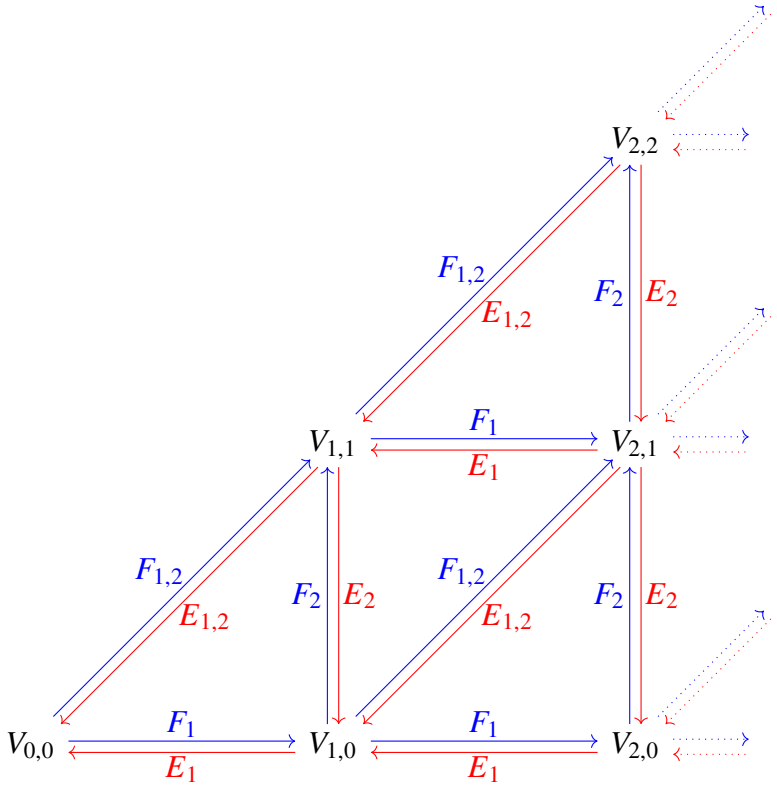


Figure 3.1: The bottom left corner of the lattice for symmetric representations of $U_q(\mathfrak{sl}_3)$. For the $k$'th symmetric representation, this lattice will stop at the line $V_{k,0}, \cdots, V_{k,k}$ where for $i \leq j$, $V_{i,j}$ refers to the eigenspace spanned by $v_{(i,j)}$.

$$K_1 \cdot v_{\mathbf{a}} = x^{\frac{1}{2}} q^{\frac{a_2 - 2a_1}{2}} v_{\mathbf{a}} \qquad K_i \cdot v_{\mathbf{a}} = q^{\frac{a_{i-1} + a_{i+1} - 2a_i}{2}} v_{\mathbf{a}}$$

**Proposition 3.1.1.** *The above definitions are well-defined and give $V_N^x$ the structure of an infinite dimensional Verma Module.*

Most of the relations are identical to the ones required to check Proposition 2.1.6 and so follow from the identifies given below it. The only differences occur with relations involving $K_1$ and $F_1$. Let us explicitly check one of these:

$$F_2^2 F_1 - [2]_q F_2 F_1 F_2 + F_1 F_2^2 = 0.$$

Plugging in an arbitrary eigenvector, we find:

$$\begin{aligned}\left(F_2^2 F_1 - [2]_q F_2 F_1 F_2 + F_1 F_2^2\right) v_{\mathbf{a}} &= \frac{[a_1 - a_2]_q \left(x^{\frac{1}{2}} q^{-\frac{a_1}{2}} - x^{-\frac{1}{2}} q^{\frac{a_1}{2}}\right)}{(q^{\frac{1}{2}} - q^{-\frac{1}{2}})} \\ &\times \left([a_1 - a_2 + 1]_q - [2]_q [a_1 - a_2]_q + [a_1 - a_2 - 1]_q\right) v_{\mathbf{a}} \\ &= 0.\end{aligned}$$

The rest of the relations follow similarly.

We can similarly extend the evaluation and co-evaluation maps to this module $V_N^x$. The co-evaluation map is identical to (2.1.9) but the evaluation becomes:

$$\overrightarrow{ev}_N^x : V_N^x \otimes (V_N^x)^* \to \mathbb{C}(q^{\frac{1}{2}}, x^{\frac{1}{2}}), \qquad v_{\mathbf{i}} \otimes v_{\mathbf{j}}^* \mapsto x^{\frac{N-1}{2}} q^{-|\mathbf{i}|} \delta_{\mathbf{i},\mathbf{j}}.$$

Again these combine to give a quantum trace and reduced quantum trace on $V_N^x$.

This module $V_N^x$ should be thought of as a type of limit of the symmetric representations $V_{N,k}^q$. In particular, when we specialise $x = q^k$, $V_{N,k}^q$ sits inside $V_N^x|_{x=q^k}$ as the irreducible subrepresentation containing $V_{\mathbf{0}}$. It is worth noting that this property does not uniquely characterise $V_N^x$. From the perspective of the polynomial representations we discussed earlier, $V_N^x$ corresponds to sending the exponent of $z_1$ to infinity while keeping the other exponents finite. This naturally leads to a host of other possible limits where, instead of $z_1$, the exponent of $z_j$ is sent to infinity. The highest weight module in [Par20b] and its $\mathfrak{sl}_N$ extension corresponds to the $j = N$ case.

### 3.1.2 The $\mathfrak{sl}_N$ Symmetrically Large Coloured R-matrix

In what follows by $R$-matrix we implicitly include the permutation operator, so technically these are all $\widetilde{R}$ matrices. Let us specialise the R-matrix given in (2.1.5) to the Verma module defined above. The result is an infinite summation over a collection of non-negative integers $\mathbf{r} = r_i^j$ with $1 \leq i \leq j \leq N-1$. For $i \leq j \leq k \leq l$, define $\mathbf{r}_{(i,j)}^{(k,l)}$ as the vector $(r_i^k, \cdots, r_i^l, r_{i+1}^k, \cdots, r_j^l)$ and denote

$$\mathbf{r}^j = \mathbf{r}_{(1,j)}^{(j,j)} = (r_1^j, \cdots, r_j^j), \qquad \mathbf{r}_j = \mathbf{r}_{(j,j)}^{(j,N-1)} = (r_j^j, \cdots, r_j^{N-1}).$$

Letting $|\cdot|$ denote the $l^1$ norm, we find that[1]:

$$\begin{aligned} {}_{\mathfrak{sl}_N} R\,|\mathbf{a},\mathbf{b}\rangle = q^{\frac{(N-1)\log_q(x)^2}{2N}} \\ \times \sum_{\mathbf{r}>0} \frac{(-1)^{|\mathbf{r}|} q^{C_N} x^{-\frac{1}{2}(a_1+b_1+|\mathbf{r}_1|)} (xq^{-b_1};q^{-1})_{|\mathbf{r}_1|} (q^{a_1-a_2+|\mathbf{r}_2|};q^{-1})_{|\mathbf{r}^1|}}{(q;q)_{\mathbf{r}}} \end{aligned} \tag{3.1.2}$$

[1]Here we present the single coloured $R$-matrix which acts on $V_N^x \otimes V_N^x$. For link invariants, we should consider the multicoloured $R$-matrix which acts on $V_N^x \otimes V_N^y$. The matrix is essentially identical, we simply need to make the following replacement:

$$q^{\frac{(N-1)\log_q(x)^2}{2N}} x^{-\frac{1}{2}(a_1+b_1+|\mathbf{r}_1|)} (xq^{-b_1};q^{-1})_{|\mathbf{r}_1|} \mapsto q^{\frac{(N-1)\log_q(x)\log_q(y)}{2N}} x^{-\frac{1}{4}(2b_1+|\mathbf{r}_1|)} y^{-\frac{1}{4}(2a_1+|\mathbf{r}_1|)} (yq^{-b_1};q^{-1})_{|\mathbf{r}_1|}.$$

$$\times \prod_{j=2}^{N-1} (q^{b_{j-1}-b_j}; q^{-1})_{|\mathbf{r}_j|} (q^{a_j - a_{j+1}+|\mathbf{r}_{j+1}|}; q^{-1})_{|\mathbf{r}^j|} \, |\mathbf{a}', \mathbf{b}'\rangle \,,$$

where

$$C_N = \frac{1}{2}\mathbf{r}\cdot\mathbf{r} + \mathbf{a}\cdot M\cdot\mathbf{b} + \sum_{j=1}^{N-1}\left(\frac{1}{4}|\mathbf{r}^j|(a_{j+1}+b_{j+1}-2) - \frac{1}{4}\left(\sum_{i=2}^{j} r_i^j (a_{i-1}+b_{i-1})\right)\right.$$
$$\left. + \sum_{i=1}^{j-1} r_i^j \left(|\mathbf{r}_{(i+1,j)}^{(j,N-1)}| + \frac{3}{4}(a_i - a_j) - \frac{1}{4}(b_i - b_j)\right)\right),$$

$$M_{ij} = \begin{cases} 1 & i = j \\ -\frac{1}{2} & |i-j| = 1 \\ 0 & \text{else.} \end{cases}, \qquad a_i' = b_i + |\mathbf{r}_{(1,i)}^{(i,N-1)}|, \qquad b_i' = a_i - |\mathbf{r}_{(1,i)}^{(i,N-1)}|.$$

Observe that the power of $x$ is always negative and, for each $\mathbf{r}$, the summand will always simplify to a polynomial. The second conclusion follows from the observation that, if we regroup the $q$-Pochhammers, we find for each $j$

$$\frac{(q^{a_j - a_{j+1}+|\mathbf{r}_{j+1}|}; q^{-1})_{|\mathbf{r}^j|}}{(q;q)_{\mathbf{r}^j}} = \frac{(q,q)_{a_j - a_{j+1}+|\mathbf{r}_{j+1}|+|\mathbf{r}^j|}}{(q;q)_{a_j - a_{j+1}+|\mathbf{r}_{j+1}|}(q;q)_{\mathbf{r}^j}}.$$

The right-hand side is simply a $q$-multinational coefficient and thus will be a polynomial in $q$. Also, while we have a prefactor $q^{\frac{(N-1)\log_q(x)^2}{2N}}$, this will be mostly cancelled out by the framing factor $q^{\frac{(N-1)\log_q(x)^2}{2N}} x^{\frac{N-1}{2}}$. As we will always work in framing 0, for computations we simply need to replace this pre-factor by $x^{-\frac{N-1}{2}}$.

To match the above description up with the R-matrix given in [Par20b] define the matrix elements

$${}_{\mathfrak{sl}_N} R_{\mathbf{a},\mathbf{b}}^{\mathbf{a}',\mathbf{b}'} = \langle \mathbf{a}', \mathbf{b}' |_{\mathfrak{sl}_N} R \, |\mathbf{a}, \mathbf{b}\rangle \,,$$

where $\langle \mathbf{a}', \mathbf{b}' | \mathbf{a}, \mathbf{b}\rangle = \delta_{\mathbf{a},\mathbf{a}'}\delta_{\mathbf{b},\mathbf{b}'}$. These matrix elements are 0 unless $\mathbf{a}+\mathbf{b} = \mathbf{b}'+\mathbf{a}'$, in which case the summand will be non 0 only when

$$|\mathbf{r}_{(1,i)}^{(i,N-1)}| = a_i - b_i' = a_i' - b_i.$$

These conditions collapse the infinite summation to a finite sum and so each matrix element will be a polynomial in $x^{-1}$, $q$ and $q^{-1}$. We can similarly compute $R^{-1}$-matrix elements via:

$$R^{-1} = PR|_{\substack{x\mapsto x^{-1} \\ q\mapsto q^{-1}}} P \qquad \Longrightarrow \qquad {}_{\mathfrak{sl}_N} R^{-1}{}_{\mathbf{a},\mathbf{b}}^{\mathbf{a}',\mathbf{b}'} = R_{\mathbf{b},\mathbf{a}}^{\mathbf{b}',\mathbf{a}'}|_{\substack{x\mapsto x^{-1} \\ q\mapsto q^{-1}}}.$$

Thus $R^{-1}$-matrix elements will be a polynomial in $x$, $q$ and $q^{-1}$.

### 3.1.3 The Classical Limit

Let's start by analysing the classical limit of this $R$-matrix. When we take $q \to 1$, the denominator has a 0 of order $|\mathbf{r}|$ and the numerator has a 0 of order,

$$\sum_{j=2}^{N-1} |\mathbf{r}^j| + \sum_{j=1}^{N-1} |\mathbf{r}_j| = 2|\mathbf{r}| - |\mathbf{r}^1|.$$

Hence, in the $q \to 1$ limit, the only non 0 terms occur when $|\mathbf{r}| = |\mathbf{r}^1|$ meaning $r_i^j = 0$ for $i \geq 2$. Thus, we find (ignoring the prefactor for a moment)

$$\lim_{q\to 1} {}_{\mathfrak{sl}_N} R\,|\mathbf{a},\mathbf{b}\rangle = \sum_{\mathbf{r}_1>0} (-1)^{|\mathbf{r}_1|} x^{-\frac{1}{2}(a_1+b_1+|\mathbf{r}_1|)} (1-x)^{|\mathbf{r}_1|} \prod_{j=1}^{N-1} \binom{a_j - a_{j+1}}{r_1^j} |\mathbf{a}',\mathbf{b}'\rangle\,,$$

Passing to matrix elements, we find that the only non 0 term in the summation is at $r_i^j = (a_i - a_{i+1}) - (b'_i - b'_{i+1})$ and so our $R$-matrix elements are

$$\lim_{q\to 1} {}_{\mathfrak{sl}_N} R^{\mathbf{a}',\mathbf{b}'}_{\mathbf{a},\mathbf{b}} = (-1)^{a_1-b'_1} x^{-\frac{1}{2}(2a_1+b_1-b'_1)} (1-x)^{a_1-b'_1} \prod_{j=1}^{N-1} \binom{a_j - a_{j+1}}{b_i - b'_{i+1}}.$$

This can be made simpler by considering a different labelling of our basis. Define $c_i = a_i - a_{i+1}$ and $d_i = b_i - b_{i+1}$. Then with respect to this labelling (and reintroducing the prefactor modified by the framing) we have:

$$\lim_{q\to 1} {}_{\mathfrak{sl}_N} R^{\mathbf{c}',\mathbf{d}'}_{\mathbf{c},\mathbf{d}} = x^{\frac{N-1}{2}} \prod_{i=1}^{N-1} (-1)^{c_i-d'_i} x^{-\frac{1}{2}(2c_i+d_i-d'_i)} (1-x)^{c_i-d'_i} \binom{c_i}{d'_i}.$$

We immediately see that we have $n-1$ non-interacting copies of the classical limit of ${}_{\mathfrak{sl}_2}R$. Hence, similarly to [Par20b], if we compute the trace of a braid we will recover $\frac{1}{\Delta_K(x)^{(N-1)}}$. This proves the $q \to 1$ limit obeys property (2.4.8) for knots where the $R$-matrix sum converges absolutely.

As a brief side comment, note that in this $q \to 1$ limit the theory is identical to the theory coming from $U_q(\mathfrak{sl}_2)^{N-1}$. Similarly, if we study how the $R$-matrix acts on one particle states[2], our theory is again identical to $U_q(\mathfrak{sl}_2)^{N-1}$. The difference arises when $q$ is turned on, where some multiparticle transitions occur only in the $U_q(\mathfrak{sl}_N)$ theory. This is one of the obstacles which currently prevents the generalization of the theorems in [Par21] from $\mathfrak{sl}_2$ to $\mathfrak{sl}_N$.

Let us turn now to Theorem 1.0.5 which we restate and make more precise here[3].

[2] These states are simplest to study in the $\mathbf{c}$, $\mathbf{d}$ basis. In this basis, the one particle states are states where exactly one of the $c_i, d_i$ is 1 and the rest are 0.

[3] Note that while we only deal with positive braid knots here an identical theorem extends to negative braid knots

**Theorem 3.1.3** ($F_K$ for $\mathfrak{sl}_N$)**.** *For every positive braid knot $K$ and integer $N \in \mathbb{N}$ there exists a 2 variable series*

$$F_K^N(x,q) = x^p \sum_{m=0}^{\infty} f_m(q) x^m, \qquad f_m(q) \in \mathbb{Z}[q^{-1}, q]$$

*such that the asymptotic expansion agrees with the $\mathfrak{sl}_N$ MMR expansion*

$$F_K^N(x, q = e^{\hbar}) = \frac{1}{\Delta_K(x)^{N-1}} + \sum_{k=1}^{\infty} \frac{R_k(x,N)}{\Delta^{N+2k-1}(x)} \hbar^k. \tag{3.1.4}$$

*Moreover, this is annihilated by the quantum super A-polynomial at $a = q^N$*

$$\hat{A}_K(\hat{x}, \hat{y}, q^N, q) F_K^N(x,q) = 0.$$

### 3.1.4 Proof of Theorem 3.1.3

The proof is similar to one given in [Par20b] for the $\mathfrak{sl}_2$ case. We first need to justify that the state sum converges absolutely for positive braid knots. To do this, let's look more closely at the $R$-matrix given in equation (3.1.2). In particular, observe that for each choice of $\mathbf{r}$, the highest and lowest $x$ exponents which appear when we expand out the $q$-Pochhammers will be

$$\begin{aligned} \text{Highest: } & x^{-\frac{1}{2}(a_1+b_1-\mathbf{r}_1)} = x^{-\frac{1}{2}(b_1+b_1')} \\ \text{Lowest: } & x^{-\frac{1}{2}(a_1+b_1+\mathbf{r}_1)} = x^{-\frac{1}{2}(a_1+a_1')}. \end{aligned}$$

We see that if the incoming strands are labelled **a** and **b** then, regardless of the labelling on the outgoing strands, we will have an $x$ power of at most $x^{-\frac{b_1}{2}}$. As, when considering just the $x$ power, only the 1st component of the states **a**, **b**, **a'**, **b'** appear, the situation is identical to the $\mathfrak{sl}_2$ case and so the argument in [Par20b] will easily carry across. That argument essentially proves the following lemma[4]:

**Lemma 3.1.5.** *Let $\beta_K$ be an $n+1$ strand braid representation of a knot $K$. Then*

$$\langle \boldsymbol{0}, \boldsymbol{b}_1, \cdots, \boldsymbol{b}_n | \, \beta_K \, | \boldsymbol{0}, \boldsymbol{b}_1, \cdots, \boldsymbol{b}_n \rangle$$

*is a finite polynomial in $x^{-1}, q, q^{-1}$ with maximal $x$ coefficient*

$$x^{-\frac{1}{2}(b_{1,1}+\cdots+b_{n,1})}.$$

For a graphical representation of $\langle \mathbf{0}, \mathbf{b}_1, \cdots, \mathbf{b}_n | \, \beta_K \, | \mathbf{0}, \mathbf{b}_1, \cdots, \mathbf{b}_n \rangle$, see Figure 3.2.

[4] Technically [Par20b] proves a slightly weaker lemma, but the proof easily extends.

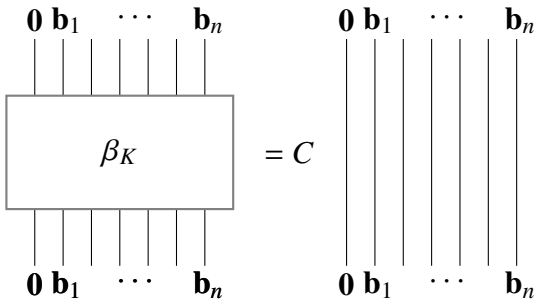


Figure 3.2: The graphical picture defining the tensor elements

$$C = \langle \mathbf{0}, \mathbf{b}_1, \cdots, \mathbf{b}_n | \, \beta_K \, | \mathbf{0}, \mathbf{b}_1, \cdots, \mathbf{b}_n \rangle \, .$$

The proof of this lemma follows from simple analysis of how weight can move around on a braid. Let us study the strand labelled by $\mathbf{b}_i$ noting that, as we are dealing with a knot, $\sigma_i$ must appear at least once for all $i$. If $i = n$, then the first occurrence of $\sigma_n$ has bottom right strand $\mathbf{b}_n$ and thus the corresponding $R$-matrix has maximal $x$ power $x^{-\frac{b_{n,1}}{2}}$. If $i < n$ then there might be some number of $\sigma_{i+1}$ before the first occurrence of $\sigma_i$.

For any crossing going from state $|\mathbf{a}, \mathbf{b}\rangle$ to $|\mathbf{a}', \mathbf{b}'\rangle$, we immediately know $\mathbf{a} \leq \mathbf{a}' + \mathbf{b}'$ and that the corresponding $R$-matrix element has maximal $x$ power lower than $-\frac{b'_1}{2}$. Assume we encounter $j$ $\sigma_{i+1}$ elements before we reach the first $\sigma_i$ element. Let the $k$'th $\sigma_{i+1}$ go from $|\mathbf{a}_{k-1}, \mathbf{c}_k\rangle$ to $\left|\mathbf{a}_k, \mathbf{c}'_k\right\rangle$ where $\mathbf{a}_0 = \mathbf{b}_i$. Then the overall maximum exponent power of $x$ coming from this chain of crossings is less than

$$-\frac{1}{2}(\mathbf{c}'_1 + \cdots + \mathbf{c}'_j + \mathbf{a}_j) \leq -\frac{1}{2}(\mathbf{c}'_1 + \cdots + \mathbf{c}'_{j-1} + \mathbf{a}_{j-1}) \leq \cdots \leq -\frac{\mathbf{a}_0}{2} = -\frac{\mathbf{b}_i}{2},$$

Note that in this argument we have completely ignored the right incoming strand of $\sigma_{i+1}$ and so we can freely apply this argument for all $i$ to conclude Lemma 3.1.5.

Next, observe that if we fix the incoming labels, all summations over internal variables are finite. This is due to the fact that all labellings must be positive and, at every level, the sum of the labellings is $\mathbf{b}_1 + \cdots + \mathbf{b}_n$. This proves that the normalized reduced trace $f_{V_N^x}(q)^{-\omega(\beta_K)}\widetilde{\mathrm{Tr}}^q_{V_N^x}(\beta_K)$ converges absolutely for all positive braids $\beta_K$ to a series in $x^{-1}$ with coefficients, Laurent polynomials[5] in $q$.

Consider the properties of this series. In particular, observe that when we specialise $x = q^k$, we recover the quantum invariant $\mathcal{P}^N_k(K)$. This follows from the fact that under the specialisation $x = q^k$, our module $V_N^x|_{x=q^k}$ contains $V^q_{N,k}$ as the irreducible

[5] From studying simple examples, we expect this can be improved to coefficients being simply polynomials in $q$ with $q^{-1}$ not appearing.

| Knot | Braid | Torus Knot? |
|---|---|---|
| $3_1^r$ | $\sigma_1^3$ | $T(2,3)$ |
| $5_1^r$ | $\sigma_1^5$ | $T(2,5)$ |
| $7_1^r$ | $\sigma_1^7$ | $T(2,7)$ |
| $8_{19}$ | $\sigma_1^3\sigma_2\sigma_1^3\sigma_2$ | $T(3,4)$ |
| $9_1^r$ | $\sigma_1^9$ | $T(2,9)$ |
| $10_{124}$ | $\sigma_1^5\sigma_2\sigma_1^3\sigma_2$ | $T(3,5)$ |
| $10_{139}$ | $\sigma_1^4\sigma_2\sigma_1^3\sigma_2^2$ | No |
| $10_{152}$ | $\sigma_1^3\sigma_2^2\sigma_1^2\sigma_2^3$ | No |

Table 3.1: Positive Braid knots with 10 or fewer crossings. Data from [LM22].

component containing $V_{\mathbf{0}}$. As the open strand is coloured[6] $v_{\mathbf{0}}$ and we are dealing with a knot[7], the trace restricts to the trace over this submodule $V_{N,k}^q$ which exactly computes $\mathcal{P}_k^N(K)$.

As this is true for all $k$, it follows that $F_K^N(x,q) = f_N(x,q)^{-\omega(\beta_K)}\widetilde{\mathrm{Tr}}_{V_N^x}^q(\beta_K)$ is indeed an invariant of positive braid knots, which satisfies precisely the properties required by 3.1.3.

## 3.2 Positive Braid Knots

We now turn to computing this invariant for some positive braid knots. As can be seen in Table 3.1, there are 8 positive braid knots with 10 or fewer crossings. Of these, 6 are torus knots, 4 of which are $T(2,2p+1)$ torus knots.

Conjecture 2.4.10 has been verified to a different extent for each of these knots, as we will discuss in Chapter 4. For $T(2,2p+1)$ torus knots, Theorem 4.1.3 gives $F_K(x,a,q)$ in full generality. For more general torus knots, $F_K(x,a,q)$ is not generally known (Except for $T(3,4)$) but it is possible to compute $F_K(x,q^N,q)$ for any $N \in \mathbb{N}$ via surgeries on plumbings [Par20a]. Finally, for non torus positive braid knots, only $F_K(x,q) = F_K(x,q^2,q)$ is known [Par20b].

Thus, we first compute $F_K$ for a couple of torus knots as a cross-check before focusing on $10_{139}$ and $10_{152}$.

### Torus Knots

We start with 3 torus knots, the trefoil, cinquefoil and $8_{19}$ knot. In the first two cases, the general $a$ deformed expression appears in Theorem 4.1.3 case, and a prediction

[6] A similar but more complicated argument still works if we had coloured the open strand by a different element.

[7] It should be possible to extend this argument to work for positive braid links as well.

for $F_{8_{19}}(x, a, q)$ was given in [EGGKPSS22]. As well as cross-checking, this gives us an opportunity to discuss how to efficiently perform these calculations. The main step is producing a labelled braid diagram[8] as in Figure 3.3. To produce this diagram for a knot $K$, start with a braid whose closure is $K$. Give matching labels to corresponding left/right outgoing strands with the top stand labelled[9] $\mathbf{0}$.

Next, at each crossing, ensure that the sum of incoming and outgoing labels are equal and that the label on the overstrand decreases. In particular, this means that if the upper incoming/outgoing strand is labelled $\mathbf{0}$, the diagonally opposite strand must also be labelled $\mathbf{0}$. For simple knots such as the $3_1$ knot, this fixes all labels based off the external labels, but in general this will introduce internal labellings which we need to sum over.

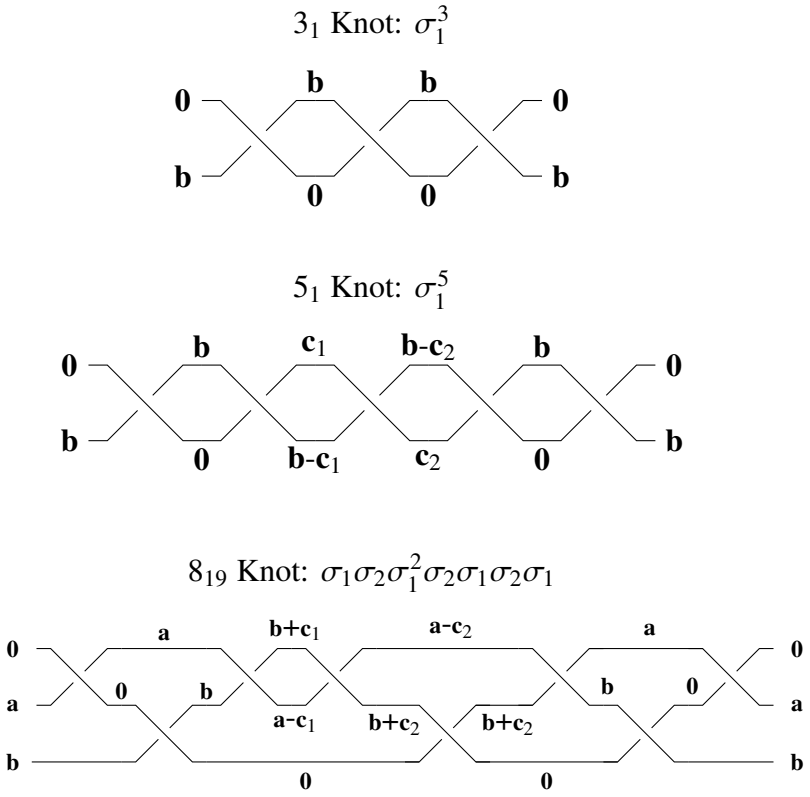


Figure 3.3: Labelled braid diagrams for the trefoil ($3_1$) and cinquefoil ($5_1$) and $8_{19}$ knots.

Finally, we apply the quantum trace, reading the $R$-matrix elements directly off the

[8] While usually these diagrams are drawn top to bottom, note we have drawn them left to right here.

[9] In principle the top strand can carry any label as the choice of label will not affect the final answer, but $\mathbf{0}$ is by far the simplest for computations.

diagram to get

$$\sum_{\mathbf{a}_1,\cdots,\mathbf{a}_n,\mathbf{c}_1,\cdots\mathbf{c}_m} \prod_{i=1}^{n} x^{\frac{N-1}{2}} q^{-|\mathbf{a}_i|} \prod_{\alpha\in\text{crossings}} {}_{\mathfrak{sl}_N} R^{\mathbf{i}'_\alpha,\mathbf{j}'_\alpha}_{\mathbf{i}_\alpha,\mathbf{j}_\alpha}. \tag{3.2.1}$$

This will give a series in $x^{-1}$ so, as a final step, we apply Weyl symmetry sending $x^{-1} \longrightarrow q^N x$ to get a series in $x$.

Let's start by applying this to the right-handed trefoil, for which it is possible to use the $R$-matrix approach for generic $N$. Following the labelled braid diagram in Figure 3.3 the $R$-matrices we need are (Ignoring prefactors)

$$R^{\mathbf{b},\mathbf{0}}_{\mathbf{0},\mathbf{b}} = x^{\frac{-b_1}{2}}, \qquad R^{\mathbf{b},\mathbf{0}}_{\mathbf{b},\mathbf{0}} = (-1)^{b_1} q^{\frac{b_1^2-b_1}{2}} x^{-b_1} (x;q^{-1})_{b_1}, \qquad R^{\mathbf{0},\mathbf{b}}_{\mathbf{b},\mathbf{0}} = x^{\frac{-b_1}{2}}.$$

Taking the quantum trace we get the general formula:

$$F^{\mathfrak{sl}_N}_{3^r_1}(x,q) = x^{1-N} \sum_{\mathbf{b}} q^{-|\mathbf{b}|} (-1)^{b_1} q^{\frac{1}{2}(b_1-1)b_1} x^{-2b_1} (x;q^{-1})_{b_1}.$$

Apply Weyl symmetry to send $x^{-1} \longrightarrow q^N x$ and compute the sum over the $b_i$ variables for $i > 1$ to get:

$$F^{\mathfrak{sl}_N}_{3^r_1}(x,q) = q^{(\log_q(x)+N)(N-1)} \sum_{b_1=0}^{\infty} (-1)^{b_1} q^{\frac{(b_1+N+1)b_1}{2}} x^{2b_1} \frac{(q^{b_1+1})_{N-2} (q^{-N}x^{-1};q^{-1})_{b_1}}{(q)_{N-2}}.$$

While this is already an expression which will work for all integer $N$, it is not quite in the right form for an $a$ deformation due to where the $N$'s appear in the $q$-Pochhammers. We can fix this by observing that

$$\frac{(q^{b_1+1})_{N-2}}{(q)_{N-2}} = \frac{(q)_{N-2+b_1}}{(q)_{b_1}(q)_{N-2}} = \frac{(q^{N-1})_{b_1}}{(q)_{b_1}}$$

which allows us to produce an $a$ deformed series

$$F_{3^r_1}(x,a,q) = q^{(\log_q(x)+\log_q(a))(\log_q(a)-1)} \sum_{b_1=0}^{\infty} q^{b_1} x^{b_1} \frac{(aq^{-1})_{b_1} (ax,q)_{b_1}}{(q)_{b_1}}. \tag{3.2.2}$$

As we will show in Chapter 4, once we correct for the difference in orientation, this exactly agrees with the $F_{3^l_1}(x,a,q)$ expression from Theorem 4.1.3 giving a quantum group proof in for the $p = 1$ case. Specialising $a = q^2$, it also matches the computation for the $\mathfrak{sl}_2$ $F_K$ invariant for the trefoil computed in [GM21].

For more complicated knots, we can make progress only after specialising $N$. For the $5_1$ knot, Figure 3.3 shows

$$F^{\mathfrak{sl}_N}_{5^r_1}(x,q) = x^{2(1-N)} \sum_{\mathbf{b},\mathbf{c}_1,\mathbf{c}_2} q^{-|\mathbf{b}|} x^{-b_1} R^{\mathbf{c}_1,\mathbf{b}-\mathbf{c}_1}_{\mathbf{b},\mathbf{0}} R^{\mathbf{b}-\mathbf{c}_2,\mathbf{c}_2}_{\mathbf{c}_1,\mathbf{b}-\mathbf{c}_1} R^{\mathbf{0},\mathbf{b}}_{\mathbf{b}-\mathbf{c}_2,\mathbf{c}_2}$$

| | $F_{5_1^r}(x,q)$ |
|---|---|
| $\mathfrak{sl}_2$ | $1+qx-(-1+q)q^2x^2-(-1+q)q^3x^3-(-1+q)q^4x^4-q^5(-1+q+q^4)x^5-q^6(-1+q+q^4)x^6+q^7(1-q-q^4+q^7)x^7+q^8(1-q-q^4+q^7)x^8+O(x^9)$ |
| $\mathfrak{sl}_3$ | $1+q(1+q)x+(q^2+q^3-q^5)x^2-q^3(-1-q+q^3+q^4)x^3-q^4(-1-q+q^3+q^4)x^4-q^5(-1-q+q^3+q^4+q^8+q^9)x^5-q^6(-1-q+q^3+q^4+q^8+2q^9+q^{10})x^6+q^7(1+q-q^3-q^4-q^8-2q^9-2q^{10}+q^{12}+q^{13}+q^{14})x^7+q^8(1+q-q^3-q^4-q^8-2q^9-2q^{10}-q^{11}+q^{12}+2q^{13}+2q^{14}+q^{15})x^8+O(x^9)$ |
| $\mathfrak{sl}_4$ | $1+q(1+q+q^2)x+(q^2+q^3+2q^4-q^7)x^2+q^3(1+q+2q^2+q^3-2q^5-q^6-q^7)x^3+q^4(1+q+2q^2+q^3+q^4-2q^5-2q^6-2q^7)x^4-q^5(-1-q-2q^2-q^3-q^4+q^5+2q^6+3q^7+q^8-q^{10}+q^{12}+q^{13}+q^{14})x^5-q^6(-1-q-2q^2-q^3-q^4+q^5+q^6+3q^7+2q^8+q^9-q^{10}-q^{11}+q^{12}+2q^{13}+3q^{14}+2q^{15}+q^{16})x^6+q^7(1+q+2q^2+q^3+q^4-q^5-q^6-2q^7-2q^8-2q^9+q^{11}-2q^{13}-4q^{14}-4q^{15}-3q^{16}+q^{18}+2q^{19}+q^{20}+q^{21})x^7+q^8(1+q+2q^2+q^3+q^4-q^5-q^6-2q^7-q^8-2q^9-q^{10}-q^{13}-4q^{14}-5q^{15}-5q^{16}-2q^{17}+q^{18}+4q^{19}+4q^{20}+4q^{21}+2q^{22}+q^{23})x^8+O(x^9)$ |
| $\mathfrak{sl}_N$ | $\sum_{d1,d2} a^{2d_2}x^{d_1+3d_2}q^{d_1+d_2^2}\frac{(a^{-1}q,q^{-1})_{d_1+d_2}(ax,q)_{d_1+d_2}}{(q,q)_{d_1}(q,q)_{d_2}}$ |

Table 3.2: Computation of $F_{5_1^r}^N$ for small $N$. The $a$ deformation is given in Theorem 4.1.3 under orientation reversal.

There are 2 types of bounds on these summations. Internal bounds come from ensuring that labels are valid, whereas external bounds come from crossings and the requirement that the label decreases along the overstrand. Recall that a label $\mathbf{b}$ is valid if and only if $b_1 \geq b_2 \geq \cdots \geq b_{N-1} \geq 0$ for all $i$. In this case, the labels are $\mathbf{b}, \mathbf{c}_1, \mathbf{c}_2, \mathbf{b}-\mathbf{c}_1, \mathbf{b}-\mathbf{c}_2$ meaning that we need:

$$0 \leq b_{i+1} \leq b_i$$
$$0, b_{i+1}+c_{1,i}-b_i \leq c_{1,i+1} \leq c_{1,i}, b_{i+1}$$
$$0, b_{i+1}+c_{2,i}-b_i \leq c_{2,i+1} \leq c_{2,i}, b_{i+1}$$

In this case, the only external bound is $\mathbf{c}_1 \geq \mathbf{c}_2$. Using these bounds, we compute $F_{5_1^r}^{\mathfrak{sl}_N}$ for $N = 2, 3, 4$ with the result shown in Table 3.2 (dropping the prefactor and applying Weyl symmetry). It is certainly possible to compute $F_K^N$ for larger $N$ but becomes increasingly time-consuming as the number of summations is roughly quadratic in $N$.

We play a similar game for the $8_{19}$ knot. Note that there is a choice in the braid we use.

In particular, while the $8_{19}$ knot is usually represented as the closure of $\sigma_1^3\sigma_2\sigma_1^3\sigma_2$, we represent it as the closure of $\sigma_1\sigma_2\sigma_1^2\sigma_2\sigma_1\sigma_2\sigma_1$. Whilst the first is conceptually simpler and cleaner, the second more naturally lends itself to these computations as more crossings are fixed by $\mathbf{0}$ labels, so we end up with fewer internal summations. Figure 3.3 shows

$$F_{8_{19}}^{\mathfrak{sl}_N}(x,q) = x^{3(N-1)} \sum_{\mathbf{a},\mathbf{b},\mathbf{c}_1,\mathbf{c}_2} x^{-a_1-b_1} q^{-|\mathbf{a}|-|\mathbf{b}|} R_{\mathbf{a},\mathbf{b},}^{\mathbf{b}+\mathbf{c}_1,\mathbf{a}-\mathbf{c}_1} R_{\mathbf{b}+\mathbf{c}_1,\mathbf{a}-\mathbf{c}_1}^{\mathbf{b}+\mathbf{c}_2,\mathbf{a}-\mathbf{c}_2} R_{\mathbf{b}+\mathbf{c}_2,\mathbf{0}}^{\mathbf{b}+\mathbf{c}_2,\mathbf{0}} R_{\mathbf{b}+\mathbf{c}_2,\mathbf{a}-\mathbf{c}_2}^{\mathbf{a},\mathbf{b}}.$$

From here, similarly to the $5_1$ case, we compute $F_{8_{19}}^{\mathfrak{sl}_N}$ for $N = 2, 3, 4$ and results are shown in Table 3.3.

One immediate observation we can make is that, even though we are only looking at a few values of $N$, we can already make prediction as to what an $a$ deformation should look like, and we can check that these agree with the deformations presented in Theorem 4.1.3 and [EGGKPSS22].

### Non Torus Knots

Let us now consider a couple of positive braid non torus knots. Up to 10 crossing there are only 2 of these namely, $10_{139}$ and $10_{152}$ and labelled braid diagrams for them are shown in Figure 3.4. For each $N = 2, 3, 4$, we can compute $F_K^N$ as described above, and the results are given in Tables 3.4 and 3.5.

$10_{139}$ Knot: $\sigma_1\sigma_2^2\sigma_1^3\sigma_2\sigma_1\sigma_2\sigma_1$

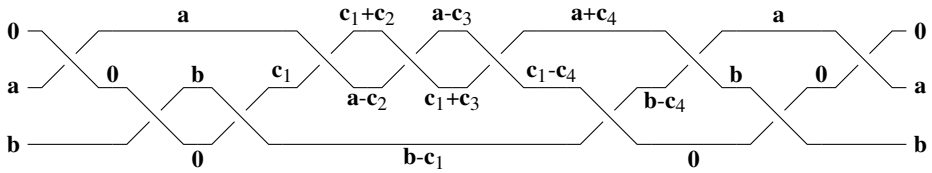


$10_{152}$ Knot: $\sigma_1\sigma_2^3\sigma_1^3\sigma_2^2\sigma_1$

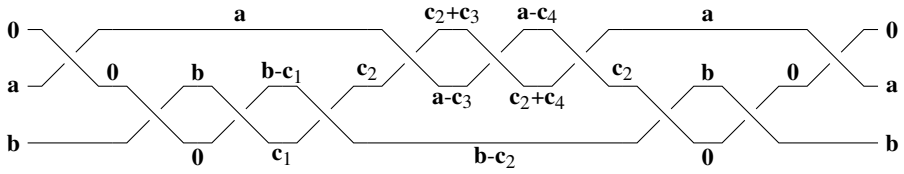


Figure 3.4: Labelled braid diagrams for the $10_{139}$ and $10_{152}$ knots.

We are interested in trying to predict the $a$ deformation from the computations at small $N$. Note that as stated so far this problem is inherently under determined as we

| | $F_{8_{19}}(x,q)$ |
|---|---|
| $\mathfrak{sl}_2$ | $1+qx+q^2x^2+(q^3-q^5)x^3-q^4(-1+q^2+q^3)x^4-q^5(-1+q^2+q^3)x^5-$ $q^6(-1+q^2+q^3)x^6+q^7(1-q^2-q^3+q^7)x^7+q^8(1-q^2-q^3+q^7)x^8+O(x^9)$ |
| $\mathfrak{sl}_3$ | $1+q(1+q)x+q^2(1+q+q^2)x^2-q^3(1+q)(-1-q^2+q^4)x^3-q^4(-1-q-$ $q^2-q^3+2q^5+2q^6+q^7)x^4-q^5(1+q)(-1-q^2+q^5+2q^6+q^7)x^5-q^6(1+$ $q)(-1-q^2+q^5+q^6+3q^7)x^6+q^7(1+q)^2(1-q+2q^2-2q^3+2q^4-3q^5+$ $2q^6-4q^7+2q^8-2q^9+2q^{10}-q^{11}+q^{12})x^7+q^8(1+q+q^2+q^3-q^5-$ $2q^6-3q^7-3q^8-3q^9-2q^{10}+q^{11}+2q^{12}+3q^{13}+2q^{14}+q^{15})x^8+O(x^9)$ |
| $\mathfrak{sl}_4$ | $1+q(1+q+q^2)x+q^2(1+q^2)(1+q+q^2)x^2-q^3(-1-q-2q^2-2q^3-2q^4-$ $q^5+q^7+q^8)x^3-q^4(1+q+q^2)(-1-q^2-q^3-q^4+q^7+q^8+q^9)x^4-q^5(1+q+$ $q^2)(-1-q^2-q^3-q^4-q^5+q^7+q^8+2q^9+2q^{10}+q^{11})x^5-q^6(-1-q-2q^2-$ $2q^3-3q^4-3q^5-3q^6-q^7+q^8+4q^9+6q^{10}+8q^{11}+7q^{12}+5q^{13}+2q^{14})x^6+$ $q^7(1+q+q^2)(1+q^2+q^3+q^4+q^5+q^6-q^8-2q^9-3q^{10}-4q^{11}-3q^{12}-2q^{13}-$ $q^{14}+q^{16}+q^{17}+q^{19})x^7+q^8(1+q+q^2)(1+q^2+q^3+q^4+q^5+q^6-2q^9-3q^{10}-$ $4q^{11}-4q^{12}-4q^{13}-2q^{14}-q^{15}+2q^{17}+2q^{18}+3q^{19}+q^{20}+q^{21})x^8+O(x^9)$ |
| $\mathfrak{sl}_N$ | $1+\dfrac{(q^{-1}a)_1}{(q)_1}qx+\dfrac{(q^{-1}a)_2}{(q)_2}q^2x^2+\left(\dfrac{(q^{-1}a)_3}{(q)_3}q^3-a^2\dfrac{(q^{-1}a)_1}{(q)_1}q\right)x^3$ $+\left(\dfrac{(q^{-1}a)_4}{(q)_4}q^4-a^2\dfrac{1-q^2}{1-q}\dfrac{(q^{-1}a)_2}{(q)_2}q^2\right)x^4$ $+\left(\dfrac{(q^{-1}a)_5}{(q)_5}q^5-a^2\dfrac{1-q^3}{1-q}\dfrac{(q^{-1}a)_3}{(q)_3}q^3+a^4\dfrac{(q^{-1}a)_1}{(q)_1}q\right)x^5$ $+\left(\dfrac{(q^{-1}a)_6}{(q)_6}q^6-a^2\dfrac{1-q^4}{1-q}\dfrac{(q^{-1}a)_4}{(q)_4}q^4\right.$ $\left.+a^4(1+2q)\dfrac{(q^{-1}a)_2}{(q)_2}q^2-a^5\dfrac{(q^{-1}a)_1}{(q)_1}q\right)x^6$ $+\left(\dfrac{(q^{-1}a)_7}{(q)_7}q^7-a^2\dfrac{1-q^5}{1-q}\dfrac{(q^{-1}a)_5}{(q)_5}q^5\right.$ $\left.+a^4(1+2q+2q^2+q^3)\dfrac{(q^{-1}a)_3}{(q)_3}q^3-a^5(1+q)\dfrac{(q^{-1}a)_2}{(q)_2}q^2\right)x^7$ |

Table 3.3: Computation of $F^N_{8_{19}}$ for small $N$. The guess for the $a$ deformation is written suggestively to show the structure present.

only know the solution for $N = 0, \cdots, 4$ and so any guess can always be modified by a term containing $(a^{-1})_5$ (or similar expressions) which are exactly 0 in these cases. However, we do have one extra constraint, namely the $a = q^N, q \to 1$ limit for each $N$ upon which the series should collapse to $\frac{1}{\Delta_K(X)^{N-1}}$. Additionally, making use of the knots-quivers correspondence [KRSS17, KRSS19, Kuc20] mentioned earlier, we can provide a useful ansatz (2.4.19) for this $a$ deformation. In practice, instead of using Equation (2.4.19), a more useful ansatz seems to be (Ignoring the prefactor for a moment)

$$\sum_{\mathbf{d}} (-q)^{\frac{1}{2}\mathbf{d}M\mathbf{d}^T} q^{\mathbf{q}\cdot\mathbf{d}} a^{\mathbf{a}\cdot\mathbf{d}} x^{\mathbf{x}\cdot\mathbf{d}} \frac{(q^{-1}a;q)_{\mathbf{d}}}{(q;q)_{\mathbf{d}}}$$

This is essentially equivalent to Equation (2.4.19) but hard-codes the $a = q$ specialisation as $F_K(x, q, q) = 1$ as well as making it clear that the $a = q^N, q \to 1$ limit is well-defined. As we can see in Tables 3.3, 3.4, 3.5 this simple ansatz does an excellent job of allowing us to guess the $a$ deformations of the first couple of terms. We can check that the $a$ deformation of $8_{19}$ is correct, and we conjecture that the $a$ deformations for the $10_{139}, 10_{152}$ will also yield the correct series. Unfortunately, it is difficult to pass from these initial terms to a full quiver form, so we only have these $a$ deformations perturbatively. As we will see in section 4.4.3, it is in principle possible to produce quiver forms for fixed $N$ but these end up being too large to be particularly useful.

### 3.2.1 Stratified State Sum

A natural question to ask is what happens if we try to apply this technology to other knots. While in general this state sum will not converge, in certain cases can get conditional convergence by stratifying the summation [Par20b].

Observe that the induced braid group representation on $(V_N^x)^{\otimes(n+1)}$ is not irreducible. In particular, if we define the total weight of a set of states as the sum of the labels $\mathbf{w} = \mathbf{b}_0 + \mathbf{b}_1 + \cdots + \mathbf{b}_n$, we immediately observe that $\mathbf{w}$ is fixed by the action of the $R$, $R^{-1}$-matrices. Hence, letting $V_{\mathbf{w}}^{\otimes(n+1)}$ denote the subspace of total weight $\mathbf{w}$ we can stratify by total weight, yielding

$$\widetilde{\mathrm{Tr}}^{q,x}_{V^{\otimes(n+1)}}(\beta) = \lim_{\eta\to 1} \sum_{\mathbf{w}} \eta^{|\mathbf{w}|} \widetilde{\mathrm{Tr}}^{q}_{V_{\mathbf{w}}^{\otimes n}}(\beta).$$

When this converges we conjecture that it produces the correct $F_K$ invariant. Two examples of this are the $m(5_2)$ and $m(7_3)$ knots. For both of these knots, the Alexander polynomial is not monic which means that we should expect each coefficient in $x$ to

| | $F_{10_{139}}(x,q)$ |
|---|---|
| $\mathfrak{sl}_2$ | $1+qx+q^2x^2-q^3(-1+2q^2)x^3+(-1+q)q^4(-1-q+q^2)x^4-q^5(-1+2q^2-q^3+q^4)x^5+q^6(1-2q^2+q^3-q^4+2q^5+q^6)x^6-q^7(-1+2q^2-q^3+q^4-2q^5+q^6+2q^7)x^7+q^8(1-2q^2+q^3-q^4+2q^5-q^6-2q^7+3q^8+q^9)x^8+O(x^9)$ |
| $\mathfrak{sl}_3$ | $1+q(1+q)x+q^2(1+q+q^2)x^2-(-1+q)q^3(1+q)^2(1+2q^2)x^3+q^4(1+q+q^2+q^3-q^4-4q^5-q^6+q^7)x^4-q^5(1+q)^2(-1+q-2q^2+2q^3-q^4+3q^5-2q^6+q^7)x^5+q^6(1+q+q^2+q^3-q^4-3q^5-2q^6-2q^7-q^8+2q^9+2q^{10}+3q^{11}+q^{12})x^6-q^7(1+q)(-1-q^2+q^4+2q^5+q^7+2q^8-3q^9-2q^{10}-q^{11}+q^{12}+2q^{13})x^7+q^8(1+q)(1+q^2-q^4-2q^5-q^7-q^8+4q^{10}+2q^{11}-2q^{12}-q^{13}-q^{14}+3q^{15}+q^{16})x^8+O(x^9)$ |
| $\mathfrak{sl}_4$ | $1+q(1+q+q^2)x+q^2(1+q^2)(1+q+q^2)x^2-q^3(1+q)(-1-2q^2-2q^4+q^5+2q^7)x^3+(-1+q)q^4(1+q)(1+q+q^2)(-1-2q^2-q^3-3q^4-q^5-2q^6+q^7)x^4-q^5(1+q+q^2)(-1-q^2-q^3-q^4-q^5+q^6+2q^7+3q^8+q^9+q^{10}-q^{11}+q^{12})x^5+q^6(1+q^2)(1+q+q^2+q^3+2q^4+2q^5-3q^7-5q^8-4q^9-3q^{10}-q^{11}-q^{12}+2q^{13}+2q^{14}+3q^{15}+q^{16})x^6-q^7(1+q+q^2)(-1-q^2-q^3-q^4-q^5+q^7+3q^8+2q^9+4q^{10}+2q^{11}+2q^{12}-2q^{13}-q^{14}-6q^{15}-q^{16}-q^{17}+q^{18}+2q^{19})x^7+q^8(1+q+q^2)(1+q^2+q^3+q^4+q^5-q^7-2q^8-2q^9-4q^{10}-3q^{11}-4q^{12}+q^{13}+q^{14}+7q^{15}+3q^{16}+5q^{17}-2q^{18}-2q^{19}-q^{21}+3q^{22}+q^{23})x^8+O(x^9)$ |
| $\mathfrak{sl}_N$ | $1+\frac{(q^{-1}a)_1}{(q)_1}qx+\frac{(q^{-1}a)_2}{(q)_2}q^2x^2+\left(\frac{(q^{-1}a)_3}{(q)_3}q^3-2a^2\frac{(q^{-1}a)_1}{(q)_1}q\right)x^3$ $+\left(\frac{(q^{-1}a)_4}{(q)_4}q^4-2a^2\frac{1-q^2}{1-q}\frac{(q^{-1}a)_2}{(q)_2}q^2+3a^3\frac{(q^{-1}a)_1}{(q)_1}q\right)x^4$ $+\left(\frac{(q^{-1}a)_5}{(q)_5}q^5-2a^2\frac{1-q^3}{1-q}\frac{(q^{-1}a)_3}{(q)_3}q^3+3a^3\frac{1-q^2}{1-q}\frac{(q^{-1}a)_2}{(q)_2}q^2-2a^4\frac{(q^{-1}a)_1}{(q)_1}q\right)x^5$ $+\left(\frac{(q^{-1}a)_6}{(q)_6}q^6-2a^2\frac{1-q^4}{1-q}\frac{(q^{-1}a)_4}{(q)_4}q^4+3a^3\frac{1-q^3}{1-q}\frac{(q^{-1}a)_3}{(q)_3}q^2-a^4(2-q-q^2)\frac{(q^{-1}a)_1}{(q)_1}q\right)x^6+O(x^7)$ |

Table 3.4: $F_K^N$ invariant for the $10_{139}$ knot with lie algebra $\mathfrak{sl}_N$ for small $N$.

| | $F_{10_{152}}(x,q)$ |
|---|---|
| $\mathfrak{sl}_2$ | $1+qx+q^2(1+q)x^2-q^3(-1-q+3q^2)x^3+q^4(1+q-2q^2+2q^3)x^4-q^5(-1-q+2q^2+5q^4+q^5)x^5+q^6(1+q-2q^2+q^3-4q^4+6q^5+4q^6)x^6-q^7(-1-q+2q^2-q^3+6q^4-4q^5+5q^6+9q^7+3q^8)x^7+q^8(1+q-2q^2+q^3-5q^4+5q^5-q^6+15q^8+11q^9+3q^{10})x^8+O(x^9)$ |
| $\mathfrak{sl}_3$ | $1+q(1+q)x+q^2(1+q+2q^2+q^3)x^2-q^3(1+q)(-1-2q^2-q^3+3q^4)x^3+q^4(1+q+2q^2+3q^3+q^4-4q^5+2q^7)x^4-q^5(1+q)(-1-2q^2-q^3+q^5+2q^6+q^7+5q^8+q^9)x^5+q^6(1+q+2q^2+3q^3+q^4-q^5+q^6-5q^7-9q^8-2q^9+5q^{10}+10q^{11}+4q^{12})x^6-q^7(1+q)(-1-2q^2-q^3+q^5-2q^6+3q^7+10q^8-q^9-q^{10}-q^{11}+8q^{12}+9q^{13}+3q^{14})x^7+q^8(1+q+2q^2+3q^3+q^4-q^5+q^6-q^7-8q^8-12q^9-3q^{10}+5q^{11}-q^{12}-3q^{13}+9q^{14}+26q^{15}+29q^{16}+14q^{17}+3q^{18})x^8+O(x^9)$ |
| $\mathfrak{sl}_4$ | $1+q(1+q+q^2)x+q^2(1+q+q^2)(1+q^2+q^3)x^2+q^3(1+q+2q^2+3q^3+4q^4+4q^5-2q^7-3q^8)x^3+q^4(1+q+q^2)(1+q^2+2q^3+2q^4+2q^5-2q^7-2q^8+2q^9)x^4-q^5(1+q+q^2)(-1-q^2-2q^3-2q^4-3q^5-q^6+2q^8+q^9+3q^{10}+q^{11}+5q^{12}+q^{13})x^5+q^6(1+q+2q^2+3q^3+5q^4+7q^5+7q^6+6q^7+3q^8+q^9-5q^{10}-9q^{11}-17q^{12}-12q^{13}-9q^{14}+7q^{15}+9q^{16}+10q^{17}+4q^{18})x^6-q^7(1+q+q^2)(-1-q^2-2q^3-2q^4-3q^5-2q^6-2q^7-q^8-2q^9+4q^{10}+5q^{11}+12q^{12}+5q^{13}+7q^{14}-8q^{15}+2q^{16}+2q^{17}+8q^{18}+9q^{19}+3q^{20})x^7+q^8(1+q+q^2)(1+q^2+2q^3+2q^4+3q^5+2q^6+2q^7+2q^8+3q^9-2q^{10}-4q^{11}-12q^{12}-8q^{13}-12q^{14}+2q^{15}-4q^{16}+4q^{17}-6q^{18}-2q^{19}+9q^{20}+11q^{21}+18q^{22}+11q^{23}+3q^{24})x^8+O(x^9)$ |
| $\mathfrak{sl}_N$ | $1+\frac{(q^{-1}a)_1}{(q)_1}qx+\left(\frac{(q^{-1}a)_2}{(q)_2}q^2+a\frac{(q^{-1}a)_1}{(q)_1}q\right)x^2$ $+\left(\frac{(q^{-1}a)_3}{(q)_3}q^3+a\frac{1-q^2}{1-q}\frac{(q^{-1}a)_2}{(q)_2}q^2-4a^2\frac{(q^{-1}a)_1}{(q)_1}q\right)x^3$ $+\left(\frac{(q^{-1}a)_4}{(q)_4}q^4+a\frac{1-q^3}{1-q}\frac{(q^{-1}a)_3}{(q)_3}q^3 -a^2(3+4q)\frac{(q^{-1}a)_2}{(q)_2}q^2+5a^3\frac{(q^{-1}a)_1}{(q)_1}q\right)x^4$ $+\left(\frac{(q^{-1}a)_5}{(q)_5}q^5+a\frac{1-q^4}{1-q}\frac{(q^{-1}a)_4}{(q)_4}q^4-3a^2\frac{1-q^3}{1-q}\frac{(q^{-1}a)_3}{(q)_3}q^3 +a^3(2+q-q^2)\frac{(q^{-1}a)_2}{(q)_2}q^2-4a^4\frac{(q^{-1}a)_1}{(q)_1}q\right)x^5+O(x^6)$ |

Table 3.5: $F_K$ invariant for the $10_{152}$ knot and symmetric series of representations on $\mathfrak{sl}_N$ for small $N$.

itself be a power series in $q$. Writing $F_N^K$ in a general form

$$F_K^N(x,q) = x^{\frac{(N-1)}{2}(\#Tr\,+\,\#R^{-1}\,-\,\#R)} \sum_{x=0}^{\infty} f_k^N(n;q)x^n,$$

where $\#Tr$ is the number of strands we are tracing over and $R^{\pm}$ is the number of $\pm$ crossings which appear in the braid. We can use the labelled braid diagrams in Figure 3.5 to compute:

$$\begin{aligned}
f^3_{m(5_2)}(0;q) &= 1 - q - q^2 + q^3 + q^4 + q^5 - q^6 - q^7 - q^8 - q^9 + q^{10} + q^{11} + O(q^{12}) \\
f^3_{m(5_2)}(1;q) &= 2q - 4q^3 - q^4 + 3q^5 + 5q^6 + 2q^7 - 2q^8 - 4q^9 - 6q^{10} + O(q^{11}) \\
f^3_{m(5_2)}(2;q) &= 3q^2 + q^3 - 5q^4 - 7q^5 + q^6 + 11q^7 + 11q^8 + 5q^9 - 6q^{10} + O(q^{11})
\end{aligned}$$

and

$$\begin{aligned}
f^3_{m(7_3)}(0;q) &= 1 - q - q^2 + q^3 + q^4 + q^5 - q^6 - q^7 - q^8 - q^9 + q^{10} + q^{11} + O(q^{12}) \\
f^3_{m(7_3)}(1;q) &= 2q - q^2 - 3q^3 + 3q^5 + 4q^6 - 2q^8 - 4q^9 - 4q^{10} - q^{11} + O(q^{12}) \\
f^3_{m(7_3)}(2;q) &= -q + 4q^2 - 5q^4 - 4q^5 + 2q^6 + 9q^7 + 5q^8 + 2q^9 - 6q^{10} + O(q^{11}).
\end{aligned}$$

Further terms can be easily computed via recursion on the quantum A-polynomial as described in Section 4.2 with the terms here giving the initial conditions. In the $m(5_2)$ case, we can cross-check this with the quiver form for $F_{m(5_2)}(x,a,q)$ given in [EGGKPSS22]. With a little effort[10] we simplify the form yielding the infinite sum expressions:

$$\begin{aligned}
f_{m(5_2)}(0;a,q) &= \sum_{d=0}^{\infty} (-1)^d q^{\frac{d(d+1)}{2}} \frac{(aq^{-1},q)_d}{(q,q)_d} \\
f_{m(5_2)}(1;a,q) &= \sum_{d=0}^{\infty} (-1)^d q^{\frac{d(d+1)}{2}} \frac{\left(q(2-q^{-d})(aq^{-1},q)_d - a(1+aq^d)(a,q)_d\right)}{(q,q)_1(q,q)_d}.
\end{aligned}$$

It is an easy check that when $a = q$, $f_{5_2}(0;a=q,q) = 1$ and $f_{5_2}(1;a=q,q) = 0$. Similarly, specialising $a = q^2$ yields the expressions in [Par20b] and $a = q^3$ yields the expressions above.

[10] We take the quiver form, consider all terms contributing to a particular power of $x$ and apply the following identity:

$$\sum_{d1,d2=0}^{\infty} \frac{\left(-q^{\frac{1}{2}}\right)^{d1^2+2d1d2+2d2^2} b^{d1}a^{d2}q^{\frac{d1}{2}}}{(q,q)_{d1}(q,q)_{d2}} = \sum_{d=0}^{\infty} (-1)^d q^{\frac{d(d+1)}{2}} b^d \frac{(ab^{-1},q)_d}{(q,q)_d}.$$

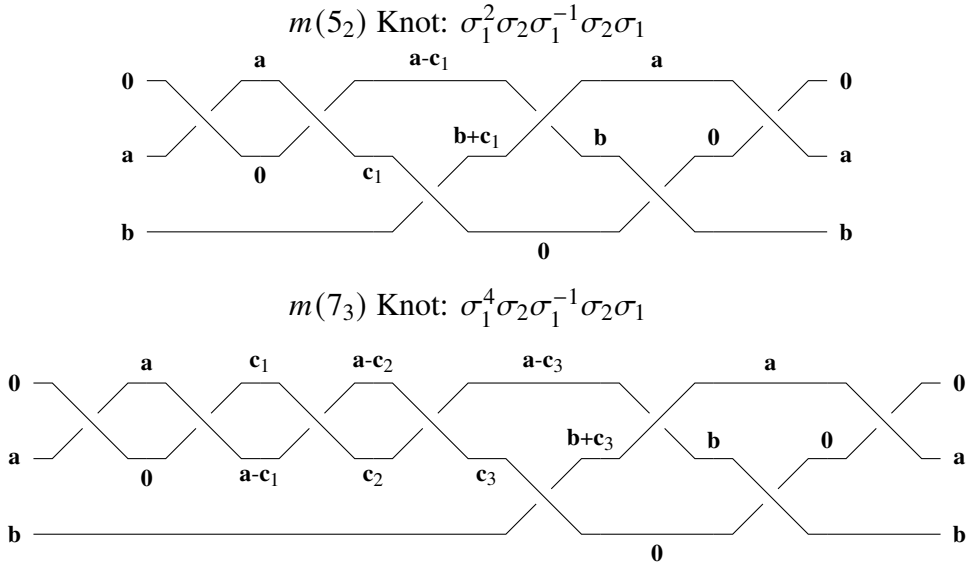


Figure 3.5: Labelled braid diagrams for the $m(5_2)$ and $m(7_3)$ knots.

In general, the stratified state sum will converge provided that, for each incoming state $\mathbf{b}_i$, either[11] the minimal $x^{-1}$ or $q$ power strictly increases as $\mathbf{b}_i$ increases. It would be nice to have an easy way to check this in a labelled braid diagram, but currently we can only easily check the behaviour of the $x$ power.

### 3.3 The Inverted State Sum Technique

In cases where the stratified state sum does not converge, there is one final technique we can try to apply. This technique, called the inverted state sum, was recently introduced in [Par21] for the $\mathfrak{sl}_2$ case and extended the $R$-matrix computations to signed braid links. We take a very computational approach here as the proof in [Par21] does not currently extend to $\mathfrak{sl}_N$ but we conjecture that the method still works.

The basic observation is that many $q$-Hypergeometric identities remain true if you invert the direction of the sum. The simplest example of this phenomenon is

$$\sum_{n=0}^{\infty} q^n = \frac{1}{1-q} = -\frac{1}{q}\frac{1}{1-\frac{1}{q}} = -\sum_{n<0} q^n.$$

This example can be easily generalized to

$$\sum_{n=0}^{\infty} \frac{(q^{n+m}, q^{-1})_m}{(q;q)_m} x^n = \frac{1}{(x;q)_{m+1}}$$

[11] If both the minimal $x^{-1}$ and $q$ powers strictly increase as $\mathbf{b}_i$ increase then the sum converges absolutely.

$$
\begin{aligned}
&= \frac{(-1)^{m+1}}{x^{m+1}q^{\frac{m(m+1)}{2}}} \frac{1}{(x^{-1};q^{-1})_{m+1}} \\
&= \frac{(-1)^{m+1}}{x^{m+1}q^{\frac{m(m+1)}{2}}} \sum_{n=0}^{\infty} \frac{(q^{-n-m},q)_m}{(q^{-1};q^{-1})_m} x^{-n} \\
&= -\sum_{n=0}^{\infty} \frac{(q^{-n-1},q^{-1})_m}{(q;q)_m} x^{-n-m-1} \\
&= -\sum_{n<-m} \frac{(q^{n+m},q^{-1})_m}{(q;q)_m} x^{n}.
\end{aligned}
$$

While the sum is $< -m$, it can be trivially extended to $< 0$ as the expression is exactly 0 for $0 > n \geq -m$. Additionally, note that the initial equality is more commonly written as

$$\sum_{n=0}^{\infty} \frac{(q;q)_{m+n}}{(q;q)_n (q;q)_m} x^n = \frac{1}{(x;q)_{m+1}}.$$

But in this form the left-hand side is not well-defined when $n < 0$.

The inverted state sum can be thought of as another example of this phenomenon. Given a knot $K$ with a chosen $n+1$ strand braid diagram recall, as in Equation 3.2.1, that we have a formal expansion:

$$\sum_{\substack{\mathbf{a}_1,\cdots,\mathbf{a}_n \\ \mathbf{c}_1,\cdots\mathbf{c}_m}} \prod_{i=1}^{m} x^{\frac{N-1}{2}} q^{-|\mathbf{a}_i|} \prod_{\alpha\in\text{crossings}} {}_{\mathfrak{sl}_N} R^{e_\alpha}{}_{\mathbf{i}_\alpha,\mathbf{j}_\alpha}^{\mathbf{i}'_\alpha,\mathbf{j}'_\alpha}.$$

The idea is, as above, to invert some of these summations, choosing 2 subsets $P \subset \{1,\cdots,n\}$ and $Q \subset \{1,\cdots,m\}$, and computing:

$$(-1)^{|P|+|Q|} \sum_{\substack{-\mathbf{a}_i, i\in P \\ -\mathbf{c}_j, j\in Q}} \sum_{\substack{\mathbf{a}_i, i\notin P \\ \mathbf{c}_j, j\notin Q}} \prod_{i=1}^{m} x^{\pm\frac{N-1}{2}} q^{\pm|\mathbf{a}_i|} \prod_{\alpha\in\text{crossings}} {}_{\mathfrak{sl}_N} R^{e_\alpha}{}_{\mathbf{i}_\alpha,\mathbf{j}_\alpha}^{\mathbf{i}'_\alpha,\mathbf{j}'_\alpha}.$$

Here the $\pm$ in the $q$ power is $+$ if $i \in P$ and $-$ otherwise. Additionally, a negative state $-\mathbf{a}$ is a sequence of integers $0 < a_n < \cdots < a_1$. Note that we use $<$ and not $\leq$. This is a reflection of our choice of basis, and in the quantum polynomial representation corresponds to summing over monomials with strictly negative powers. Computationally, what is going on is that when $\mathbf{b}, \mathbf{b}'$ are negative[12], we can still make sense of the ${}_{\mathfrak{sl}_N} R^{-1}{}_{\mathbf{a},\mathbf{b}}^{\mathbf{a}',\mathbf{b}'}$ matrix elements and this will give a series in $x^{-1}$. Thus, if we can give 'inverted' $\mathbf{b}$ inputs to all $R^{-1}$-matrices, the state sum will converge. The surprising result proven in [Par21] is that, if the state sum converges absolutely, then the result is precisely the $F_K$ invariant that we are looking for.

[12] The method in [Par21] is slightly more general than this, but we ignore this here.

### 3.3.1 The $R^{-1}$-Matrix for Inverted States

Let's study how to interpret the $R^{-1}$-matrix for negative states. For simplicity, we focus on $\mathfrak{sl}_{2,3}$ but this method extends to all $N$. Starting with $\mathfrak{sl}_2$, each state $|\mathbf{a}\rangle$ is defined by a single number $a \geq 0$ and so the $R^{-1}$-matrix elements coming from Equation (3.1.2) specialise to

$$ {}_{\mathfrak{sl}_2}R^{-1}{}^{\mathbf{a}',\mathbf{b}'}_{\mathbf{a},\mathbf{b}} = (-1)^{b+a'} q^{\frac{b}{2}+\frac{a^2}{2}-aa'-\frac{a'}{2}-\frac{(b')^2}{2}} x^{\frac{1}{2}(b+b')} \frac{(q^{-b};q)_{b-a'}(x^{-1}q^a;q)_{b-a'}}{(q^{-1};q^{-1})_{b-a'}}. $$

In comparison to the generic case, note that the summation over $r$ disappears[13] as the only non 0 term occurs at $r = a - b'$. Additionally, we have used the equality $(xq^b;q)_r = (-1)^r x^r q^{rb} q^{\frac{r(r-1)}{2}} (x^{-1}q^{-b};q^{-1})_r$. Next, observe that

$$ \frac{(q^{-b};q)_{b-a'}}{(q^{-1};q^{-1})_{b-a'}} = \frac{(q^{-1},q^{-1})_b}{(q^{-1};q^{-1})_{b-a'}(q^{-1};q^{-1})_{a'}} = \frac{(q^{-b};q)_{a'}}{(q^{-1};q^{-1})_{a'}}. $$

The beauty of this equality is that while all terms are equal for the usual $b > a' > 0$ situation, if $a' > 0 > b$ the right-hand side still makes sense and similarly if $0 > b > a$ then we can use the left-hand side. Mostly we will be concerned with the former situation and so use the $R^{-1}$-matrix

$$ (-1)^{b+a'} q^{\frac{b'}{2}+\frac{a^2}{2}-aa'-\frac{a}{2}-\frac{(b')^2}{2}} x^{\frac{1}{2}(b+b')} \frac{(q^{-b};q)_{a'}(x^{-1}q^a;q)_{b-a'}}{(q^{-1};q^{-1})_{a'}} $$

The point, as mentioned earlier, is that if $b, b'$ are less than 0, this matrix element remains well-defined and produces a series in $x^{-1}$.

We take a similar approach for $\mathfrak{sl}_3$. In this case, each state $|\mathbf{a}\rangle$ is defined by a pair of numbers $a_1 \geq a_2 \geq 0$ and so we get:

$$ \begin{aligned} {}_{\mathfrak{sl}_3}R^{-1}{}^{\mathbf{a}',\mathbf{b}'}_{\mathbf{a},\mathbf{b}} &= \sum_{r\geq 0} (-1)^{b_1+a_1'+b_2+a_2'+r} q^{-C_3(r)} x^{\frac{1}{2}(b_1+b_1')} (x^{-1}q^{a_1};q)_{b_1-a_1'} \\ &\quad \times \frac{(q^{-b_2};q)_{a_2'+r}(q^{a_2-a_1};q)_{b_2-a_2'-r}(q^{a_2'-b_1+r};q)_{a_1'-a_2'}}{(q^{-1};q^{-1})_{a_1'-a_2'}(q^{-1};q^{-1})_{a_2'}(q^{-1};q^{-1})_r} \\ C_3(r) &= \frac{1}{4}\big(2(b_1^2+b_2^2+{a_1'}^2+{a_2'}^2+r^2) + (2+4r-4b_1-a_2-b_2)a_1' + 2r \\ &\quad + (2+a_1+b_1-4b_2)a_2' + (4a_1-2-a_2)b_1 - (2+3a_1-4a_2+4r)b_2\big) \end{aligned} $$

Note that as mentioned previously, the summand is 0 unless

$$ 0, a_2+b_2-a_1-a_2' \leq r \leq b_1-a_1', b_2-a_2'. $$

[13] In general the ${}_{\mathfrak{sl}_N}R^{\mathbf{a}_2,\mathbf{b}_2}_{\mathbf{a}_1,\mathbf{b}_1}$ matrix element will be a sum over $\frac{(N-1)(N-2)}{2}$ $r$ variables.

and so once we specialise **a** and **b** this is a finite sum. Our work has essentially been done for us already, as these expressions already produce sensible answers for $0 < b_2 < b_1$.

This method is very robust and continues to work for higher $\mathfrak{sl}_N$. It can also be combined with the stratified state sum method to produce predictions for far more knots. The downside is that it is more computationally expensive, particularly for large $N$, hence why we only present computations in the $N = 2, 3$ cases here.

### 3.3.2 Homogeneous braid knots

A homogeneous braid is a braid such that for every $i$, either $\sigma_i$ or $\sigma_i^{-1}$ appears, but never both. These are exactly the braids for which the inverted state sum technique works most easily.

The simplest knots which have homogeneous braid representatives are the $4_1, 6_2$ and $6_3$ knots. Labelled braid diagrams for these knots are in Figure 3.6 and the corresponding $F_N^K$ are given in Tables 3.6, 3.7 and 3.8. The $N = 2$ results previously appeared in [Par21] but we give them here both for a consistency check[14] and to give hints towards possible $a$ deformations.

It can be easily checked that the expressions in Table 3.6 match the $a = q^2, q^3$ specialisations of the $F_{4_1}(x, a, q)$ given in Equation (4.2.13). Similarly, the $\mathfrak{sl}_2$ rows in Tables 3.7, 3.8 match the computations in [Par21]. The $6_2, 6_3$ examples are also interesting as they are the smallest knots (along with $6_1$ where the $a$ deformation is still unknown[15]. Thus, these $\mathfrak{sl}_3$ examples can serve as an important cross-check for future work in that direction. Unfortunately, there is not enough data here to provide a sensible guess for what the $a$ deformations might be.

[14] As usual, to compare these results we first need to align conventions.

[15] There was an $a$ deformation for the $6_2$ knot presented in [EGGKPSS22] but that was an error.

$4_1$ Knot: $\sigma_1\sigma_2^{-1}\sigma_1\sigma_2^{-1}$

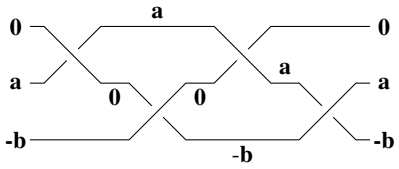


$6_2$ Knot: $\sigma_1^3\sigma_2^{-1}\sigma_1\sigma_2^{-1}$

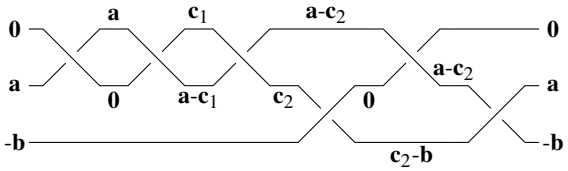


$6_3$ Knot: $\sigma_1^2\sigma_2^{-1}\sigma_1\sigma_2^{-2}$

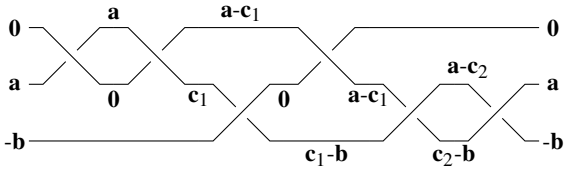


Figure 3.6: Labelled braid diagrams for the $4_1$ and $6_2$ and $6_3$ knots.

| | $F_{4_1}(x,q)$ |
|---|---|
| $\mathfrak{sl}_2$ | $1+3qx+q(1+6q+q^2)x^2+q(2+3q+11q^2+3q^3+2q^4)x^3+(1+3q+6q^2+8q^3+19q^4+8q^5+6q^6+3q^7+q^8)x^4+(2q^{-1}+2+7q+10q^2+16q^3+18q^4+34q^5+18q^6+16q^7+10q^8+7q^9+2q^{10}+2q^{11})x^5+O(x^6)$ |
| $\mathfrak{sl}_3$ | $1+3q(1+q)x+q(1+7q+9q^2+7q^3+q^4)x^2+q(2+5q+16q^2+22q^3+22q^4+16q^5+5q^6+2q^7)x^3+(1+4q+10q^2+18q^3+38q^4+51q^5+56q^6+51q^7+38q^8+18q^9+10q^{10}+4q^{11}+q^{12})x^4+(2q^{-1}+4+11q+21q^2+37q^3+57q^4+92q^5+119q^6+134q^7+134q^8+119q^9+92q^{10}+57q^{11}+37q^{12}+21q^{13}+11q^{14}+4q^{15}+2q^{16})x^5+O(x^6)$ |

Table 3.6: $F_K$ invariant for the $4_1$ knot. This can be matched against the specialisations of the $a$ deformed series given in Equation (4.2.13).

| | $F_{6_2}(x,q)$ |
|---|---|
| $\mathfrak{sl}_2$ | $1+3qx+(q+6q^2-q^3)x^2+q(2+3q+10q^2-3q^3)x^3+(1+3q+6q^2+6q^3+14q^4-6q^5+2q^7)x^4+(2q^{-1}+2+7q+9q^2+12q^3+8q^4+18q^5-10q^6+q^7+6q^8+2q^9)x^5+O(x^6)$ |
| $\mathfrak{sl}_3$ | $1+2q(1+2q)x+q(2+3q+8q^2+9q^3-q^4)x^2+2q(2+2q+6q^2+6q^3+9q^4+7q^5-2q^6)x^3+(3+6q+8q^2+22q^3+20q^4+35q^5+25q^6+29q^7+17q^8-9q^9+q^{10}+3q^{11})x^4+(6q^{-1}+6+14q+24q^2+36q^3+38q^4+66q^5+50q^6+67q^7+37q^8+38q^9+19q^{10}-13q^{11}+10q^{12}+11q^{13}+5q^{14})x^5+O(x^6)$ |

Table 3.7: $F_K$ invariant for the $6_2$ knot and symmetric series of representations on $\mathfrak{sl}_N$ for small $N$.

| | $F_{6_3}(x,q)$ |
|---|---|
| $\mathfrak{sl}_2$ | $1+3qx-q(1-6q+q^2)x^2-(-1+q)^2q(2+7q+2q^2)x^3-2q(1+3q+3q^2-8q^3+3q^4+3q^5+q^6)x^4+(2-2q-6q^2-12q^3-8q^4+25q^5-8q^6-12q^7-6q^8-2q^9+2q^{10})x^5+O(x^6)$ |
| $\mathfrak{sl}_3$ | $1+3q(1+q)x-q(1-5q-9q^2-5q^3+q^4)x^2-q(2+5q-4q^2-15q^3-15q^4-4q^5+5q^6+2q^7)x^3-q(2+8q+17q^2+6q^3-16q^4-26q^5-16q^6+6q^7+17q^8+8q^9+2q^{10})x^4+(2-6q^2-22q^3-43q^4-32q^5+4q^6+34q^7+34q^8+4q^9-32q^{10}-43q^{11}-22q^{12}-6q^{13}+2q^{15})x^5+O(x^6)$ |

Table 3.8: $F_K$ invariant for the $6_3$ knot and symmetric series of representations on $\mathfrak{sl}_N$ for small $N$.

*Chapter 4*

# A-DEFORMED $F_K$

While we have a method which allows us to compute $F_N^K$ for a large class of knots, finding an $a$ deformation from these computations is difficult at best. Thus, to investigate Conjecture 2.4.10 it is valuable to try out other possible methods.

One approach is to start with the general formula for symmetrically coloured HOMFLY-PT polynomials of a knot $K$ and try to manipulate the formula into a formula for the $a$ deformed $F_K$. This approach works well in the case of $(2, 2p+1)$ torus knots.

## 4.1 Explicit $F_K$ Formula for $(2, 2p+1)$ Torus Knots

We start with symmetrically coloured HOMFLY-PT polynomials given in [FGSS12]

$$P_k(T^{(2,2p+1)}; a, q) = \sum_{0\le j_p\le\ldots\le j_1\le j_0=k} a^{pk} q^{-pk} q^{(2k+1)(j_1+j_2+\ldots+j_p)-\sum_{i=1}^{p} j_{i-1}j_i} \times \frac{(q^k;q^{-1})_{j_1}(aq^{-1};q)_{j_1}}{(q;q)_{j_1}} \binom{j_1}{j_2}_q \cdots \binom{j_{p-1}}{j_p}_q, \tag{4.1.1}$$

Changing the summation to infinity, substituting $q^k = x$ and pulling out the prefactor leads to

$$x^{p(\frac{\log a}{\hbar}-1)} \sum_{0\le j_p\le\ldots\le j_1} x^{2(j_1+\ldots+j_p)-j_1} q^{(j_1+j_2+\ldots+j_p)-\sum_{i=2}^{p} j_{i-1}j_i} \times \frac{(aq^{-1};q)_{j_1}(x;q^{-1})_{j_1}}{(q;q)_{j_1}} \binom{j_1}{j_2}_q \cdots \binom{j_{p-1}}{j_p}_q. \tag{4.1.2}$$

We claim that this is precisely $F_K(x, a, q)$ for $K$ a $(2, 2p+1)$ torus knot. Making Theorem 1.0.7 more explicit, we want to prove

**Theorem 4.1.3.** *Conjecture 2.4.10 is true for $(2, 2p+1)$ torus knots. Specifically,*

$$F_{T^{(2,2p+1)}}(x, a, q) = x^{p(\frac{\log a}{\hbar}-1)} \sum_{0\le j_p\le\ldots\le j_1} x^{2(j_1+\ldots+j_p)-j_1} q^{(j_1+j_2+\ldots+j_p)-\sum_{i=2}^{p} j_{i-1}j_i} \times \frac{(aq^{-1};q)_{j_1}(x;q^{-1})_{j_1}}{(q;q)_{j_1}} \binom{j_1}{j_2}_q \cdots \binom{j_{p-1}}{j_p}_q. \tag{4.1.4}$$

*exhibits all properties of Conjecture 2.4.10.*

*Proof of Theorem 4.1.3.* Constructing $F_{T^{(2,2p+1)}}(x,a,q)$ from the HOMFLY-PT polynomials automatically guarantees properties (2.4.11-2.4.12) and (2.4.16).

The Alexander polynomial of the $(2,2p+1)$ torus knot is given by

$$\begin{aligned}\Delta_{T^{(2,2p+1)}}(x) = x^{-p}\frac{1+x^{2p+1}}{1+x} &= x^{-p} - x^{1-p} + x^{2-p} - \cdots + x^{p} \\ &= x^{-p}(1 - x(1-x)(1 + x^2 + \ldots + x^{2(p-1)})).\end{aligned}$$

When we put $a = 1$ in (4.1.4), the $q$-Pochhammer $(q^{-1};q)_{j_1}$ is non-zero only for $j_1 = 0, 1$. Hence, all $j_i$ must be 0 or 1 and the summation contains exactly $p+1$ terms, where the $i$-th term has $j_n = 1$ for $n \leq i$ and $j_n = 0$ for $n > i$. Simple computations yield 1 for $i = 0$ and

$$x^{2i-1}q^{i-(i-1)}\frac{(1-q^{-1})(1-x)}{(1-q)} = -x^{2i-1}(1-x)$$

for $i > 0$. Therefore,

$$F_{T^{(2,2p+1)}}(x,1,q) = x^{-p}(1 - x(1-x)\sum_{i=1}^{p} x^{2i-2}) = \Delta_{T^{(2,2p+1)}}(x), \tag{4.1.5}$$

proving property (2.4.13).

Property (2.4.14) follows immediately from observing that $F_{T^{(2,2p+1)}}(x,q,q)$ contains the $q$-Pochhammer $(1;q)_{j_1}$, which is non-zero only for $j_1 = 0$, in which case the whole expression is equal to 1. Additionally, when $a = q$, $\frac{\log a}{\hbar} - 1 = 0$ so the prefactor vanishes as expected.

In order to show (2.4.15), we start with two simple combinatorial identities:

$$\begin{aligned}\left(\frac{1}{1-x}\right)^{N} &= \sum_{i=0}^{\infty}\binom{N+i-1}{i}x^{i} \\ \left(1 + x + \cdots x^{p-1}\right)^{j_1} &= \sum_{0\leq j_p \leq \cdots \leq j_2 \leq j_1} x^{(j_2+\cdots+j_p)}\binom{j_1}{j_2}\cdots\binom{j_{p-1}}{j_p}.\end{aligned}$$

These both follow from counting arguments. The first is the number of ways to divide $i$ balls into $N$ buckets, and the second is essentially the multinomial theorem with a simple change of variables. Combining them, we expand,

$$\left(\frac{1}{\Delta_{T^{(2,2p+1)}}(x)}\right)^{N-1} = \left(\frac{x^{p}}{(1-x(1-x)(1+x^2+\ldots+x^{2(p-1)})}\right)^{N-1}$$

$$
\begin{aligned}
&= x^{p(N-1)} \sum_{j_1} \binom{N-2+j_1}{j_1} x^{j_1} (1-x)^{j_1} (1+x^2+\ldots+x^{2(p-1)})^{j_1} \\
&= x^{p(N-1)} \sum_{0 \le j_p \le \cdots \le j_1} (1-x)^{j_1} x^{2(j_1+\ldots+j_p)-j_1} \qquad (4.1.6) \\
&\qquad \times \binom{N-2+j_1}{j_1} \binom{j_1}{j_2} \cdots \binom{j_{p-1}}{j_p} \qquad (4.1.7) \\
&= \lim_{q \to 1} F_{T^{(2,2p+1)}}(x, q^N, q),
\end{aligned}
$$

which completes the proof. □

### 4.1.1 The Trefoil Knot

Let's look at the simplest $(2, 2p+1)$ torus knot, the trefoil, in more detail.

For $p = 1$, equation (4.1.4) reduces to

$$
F_{3_1^l}(x, a, q) = x^{\frac{\log a}{\hbar}-1} \sum_{k=0}^{\infty} (xq)^k \frac{(x; q^{-1})_k (aq^{-1}; q)_k}{(q; q)_k}. \qquad (4.1.8)
$$

The function $F_{3_1^l}(x, a, q)$ is annihilated by the quantum $a$-deformed A-polynomial

$$
\hat{A}_{3_1^l}(\hat{x}, \hat{y}, a, q) = a_0 + a_1 \hat{y} + a_2 \hat{y}^2, \qquad (4.1.9)
$$

where[1]

$$
\begin{aligned}
a_0 =& q^4 \hat{x}^3 (q\hat{x} - 1)(1 - aq^3 \hat{x}^2), \\
a_1 =& -(1 - aq^2 \hat{x}^2)(1 + q^4 \hat{x}^2 - aq\hat{x}^2 + a^2 q^4 \hat{x}^4 + q^2 \hat{x}(-1 + q\hat{x} - aq\hat{x} - aq^2 \hat{x}^2)), \\
a_2 =& (1 - aq\hat{x})(1 - aq\hat{x}^2).
\end{aligned}
$$

When we take the semiclassical limit of $F_{3_1}(x, a, q)$ we reproduce the twisted superpotential of $T[M_{3_1}]$, the trefoil complement theory studied in [FGS13]:

$$
\begin{aligned}
&F_{3_1^l}(x, a, q) \underset{\hbar \to 0}{\to} \exp \int \frac{dz}{z} \left[ \frac{1}{\hbar} \widetilde{\mathcal{W}}(z, x, a) + O(\hbar^0) \right], \\
&\widetilde{\mathcal{W}}(z, x, a) = \log x \log z - \mathrm{Li}_2(x) + \mathrm{Li}_2(xz^{-1}) + \mathrm{Li}_2(a) - \mathrm{Li}_2(az) + \mathrm{Li}_2(z).
\end{aligned} \qquad (4.1.10)
$$

Extremization with respect to $z$ ($z_0$ denotes the extremal value) and introduction of the variable $y$ dual to $x$ leads to equations

$$
\begin{cases}
1 = \frac{x(1 - xz_0^{-1})(1 - az_0)}{(1 - z_0)}, \\
y = \frac{z_0(1-x)}{1 - xz_0^{-1}}.
\end{cases} \qquad (4.1.11)
$$

[1] Formula (4.1.9) differs from [FGS13] by the rescaling of $\hat{x}$ by $q$ mentioned earlier, and of $\hat{y}$ by $a/q$ due to the omitted prefactor.

Eliminating $z_0$, we obtain the $A$-polynomial

$$A_{3_1^l}(x,y,a) = (x-1)x^3 - \left(1 - x + 2(1-a)x^2 - ax^3 + a^2x^4\right) y + (1-ax)y^2 \quad (4.1.12)$$

which is the classical limit of (4.1.9).

We would like to compare this result to the $F_K$ invariants for $\mathfrak{sl}_2$ case from [GM21] and the $a$ deformed $F_K$ invariant we computed using the $R$-matrix in Equation (3.2.2).

The first step is to convert our expression from the left to right-handed trefoil. In order to do this we first replace

$$x \mapsto x^{-1} \qquad a \mapsto a^{-1} \qquad q \mapsto q^{-1},$$

and then use the Weyl symmetry

$$x^{-1} \mapsto ax.$$

Making these substitutions and applying the identity $\frac{(a^{-1}q,q^{-1})_k}{(q^{-1},q^{-1})_k} = a^{-k}q^{2k}\frac{(aq^{-1};q)_k}{(q;q)_k}$ yields

$$F_{3_1^r}(x,a,q) = F_{3_1^l}(ax,a^{-1},q^{-1}) = (ax)^{\frac{\log a}{\hbar}-1}\sum_{k=0}^{\infty} x^k q^k \frac{(ax;q)_k(aq^{-1};q)_k}{(q;q)_k}$$

which agrees with Equation (3.2.2) as expected. Next, to relate to the computations in [GM21] we need to specialise $a$ and adjust normalisations and conventions (see Section 2.4.3). Setting $a = q^2$ this simplifies our equation to

$$(q^2x)\sum_{k=0}^{\infty} x^k q^k (q^2x;q)_k.$$

Next we need to, switch from $x = q^r$ for $S^r$ to $x = q^n$ for $S^{n-1}$, which corresponds to $x \mapsto x/q$. Performing this transformation and expanding in $x$ we get

$$qx + qx^2 + q(1-q)x^3 + q(1-q-q^2)x^4 + q(1-q-q^2+q^5)x^5 + \dots.$$

Since [GM21] uses the unreduced normalisation, we multiply by $(x^{\frac{1}{2}} - x^{-\frac{1}{2}})$, which leaves us with the series

$$-qx^{\frac{1}{2}} + q^2x^{\frac{5}{2}} + q^3x^{\frac{7}{2}} - q^6x^{\frac{11}{2}} - q^8x^{\frac{13}{2}} + \dots$$

From here we need to switch to the balanced expansion, which – thanks to the $\mathfrak{sl}_2$ Weyl symmetry – means replacing $x^n \mapsto \frac{1}{2}(x^n - x^{-n})$, and we exactly recover $(x,q)$-series from [GM21, eq.(114)]:

$$\begin{aligned} F_{3_1^r}^{2,unreduced}(x,q) = -\frac{1}{2}\Big[&q(x^{\frac{1}{2}} - x^{-\frac{1}{2}}) - q^2(x^{\frac{5}{2}} - x^{-\frac{5}{2}}) - q^3(x^{\frac{7}{2}} - x^{-\frac{7}{2}}) \\ &+ q^6(x^{\frac{11}{2}} - x^{-\frac{11}{2}}) + q^8(x^{\frac{13}{2}} - x^{-\frac{13}{2}}) + \dots\Big]. \end{aligned} \quad (4.1.13)$$

## 4.2 Computing $F_K$ from $A$-Polynomial Recursion

Unfortunately, the strategy of substituting $q^r = x$ does not work for all knots. For example, the coloured HOMFLY-PT polynomial for the figure-eight knot is given in [FGS13] as

$$P_k(4_1; a, q) = \sum_{k=0}^{\infty} (-1)^k a^{-k} q^{-k(k-3)/2} \frac{(aq^{-1}; q)_k}{(q; q)_k} (q^{-r}; q)_k (aq^r; q)_k. \tag{4.2.1}$$

Making the substitution $q^r = x$, we get

$$\sum_{k=0}^{\infty} (-1)^k a^{-k} q^{-k(k-3)/2} \frac{(aq^{-1}; q)_k}{(q; q)_k} (x^{-1}; q)_k (ax; q)_k,$$

but this expression does not give a well-defined power series in $x$.

In a case like this, we can construct a candidate for $F_K$ invariant by solving the recursion given by the quantum $a$-deformed $A$-polynomial. The uniqueness of the solution is ensured by the following:

**Lemma 4.2.2.** *Suppose that the quantum $A$-polynomial is properly normalised so that we expect a solution $F_K(x, a, q)$ to the equation*

$$\hat{A}_K(\hat{x}, \hat{y}, a, q) F_K(x, a, q) = 0 \tag{4.2.3}$$

*of the form*

$$F_K(x, a, q) = f_0 + f_1(a, q)x + f_2(a, q)x^2 + \dots \tag{4.2.4}$$

*with $f_0 = 1$. Let us write the quantum $A$-polynomial as follows:*

$$\hat{A}_K(\hat{x}, \hat{y}, a, q) = \sum_{j=0}^{d} \alpha_j(\hat{y}, a, q) x^j.$$

*Then the equation (4.2.3) has a unique solution of the form (4.2.4) if and only if*

$$\alpha_0(1, a, q) = 0 \qquad \text{and} \qquad \alpha_0(q^j, a, q) \neq 0 \tag{4.2.5}$$

*for every $j \in \mathbb{Z}_+$. If these conditions are satisfied, then the unique solution is given recursively by*

$$f_j(a, q) = -\frac{1}{\alpha_0(q^j, a, q)} \sum_{k=0}^{j-1} \alpha_{j-k}(q^k, a, q) f_k(a, q) \tag{4.2.6}$$

*for each $j \in \mathbb{Z}_+$.*

*Proof.* The statement follows from simple computations. □

In order to show properties (2.4.13-2.4.15), we will need also the following:

**Lemma 4.2.7.** *Let $F(x,a,q)$ be a polynomial annihilated by a relation,*

$$\hat{C}(\hat{x},\hat{y},a,q) = \sum_{i=0}^{n} c_i(\hat{x},a,q)\hat{y}, \tag{4.2.8}$$

*where each $c_i$ is a rational function. Then $\hat{C}$ factors as*

$$\hat{C}(\hat{x},\hat{y},a,q) = \hat{Q}(\hat{x},\hat{y},a,q)\left(\hat{y} - \frac{F(qx,a,q)}{F(x,a,q)}\right). \tag{4.2.9}$$

As a brief comment, note that by clearing denominators, this is essentially equivalent to the case where the coefficients $c_i$ are polynomials and the factor has the form $F(x,a,q)\hat{y} - F(qx,a,q)$.

*Proof.* The proof is constructive. Define $\hat{Q}_n(\hat{x},\hat{y},a,q) = c_n(\hat{x},a,q)\hat{y}^{n-1}(\hat{y} - \frac{F(qx,a,q)}{F(x,a,q)})$ and $\hat{C}_{n-1} = \hat{C} - \hat{Q}_n$. Then $\hat{C}_{n-1}$ is an $n-1$ degree polynomial in $\hat{y}$ which annihilates $F(x,a,q)$. Repeating this procedure, we end up with a zero degree polynomial $\hat{C}_0(\hat{x},a,q)$ satisfying $\hat{C}_0(x,a,q)F(x,a,q) = 0$ which, implies $\hat{C}_0(x,a,q) = 0$. Working backwards, we reconstruct $\hat{C}$ as $\hat{Q}_1 + \cdots + \hat{Q}_n$, which manifestly factors as $\hat{Q}(\hat{x},\hat{y},a,q)(\hat{y} - \frac{F(qx,a,q)}{F(x,a,q)})$. □

Since all functions involved in the proof are rational, it is equally valid in the case where, instead of $\hat{C}_0(x,a,q)F(x,a,q) = 0$, our condition is $\hat{C}_0(q^r,a,q)F(q^r,a,q) = 0$ for all $r \in \mathbb{N}$.

Having Lemma 4.2.2 and 4.2.7, we are ready to show that our candidate for $F_K$ invariant is well-defined and exhibits properties (2.4.13-2.4.15) of Conjecture 2.4.10:

*Proof of Theorem 1.0.8.* Since the abelian branch of the considered $a$-deformed $A$-polynomial $\hat{A}_K$ is non-degenerate, conditions (4.2.5) are satisfied. Following Lemma 4.2.2, this ensures that $F_K(x,a,q)$ given by (4.2.4, 4.2.6) is a unique solution of the $q$-difference equation (4.2.3).

By construction, $F_K(x,a,q)$ solves the recurrence relation given by $\hat{A}_K(\hat{x},\hat{y},a,q)$ with leading coefficient 1, which automatically ensures (2.4.12). On the other hand, the abelian branch is the unique solution whose specialisations $a = q^N$

are non-singular in the $q \to 1$ limit. Therefore, if the $A$-polynomial factors as $\hat{A}_K(\hat{x}, \hat{y}, q^N, q) = \hat{Q}(\hat{x}, \hat{y}, q)(\hat{y} - \frac{F(qx,q)}{F(x,q)})$ with $F$ being a polynomial with constant term equal to 1, then $F_K(x, q^N, q) = F(x, q)$.

Consider the $a = 1$ limits of coloured HOMFLY-PT polynomial:

$$P_k(K; 1, q) = \Delta_K(q^k). \tag{4.2.10}$$

Then Lemma 4.2.7 shows that $\hat{y} - \frac{\Delta_K(qx)}{\Delta_K(x)}$ can be factored out from $\hat{A}_K(\hat{x}, \hat{y}, 1, q)$, which means that (2.4.13) is satisfied.[2]

Similarly, the $a = q$ limit

$$P_k(K; q, q) = 1 \tag{4.2.11}$$

combined with Lemma 4.2.7 implies that $\hat{y} - 1$ can be factored out from $\hat{A}_K(\hat{x}, \hat{y}, q, q)$, which ensures property (2.4.14).

Finally, the property (2.4.15) follows directly from enumerative geometrical arguments presented in Section 4.3 of [EGGKPS22]. □

### 4.2.1 The Figure-eight Knot

Let us see the application of Theorem 1.0.8 on the figure-eight knot. The quantum $a$-deformed $A$-polynomial is given by [FGS13]:

$$\hat{A}_{4_1}(\hat{x}, \hat{y}, a, q) = a_0 + a_1\hat{y} + a_2\hat{y}^2 + a_3\hat{y}^3, \tag{4.2.12}$$

where[3]

$$\begin{aligned}
a_0 &= -\frac{(1 - q\hat{x})(1 - q^2\hat{x})(1 - aq^4\hat{x}^2)(1 - aq^5\hat{x}^2)}{q(1 - aq\hat{x})(1 - aq^2\hat{x})(1 - aq\hat{x}^2)(1 - aq^2\hat{x}^2)}, \\
a_1 &= \frac{(1 - q^2\hat{x})(1 - aq^5\hat{x}^2)}{q^4\hat{x}^2(1 - aq\hat{x})(1 - aq^2\hat{x})(1 - aq\hat{x}^2)} \\
&\quad \times \Big(-1 + 2q^2\hat{x} + aq(1 - q - q^2 + q^3)\hat{x}^2 + aq^3(-1 + q + q^2 - q^3)\hat{x}^3 \\
&\qquad -2a^2q^5\hat{x}^4 + a^2q^7\hat{x}^5\Big), \\
a_2 &= \frac{(1 - aq^4\hat{x}^2)}{q^4\hat{x}^2(1 - aq^2\hat{x})(1 - aq^2\hat{x}^2)} \\
&\quad \times \Big(1 - 2aq\hat{x} - aq^2(1 - q)^2(1 + q)\hat{x}^2 + a^2q^3(1 - q - q^2 + q^3)\hat{x}^3 \\
&\qquad +2a^2q^7\hat{x}^4 - a^3q^8\hat{x}^5\Big),
\end{aligned}$$

[2] Note that there is a minor technicality when $\Delta_K(x)$ is not monic as in that case we should get $\frac{\Delta_K(x)}{a}$ where $a$ is the leading coefficient. However, this case doesn't occur as when $\Delta_K(x)$ is not monic the abelian branch should be degenerate.

[3] Again we rescale $\hat{x}$ by $q$, $\hat{y}$ by $a/q$ and remove common factors of $a, q$. The $A$-polynomial we use corresponds to the reduced normalisation.

$$a_3 = \frac{a^2}{q}.$$

Following Lemma 4.2.2 we see that $\alpha_0 = y - 1$, so there exists a unique solution, a candidate for the $F_K$ invariant. We take the ansatz[4]

$$F_{4_1}(x, a, q) = \sum_{k=0}^{\infty} f_k(a, q) x^k,$$

and then use $\hat{A}_{4_1}$ to recursively solve for the $f_k$. This leaves us with one free variable, $f_0$, which we set to be 1 for now.[5] The first few terms are

$$\begin{aligned}
f_0 &= 1, \\
f_1 &= -\frac{3(a-q)}{(1-q)}, \\
f_2 &= -\frac{(a-q)(1-2a+6q-6aq+2q^2-aq^2)}{(1-q)(1-q^2)}, \\
f_3 &= -\frac{(1-a)(a-q)}{(1-q)(1-q^2)(1-q^3)} \\
&\quad \times (2+3q-5aq+11q^2-6aq^2+6q^3-11aq^3+5q^4-3aq^4-2aq^5).
\end{aligned} \tag{4.2.13}$$

As written it is not immediately clear that when $a = q^N$, the $q \to 1$ limit is well-defined but if we introduce the notation

$$(a)^{(n)} = \prod_{i=1}^{n} \frac{(a-q^i)}{(1-q^i)} = \frac{a^n (a^{-1}q;q)_n}{(q;q)_n},$$

we find that we can write our functions as follows:

$$\begin{aligned}
f_0 &= (a)^{(0)} = 1, \\
f_1 &= -3(a)^{(1)}, \\
f_2 &= -(1+6q+q^2)(a)^{(1)} + (2+6q+q^2)(a)^{(2)}, \\
f_3 &= -\left(2+3q+11q^2+3q^3+2q^4\right)(a)^{(1)} \\
&\quad + \left(2+8q+17q^2+14q^3+5q^4+2q^5\right)(a)^{(2)} \\
&\quad - \left(5q+6q^2+11q^3+3q^4+2q^5\right)(a)^{(3)}.
\end{aligned} \tag{4.2.14}$$

This makes the various $q \to 1$ limits easy to compute. We can additionally check that these line up with the computations in Table 3.6 which came from the inverted state sum $R$-matrix method.

[4] The prefactor $x^{\frac{\log a}{\hbar}-1}$ is omitted.

[5] In general, we cannot simply set $f_0 = 1$; it should be determined by means other than recursion.

### 4.2.2 The $5_2$ knot

Unfortunately, there are many knots for which (4.2.5) is not satisfied (it seems that non-fiberedness is correlated with the non-uniqueness). Twist knots $K_n$ with $|n| > 1$ are good examples. For $K_n$, $\alpha_0(y, a, q)$ has a factor of $\prod_{j=0}^{|n|-1}(y - q^j)$, meaning that the first $n$ coefficients, $f_0, f_1, \ldots, f_{n-1}$ are free parameters and cannot be determined by just solving the recursion. Below, we study the example of $K_2 = 5_2$ in detail to illustrate this point.

We find that, although the first two coefficients $f_0, f_1$ seem to be free parameters, we can do better than that; in particular, by imposing the non-singularity condition for $F_K(x, e^{N\hbar}, e^{\hbar})$ in the limit $\hbar \to 0$, the term $f_1$ is determined by $f_0$. Schematically,

$$(\hat{A}_K F_K = 0) \ + \ (\text{non-singularity condition}) \Rightarrow \text{unique solution, up to a prefactor.}$$

The $5_2$ knot is just an example, and we conjecture that this procedure works for every knot. In terms of the curve of the $A$-polynomial $\{A_K = 0\}$, this means that we expect a unique wave function once a branch of the curve near $x = -\infty$ has been specified. We also note that the appearance of many branches of the curve of the $A$-polynomial indicates that the form $\log x \; d(\log y)$ is singular along the curve.

The (reduced) quantum $a$-deformed $A$-polynomial for the $5_2$ knot can be found in [NRZS12, FGSS12]. After aligning with the conventions we are using, it is given by

$$\hat{A}_{5_2}(\hat{x}, \hat{y}, a, q) = a_0 + a_1\hat{y} + a_2\hat{y}^2 + a_3\hat{y}^3 + a_4\hat{y}^4, \tag{4.2.15}$$

where

$$\begin{aligned}
a_0 &= -aq^{12}\hat{x}^7(q\hat{x} - 1)\left(q^2\hat{x} - 1\right)\left(q^3\hat{x} - 1\right)\left(aq^5\hat{x}^2 - 1\right)\left(aq^6\hat{x}^2 - 1\right)\left(aq^7\hat{x}^2 - 1\right), \\
a_1 &= q^6\hat{x}^2\left(q^2\hat{x} - 1\right)\left(q^3\hat{x} - 1\right)\left(aq^2\hat{x}^2 - 1\right)\left(aq^6\hat{x}^2 - 1\right)\left(aq^7\hat{x}^2 - 1\right) \\
&\quad \Big(a^3q^9\hat{x}^6 + a^3q^8\hat{x}^6 - 3a^2q^8\hat{x}^5 - a^2q^8\hat{x}^4 - a^2q^7\hat{x}^5 - a^2q^7\hat{x}^4 + a^2q^6\hat{x}^4 \\
&\qquad - a^2q^4\hat{x}^4 - a^2q^3\hat{x}^4 + aq^8\hat{x}^4 + aq^7\hat{x}^4 + 2a\,q^7\hat{x}^3 + aq^6\hat{x}^4 - aq^5\hat{x}^3 \\
&\qquad -aq^5\hat{x}^2 - aq^4\hat{x}^3 + 2a\,q^3\hat{x}^3 + aq^3\hat{x}^2 + aq^2\hat{x}^2 - aq\hat{x}^2 + q^4\hat{x}^2 - 2q^2\hat{x} + 1\Big), \\
a_2 &= -q\left(q^3\hat{x} - 1\right)(aq\hat{x} - 1)\left(aq\hat{x}^2 - 1\right)\left(aq^4\hat{x}^2 - 1\right)\left(aq^7\hat{x}^2 - 1\right) \\
&\quad \Big(a^4q^{16}\hat{x}^8 - 2a^3q^{15} - a^3q^{14}\hat{x}^7 - a^3q^{14}\hat{x}^6 - a^3q^{13}\hat{x}^6 - a^3q^{11}\hat{x}^6 - a^3q^{10}\hat{x}^6\hat{x}^7 \\
&\qquad + 2a^2q^{14}\hat{x}^6 + 3a^2q^{13}\hat{x}^6 + 2a^2q^{13}\hat{x}^5 + a^2q^{12}\hat{x}^5 - 2a^2q^{11}\hat{x}^5 + a^2q^{11}\hat{x}^4 \\
&\qquad - a^2q^{10}\hat{x}^5 + 2a^2q^9\hat{x}^5 + a^2q^9\hat{x}^4 + a^2q^8\hat{x}^5 + 2a^2q^8\hat{x}^4 + a^2q^7\hat{x}^4 + a^2q^5\hat{x}^4 \\
&\qquad - aq^{13}\hat{x}^5 - aq^{12}\hat{x}^5 - 2a\,q^{12}\hat{x}^4 - aq^{11}\hat{x}^5 - 2a\,q^{11}\hat{x}^4 + aq^{10}\hat{x}^4 + 2a\,q^9\hat{x}^4
\end{aligned}$$

$$
\begin{aligned}
&+2aq^9\hat{x}^3-aq^8\hat{x}^4+aq^8\hat{x}^3-2a\,q^7\hat{x}^4-2a\,q^7\hat{x}^3-aq^6\hat{x}^3-aq^6\hat{x}^2\\
&+2aq^5\hat{x}^3-aq^5\hat{x}^2+aq^4\hat{x}^3-aq^3\hat{x}^2-aq^2\hat{x}^2-q^9\hat{x}^3-q^8\hat{x}^3-q^7\hat{x}^3+2q^6\hat{x}^2\\
&+3q^5\hat{x}^2-2q^3\hat{x}-q^2\hat{x}+1\Big),\\
a_3=(aq\hat{x}-1)&\left(aq^2\hat{x}-1\right)\left(aq\hat{x}^2-1\right)\left(aq^2\hat{x}^2-1\right)\left(aq^6\hat{x}^2-1\right)\\
&\Big(a^3q^{16}\hat{x}^6-2a^2q^{14}\hat{x}^5-a^2q^{13}\hat{x}^4+a^2q^{11}\hat{x}^4+a^2q^{10}\hat{x}^4-a^2q^9\hat{x}^4+aq^{12}\hat{x}^4\\
&+2aq^{11}\hat{x}^3-aq^9\hat{x}^3-aq^8\hat{x}^3-aq^8\hat{x}^2+2a\,q^7\hat{x}^3-aq^7\hat{x}^2+aq^6\hat{x}^2\\
&-aq^4\hat{x}^2-aq^3\hat{x}^2+q^8\hat{x}^2+q^7\hat{x}^2+q^6\hat{x}^2-3q^4\hat{x}-q^3\hat{x}+q+1\Big),\\
a_4=(aq\hat{x}-1)&\left(aq^2\hat{x}-1\right)\left(aq^3\hat{x}-1\right)\left(aq\hat{x}^2-1\right)\left(aq^2\hat{x}^2-1\right)\left(aq^3\hat{x}^2-1\right).
\end{aligned}
$$

Solving the recursion, we find that the first two coefficients, $f_0$ and $f_1$, determine all the others. That is,[6]

$$F_{5_2}(x,a,q)=\sum_{j\geq 0}f_j(a,q)x^j, \tag{4.2.16}$$

where $f_j$ with $j\geq 2$ are $\mathbb{Q}(a,q)$-linear combinations of $f_0$ and $f_1$. For instance,

$$f_2=-\frac{\left(a^2+a\left(q^2-4q-2\right)+q\left(-q^2+3q+2\right)\right)}{(q-1)^2(q+1)}f_0+\frac{(aq+a-3q-1)}{q^2-1}f_1.$$

Although at this point it may seem like $f_0$ and $f_1$ are free parameters, we have additional conditions to impose, namely that $F_K(x,q^N,q)$ is non-singular in the semi-classical limit $q\to 1$. Note that this non-singularity condition is weaker than imposing the explicit limit (2.4.15), but as we will see, powers of Alexander polynomial automatically pop up just from this non-singularity condition. This non-singularity property imposes lots of conditions on the perturbative coefficients of $f_0$ and $f_1$, and in particular it determines the entire perturbative series of the ratio $f_1/f_0$:

$$
\begin{aligned}
\frac{f_1}{f_0}(a=e^{N\hbar},q=e^{\hbar})=&\frac{3}{2}(N-1)\\
&+\frac{5}{8}N(N-1)\hbar\\
&+\frac{3}{16}N(N-1)(2N-1)\frac{\hbar^2}{2!}\\
&+\frac{1}{64}N(N-1)(17N^2-17N-3)\frac{\hbar^3}{3!}\\
&+\frac{1}{320}N(N-1)(66N^3-99N^2+11N+41)\frac{\hbar^4}{4!}\cdots
\end{aligned}
$$

[6]The prefactor $x^{\frac{\log a}{\hbar}-1}$ is omitted.

Plugging this back in and setting $\lim_{q\to 1} f_0(q^N, q) = 2^{1-N}$, we see that the expected properties (2.4.13)-(2.4.15) in Conjecture 2.4.10 hold! That is, when $a = 1$, we have $f_0(q^0, q) = 2$, $f_1(q^0, q) = -3$, and

$$F_{5_2}(x, q^0, q) = 2 - 3x + 2x^2, \tag{4.2.17}$$

whereas for $a = q$ we get

$$F_{5_2}(x, q^1, q) = 1. \tag{4.2.18}$$

Similarly, when $a = q^N$ ($N$ not necessarily an integer), we have

$$\lim_{q\to 1} F_{5_2}(x, q^N, q) = \frac{1}{(2 - 3x + 2x^2)^{N-1}}. \tag{4.2.19}$$

Expressing the series in terms of $\hbar$ and $N\hbar$ instead, we get

$$\begin{aligned}
(q-1)\frac{f_1}{f_0}(a,q)\Big|_{a=e^{N\hbar},q=e^{\hbar}} &= \left(3(N\hbar/2) + \frac{5(N\hbar/2)^2}{2!} + \frac{9(N\hbar/2)^3}{3!} + \frac{17(N\hbar/2)^4}{4!}\cdots\right) \\
&+ \left(-\frac{3}{2} + \frac{(N\hbar/2)}{4} + \frac{(N\hbar/2)^2}{4\times 2!} + \frac{(N\hbar/2)^3}{4\times 3!} + \ldots\right)\hbar \\
&+ \left(-\frac{3}{2} + \frac{(N\hbar/2)}{8} + \frac{(N\hbar/2)^3}{8\times 3!} + \frac{(N\hbar/2)^5}{8\times 5!} + \ldots\right)\frac{\hbar^2}{2!} \\
&+ \left(-\frac{3}{2} + \frac{5(N\hbar/2)}{32} + \frac{(N\hbar/2)^2}{16\times 2!} + \frac{13(N\hbar/2)^3}{32\times 3!} + \ldots\right)\frac{\hbar^3}{3!}\cdots
\end{aligned}$$

It is an interesting problem to re-sum these perturbative series into expressions in $a$ and $q$.

## 4.3 Different Branches of $F_K$

The perturbative invariants of complex Chern Simons theory were extensively studied in [DGLZ09]. While the method of that paper allowed the computation of perturbative invariants up to any order, for many years they were not widely used. Indeed, $F_K$ can be viewed as a repackaging of the perturbative invariants from the abelian branch[7]

$$F_K(x,q) \overset{q=e^{\hbar}}{=\!=} e^{\frac{1}{\hbar}(S_0^{(\mathrm{ab})}(x)+S_1^{(\mathrm{ab})}(x)\hbar+S_2^{(\mathrm{ab})}(x)\hbar^2+\cdots)}.$$

It should be noted however that the method of [DGLZ09] computes perturbative invariants associated to all branches $y^{(\alpha)}(x)$. This immediately brings the following question:

[7] At finite $N$, abelian branch denotes the solution $y^{(\mathrm{ab})} = 1$ of the classical $A$-polynomial.

**Question 4.3.1.** *Are there $F_K^{(\alpha)}(x,q)$ for other branches $y^{(\alpha)}(x)$? That is, can we resum $e^{\frac{1}{\hbar}(S_0^{(\alpha)}(x)+S_1^{(\alpha)}(x)\hbar+S_2^{(\alpha)}(x)\hbar^2+\cdots)}$ into a two-variable series with integrality?*

Note that on the abelian branch, to keep notation simple, we will continue to use $F_K$ as opposed to $F_K^{(\mathrm{ab})}$. Intriguingly, through various examples, we find that the answer to this question seems to be positive. There are indeed $F_K$ for other branches that can serve as the non-perturbative Chern Simons partition functions for the knot complements.[8] One method of classifying and computing the series associated to different branches is to use the $A$-polynomial.

### 4.3.1 The edges and branches of the $A$-polynomial

The Newton polygon of the $A$-polynomial contains a wealth of information about the knot. For instance, the slope of each edge of the Newton polygon equals the boundary slope of an incompressible surface of the knot complement, [CCGLS94]. For our purposes, the important aspect is a correspondence between the edges of the Newton polygon and the branches of the $A$-polynomial.

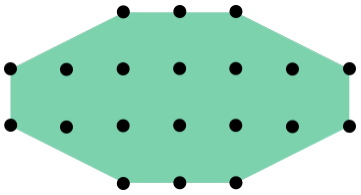

Figure 4.1: The Newton polygon for $A_{\mathbf{4}_1}$

Solving the classical $A$-polynomial equation $A_K(x,y)=0$ for $y$, we get several different branches $y^{(\alpha)}(x)$. We are interested in the behaviour of $y^{(\alpha)}(x)$ near $x=0$. Consider the Newton polygon of $A_K$. As an example, the Newton polygon for the figure-eight knot is depicted in Figure 4.1. The horizontal direction represents the $x$-degree and the vertical direction represents the $y$-degree. When $x$ is close to 0, the dominant terms are the vertices of the Newton polygon that are left-most among the vertices on the same horizontal line. Let us call such vertices "left-vertices". The equation $A_K(x,y^{(\alpha)}(x))=0$ requires that near $x=0$ we should asymptotically have $y^{(\alpha)}(x)\sim x^{-\frac{n_x}{n_y}}$ for some slope $\frac{n_y}{n_x}$ of an edge spanned by two of the left-vertices. Let us call such an edge a "left-edge". Moreover, for any given slope of a left-edge, we

[8] Physically, $F_K^{(\alpha)}(x,q)$ is a "half-index" of a 2d/3d combined system [GGP14] for the 3d theory $T[S^3\setminus K]$ with a 2d $(0,2)$ boundary condition labelled by $\alpha$ and a discrete flux, whose fugacity is $x$, cf. [GPV17, GM21].

can construct a classical solution $y^{(\alpha)}(x)$ using the asymptotic dictated by the slope. Thus, we have just shown the following proposition.

**Proposition 4.3.2.** *For any choice of branch $\alpha$, there is a left-edge $e_\alpha$ of the Newton polygon with slope $\frac{n_y}{n_x}$, such that*

$$\lim_{x\to 0} y^{(\alpha)}(x) x^{\frac{n_x}{n_y}} = C \tag{4.3.3}$$

*for some non-zero constant $C$. Moreover, the map $E : \alpha \mapsto e_\alpha$ is a surjective map onto the set of left-edges.*

While the number of branches $y^{(\alpha)}$ is the same as the total $y$-degree (which is the height of the Newton polygon), the number of left-edges is at most the height of the Newton polygon. Therefore, $E$ is not injective in general.

**Proposition 4.3.4.** *For any left-edge $e$, the number of pre-images of $E$ is $n_y$, the $y$-height of the edge $e$.*

Take any left-edge $e$ with $x$-width $n_x$ and $y$-height $n_y$. Our convention is such that $n_y > 0$ but $n_x$ can be negative. When $n_y = 1$, it is easy to see that there is a unique solution with the initial condition (4.3.3). When $n_y > 0$ but $n_x$ is coprime with $n_y$ so that the edge is non-degenerate (the endpoints are the only vertices on this edge), then (4.3.3) represents $n_y$ different initial conditions which differ by multiplication by an $n_y$'th root of unity. Each of these initial conditions gives a unique classical solution, and therefore there are $n_y$ number of branches associated to the edge. When $n_x$ is not coprime with $n_y$, the edge is degenerate (can be broken into smaller edges), and there are some genuine multiplicities associated to the initial condition (4.3.3). We will see them in an example of the edge of slope $\infty$ for the knot $5_2$.

Before we move on, we make a couple more observations

- If we look at the behaviour of $y^{(\alpha)}(x)$ near $x = \infty$, its asymptotics is determined by the slopes of the right-edge of the Newton polygon. Due to Weyl symmetry, the Newton polygon is symmetric under half-rotation, so we basically get the same set of information.
- We can similarly solve $A_K(x, y) = 0$ for $x$. With the role of $x$ and $y$ switched, everything we described in this section holds.
- When the $y$-height $n_y$ of $e_\alpha$ is 1, $y^{(\alpha)}(x)$ is a power series in $x$. In general, however, when $n_y > 1$, $y^{(\alpha)}(x)$ is a Puiseux series in $x$.

### 4.3.2 $F_K$ from the edges

So far, all our analysis has been classical, so let us turn to the quantum version of this correspondence. We are interested in solving the $q$-difference equation

$$\hat{A}_K F_K = 0,$$

where $F_K$ is expanded near $x = 0$.[9] For each left-edge, there are some natural initial conditions for the recursion that we can put, which in the semiclassical limit become the classical initial conditions that we studied in the previous section.

**Conjecture 4.3.5.** *For each left-edge $e$ with slope $\frac{n_y}{n_x}$, there is a solution to the $q$-difference equation $\hat{A}_K F_K(x,q)$ of the form*

$$F_K^{(\alpha)}(x,q) = e^{\frac{1}{\hbar}(-\frac{1}{2}\frac{n_x}{n_y}(\log x)^2 + \log C \log x)}(1 + \sum_{j\geq 1} f_j(q) x^{\frac{j}{d}}),$$

*where $d = \frac{n_y}{m}$ in case $e$ is broken into $m$ non-degenerate edges, $C$ is a monomial in $q$ determined by the coefficients of the vertices of $e$, and $f_j(q)$ are rational functions in $q$, which can be expanded into $q$-series with integer coefficients.*

- When $n_y = 1$, this conjecture is a theorem. This is because we can recursively solve for $F_K^{(\alpha)}$ uniquely, analogously to the way it was done for the abelian branch in Theorem 1.0.8 and the previous section.
- In the $a$-deformed setting, the exponential prefactor will be of the form

  $$\exp\left(\frac{p(\log x, \log a)}{\hbar}\right),$$

  where $p$ is a polynomial of degree at most 2.
- If the edge is non-degenerate but $n_y > 1$, then all the $n_y$ solutions are uniquely determined,
- If the edge is degenerate, then there are multiple solutions (the number of solutions is the same as the number of branches associated to the edge).

In this way, the solutions to the set of initial conditions determined by the left-edges span the whole $\deg_y A_K$-dimensional space of wave functions. We claim that these solutions are exactly the $F_K^{(\alpha)}$ for various branches $\alpha$ we mentioned in the beginning of this section (possibly up to an overall factor that is independent of $x$). We can formulate this in the form of the following conjecture.

[9] By the two remarks in the previous subsection, we can do the same for the expansion near $x = \infty$ or with $y$ instead of $x$.

**Conjecture 4.3.6.** *Given a knot $K$, for every branch $y^{(\alpha)}(x)$ of the A-polynomial, there is a function $F_K^{(\alpha)}(x,q)$ that is the non-perturbative partition function of the complex Chern Simons theory in the following sense:*

1. $\hat{A}_K F_K^{(\alpha)} = 0$ *with the initial conditions as in Conjecture 4.3.5.*
2. *It is associated to the branch $y^{(\alpha)}$ in the sense that*

$$\lim_{q\to 1} \frac{F_K^{(\alpha)}(qx,q)}{F_K^{(\alpha)}(x,q)} = y^{(\alpha)}(x).$$

3. *It agrees with the perturbative invariant of [DGLZ09] if we set $q = e^{\hbar}$.*

- There is always an abelian branch associated to the vertical edge whose corresponding initial condition gives the usual $F_K^{(\mathrm{ab})} = F_K$, as studied in [GM21].
- It is straightforward to generalize everything we discussed in this section to $\mathfrak{sl}_N$ and the $a$-deformed setup. As we will see later in Section 4.5, we can even consider the branches of $b$, a variable that is the conjugate of $a$. In that context, we consider solutions to $q$-difference equations with respect to the variable $a$. We will see that the branches of $b$ are canonically in one-to-one correspondence with the branches of $y$.

### 4.3.3 Examples

#### Trefoil

The quantum $A$-polynomial for the right-handed trefoil knot is given by

$$\hat{A}_{\mathbf{3}_1^r}(\hat{x},\hat{y},a,q) = a_0^{\mathbf{3}_1^r} + a_1^{\mathbf{3}_1^r}\hat{y} + a_2^{\mathbf{3}_1^r}\hat{y}^2,$$

with

$$\begin{aligned}
a_0^{\mathbf{3}_1^r} &= -aq(1-x)(1-qax^2),\\
a_1^{\mathbf{3}_1^r} &= (1-ax^2)(a^2x^2 - q^3ax^2 - qax(1+x-ax(1-x)) + q^2(1+a^2x^4)),\\
a_2^{\mathbf{3}_1^r} &= qa^2x^3(1-ax)(q-ax^2).
\end{aligned}$$

In the classical limit, after modding out by the factor $(1-ax^2)$, the Newton polygon is illustrated in Figure 4.2. While we have already discussed the abelian branch $F_{\mathbf{3}_1^r}$

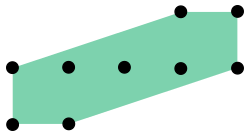

Figure 4.2: The Newton polygon of $A_{\mathbf{3}_1^r}$

is in detail, let us briefly review how to compute it from $\hat{A}_{\mathbf{3}_1^r}$. First, observe that near $x = 0$

$$a_0^{\mathbf{3}_1^r} = -qa + O(x^1), \qquad (q^{-1}a)a_1^{\mathbf{3}_1^r} = qa + O(x^1), \qquad a_2^{\mathbf{3}_1^r} = O(x^3).$$

The first two non-vanishing $O(x^0)$ terms correspond exactly to the vertical left-edge of the Newton polygon. Note that we multiplied the coefficients by powers of $q^{-1}a$ to make the sum of the two $O(x^0)$ terms vanish. This means our initial condition for solving the recursion is such that

$$F_{\mathbf{3}_1^r}(x, a, q) = x^{\frac{\log a}{\log q}-1}\Big(1 + O(x^1)\Big).$$

We can recursively solve the subsequent terms and get

$$F_{\mathbf{3}_1^r}(x, a, q) = x^{\frac{\log a}{\log q}-1}\left(1 + \frac{q-a}{1-q}x + \frac{q^2 + (-2q - q^2 + q^3)a + (1 + q - q^2)a^2}{(1-q)(1-q^2)}x^2 + \cdots\right),$$

up to an overall factor independent of $x$.

For the non-abelian branch of slope $\frac{1}{3}$, we need to consider the coefficients of the quantum $A$-polynomial near $y^{-1}x^3 = 0$. After multiplying appropriate factors, we can make the sum of the terms on this left-edge vanish:

$$\begin{aligned} a_0^{\mathbf{3}_1^r} &= O(x^0), \\ q^{-\frac{3}{2}1^2}(-q^{\frac{9}{2}}a^{-2}x^{-3})a_1^{\mathbf{3}_1^r} &= -q^5a^{-2}x^{-3} + O(x^{-2}), \\ q^{-\frac{3}{2}2^2}(-q^{\frac{9}{2}}a^{-2}x^{-3})^2a_2^{\mathbf{3}_1^r} &= q^5a^{-2}x^{-3} + O(x^{-2}). \end{aligned}$$

The extra factors we had to multiply by mean that the initial condition for solving the recursion is such that

$$F_{\mathbf{3}_1^r}^{(\frac{1}{3})}(x, a, q) = e^{\frac{-\frac{3}{2}(\log x)^2 + \log x \log\left(-a^{-2}\right)}{\log q}} x^{\frac{9}{2}}\Big(1 + O(x^1)\Big).$$

We can recursively solve the subsequent terms and get

$$F_{\mathbf{3}_1^r}^{(\frac{1}{3})}(x, a, q) = e^{\frac{-\frac{3}{2}(\log x)^2 + \log x \log\left(-a^{-2}\right)}{\log q}} x^{\frac{9}{2}}\left(1 + \frac{a}{q}x + \frac{a(q-a)}{q(1-q)}x^2 + \cdots\right),$$

up to an overall factor independent of $x$.

**Figure-eight**

The Newton polygon for the $A$-polynomial of the figure-eight knot is shown in Figure 4.1. Since all the left-edges are non-degenerate of height 1, everything can be solved term by term uniquely, just like for the trefoil knot. We computed $F_K$ for the abelian branch in Equation (4.2.13) so let's jump straight to the non-abelian ones. For the non-abelian branch of slope $-\frac{1}{2}$, we get

$$F_{\mathbf{4}_1}^{(-\frac{1}{2})}(x,a,q) = e^{\frac{(\log x)^2+\log x \log a}{\log q}} x^{-1}\left(1+\frac{q-2q^2}{1-q}x \right. \\ \left. +\frac{(q^2-2q^3-2q^4+3q^5+q^6)-q(1-q)(1-q^2)a}{(1-q)(1-q^2)}x^2+\cdots\right),$$

up to an overall factor independent of $x$.

The other non-abelian branch (with slope $\frac{1}{2}$) is conjugate to this one, and the corresponding $F_K$ can be obtained easily from this one by inverting $q$, $a$ and $x$ and then using Weyl symmetry.

## 4.4 The Knots-Quivers Correspondence

In the previous section, we have constructed $F_K$ invariants for various branches using the quantum $A$-polynomials. In this section, we focus on the relation between these newly constructed $F_K$ invariants and quivers. We start by studying how we can obtain $F_K$ invariants for some branches from the original quivers of [KRSS17, KRSS19] corresponding to knot conormals. Then we use it to construct quivers corresponding to some knot complements, generalizing [Kuc20]. Finally, we show that a slight modification of this construction leads to simpler quivers corresponding to the same $F_K$ invariant.

### 4.4.1 From knot conormal quivers to knot complement quivers

The computation of $F_K$ for abelian branches of left-handed $(2, 2p+1)$ torus knots in Theorem 4.1.3 relies on the fact that there exists a simple Fourier transform between coloured HOMFLY-PT polynomials $P_k(K;a,q)$ and $F_K(x,a,q)$, which is essentially a substitution $x = q^r$. However, as mentioned in Section 4.2, this substitution does not work in general.

One way to deal with this problem is to consider a knot $K$ with a suitable framing $f$, so that after replacing $q^r = x$, the corresponding coloured HOMFLY-PT polynomials $P_k(K;a,q)$ become a power series in $x$. In order to find the correct framing and to compute the corresponding power series, the conormal quivers become crucially

important. The framing will be the absolute value of the minimal entry of the conormal quiver matrix. Moreover, the power series in $x$ can be quickly determined and will be given in the quiver form. Finally, the obtained power series will be equal to $F_K$ invariant for the branch corresponding to the smallest slope of the knot $K$. Therefore, for each knot, $F_K$ for one branch can be obtained by this procedure. In particular, this branch will be abelian only when the corresponding framing, i.e. the smallest entry of the conormal quiver matrix, is equal to zero. In all other cases (like figure-eight knot, right-handed trefoil, etc.), the procedure that we outline below will produce $F_K$ corresponding to a certain non-abelian branch.

Let us pass to details of the connection between conormal quivers, $F_K$ invariants and their quiver forms. Given a knot $K$, let $(C, \mathbf{n}, \mathbf{a}, \mathbf{l})$ be the associated quiver data such that

$$P_k(K; a, q) = \sum_{\mathbf{d}\cdot\mathbf{n}=r} a^{\mathbf{a}\cdot\mathbf{d}} q^{\mathbf{l}\cdot\mathbf{d}} (-q^{\frac{1}{2}})^{\mathbf{d}\cdot C\cdot\mathbf{d}} \frac{(q)_r}{(q)_{\mathbf{d}}}.$$

Now suppose that

$$-C_{\min} \leq C_{ij} \leq C_{\max}, \quad i, j = 1, \ldots, m,$$

where $C_{\min}, C_{\max} \geq 0$ (must be since $C_{kk} = 0$, for some $k$), and permute rows and columns of $C$ such that $C_{11} = C_{\min}$ and $C_{mm} = C_{\max}$. Note that in the cases where conormal quivers have been computed, the largest and smallest entries are on the diagonal.

Then, we can obtain the $F_K$ invariant for the $C_{\min}$-framed knot $K$ by multiplying each $P_k$ by $q^{\frac{1}{2}C_{\min}(r^2-r)}$:

$$\begin{aligned} F_{K^{f=C_{\min}}}(x, a, q) \;=\; & (-1)^{rC_{\min}} a^{ra_1} q^{rq_1} \sum_{d_2,\cdots,d_m} (-1)^{\sum_{i\geq 2}(C_{ii}+C_{\min})d_i} a^{\sum_{i\geq 2}(a_i-a_1)d_i} \\ & \times q^{\sum_{i\geq 2}(l_i-l_1)d_i} x^{\sum_{i\geq 2}(C_{1i}+C_{\min})d_i} q^{\frac{1}{2}\sum_{i,j\geq 2}(C_{ij}-C_{i1}-C_{1j}+C_{11})d_i d_j} \\ & \times \frac{(x; q^{-1})_{d_2+\cdots+d_k}}{\prod_{i=2}^{k}(q)_{d_i}}. \end{aligned} \tag{4.4.1}$$

For the mirror image of $K$, the quiver and the change of variables are given by

$$C_{m(K)} = -C_K + I_{m\times m} - J_{m\times m}, \quad \mathbf{a}_{m(K)} = -\mathbf{a}_K, \quad \mathbf{l}_{m(K)} = -\mathbf{l}_K,$$

where $J_{m\times m}$ is the $m \times m$ matrix with all entries equal to 1. Clearly, the diagonal entries of $C_{m(K)}$ are bigger than $-C_{\max}$ and smaller than $C_{\min}$, with $(C_{m(K)})_{11} = C_{\min}$ and $(C_{m(K)})_{mm} = -C_{\max}$. In consequence, we can apply the above procedure for

the $f = C_{\max}$ framing of knot $m(K)$:

$$\begin{aligned} F_{(m(K))^{f=C_{\max}}}(x,a,q) = & \sum_{d_1,\cdots,d_{m-1}} (-1)^{\sum_i (C_{ii}+C_{\max})d_i} a^{\sum_i (a_m-a_i)d_i} \\ & \times q^{\sum_i (l_m-l_i)d_i} x^{\sum_i (C_{\max}-C_{im}-1)d_i} q^{-\frac{1}{2}\sum_{i,j} C_{ij}d_i d_j} \\ & \times q^{\sum_i C_{im}d_i \sum_i d_i} q^{-\frac{1}{2}C_{\max}(\sum_i d_i)^2} q^{-\sum_{i<j} d_i d_j} \frac{(x;q^{-1})_{d_1+\cdots+d_{m-1}}}{\prod_{i=1}^{m-1}(q)_{d_i}}. \end{aligned} \tag{4.4.2}$$

Equations (4.4.1) and (4.4.2) are very close to the quiver form. The simplest way of reaching it is an application of Lemma 4.5 from [KRSS19]:

$$\begin{aligned} \frac{(x;q^{-1})_{d_1+\ldots+d_n}}{(q)_{d_1}\cdots(q)_{d_n}} &= \frac{(x\,q^{1-\sum_i d_i};q)_{d_1+\ldots+d_n}}{(q)_{d_1}\cdots(q)_{d_n}} \\ &= \sum_{\alpha_1+\beta_1=d_1} \cdots \sum_{\alpha_n+\beta_n=d_n} (-q^{\frac{1}{2}})^{\beta_1^2+\ldots+\beta_n^2+2\sum_{i=1}^{n-1}\beta_{i+1}(d_1+\ldots+d_i)} \\ &\quad \times \frac{\left(x\,q^{\frac{1}{2}-\sum_i \alpha_i-\sum_i \beta_i}\right)^{\beta_1+\cdots+\beta_n}}{(q)_{\alpha_1}(q)_{\beta_1}\cdots(q)_{\alpha_n}(q)_{\beta_n}}. \end{aligned} \tag{4.4.3}$$

This expansion leads to expressions for the knot complement quivers found in [Kuc20]. On the other hand, we can use the following formula:

$$(x;q^{-1})_d = (xq^{1-d};q)_d = \frac{(xq^{1-d};q)_\infty}{(xq;q)_\infty} = \sum_{i,j} (-1)^i x^{i+j} q^{i+j} q^{-di} q^{\frac{1}{2}(i^2-i)} \frac{1}{(q)_i (q)_j}. \tag{4.4.4}$$

Since it only adds two nodes instead of doubling them, this will produce smaller quivers. In addition to the method presented above, quivers corresponding to knot complements can often be obtained directly by matching a quiver adjacency matrix and the change of variables against an order by order expansion of $F_K$ obtained from recursion using $\hat{A}$-polynomials, as we discussed in Sections 4.2 and 4.3.

### 4.4.2 Examples

We illustrate these techniques on the $4_1$ knot. First, we shall obtain the quiver for the slope $-\frac{1}{2}$ non-abelian branch of the figure-eight knot. We start from the expression for the coloured HOMFLY-PT polynomial for $\mathbf{4}_1$ obtained in [KRSS19]:

$$P_k(\mathbf{4}_1;a,q) = \sum_{\tilde{d}_1+\cdots+\tilde{d}_5=k} (-q^{\frac{1}{2}})^{\tilde{\mathbf{d}}\cdot C\cdot\tilde{\mathbf{d}}} a^{\tilde{d}_2-\tilde{d}_5} q^{-\tilde{d}_2-\frac{1}{2}\tilde{d}_3+\frac{1}{2}\tilde{d}_4+\tilde{d}_5} \frac{(q)_k}{(q)_{\tilde{\mathbf{d}}}}, \tag{4.4.5}$$

where

$$C = \begin{pmatrix} 0 & 0 & -1 & 0 & -1 \\ 0 & 2 & 0 & 1 & -1 \\ -1 & 0 & -1 & 0 & -2 \\ 0 & 1 & 0 & 1 & -1 \\ -1 & -1 & -2 & -1 & -2 \end{pmatrix}.$$

We need to add framing $f = 2$, i.e. to multiply by $q^{k(k-1)}$. Since

$$C + 2 \begin{pmatrix} 1 & \cdots & 1 \\ \vdots & & \vdots \\ 1 & \cdots & 1 \end{pmatrix}$$

has 0 in the bottom right corner and all entries in the last row are non-negative, we replace $\tilde{d}_5 = k - \tilde{d}_1 - \tilde{d}_2 - \tilde{d}_3 - \tilde{d}_4$ in (4.4.5) and perform the substitution $q^k \to x$. We obtain – up to an overall prefactor – the following expression:

$$F_{4_1}^{(-\frac{1}{2})}(x,a,q) = \sum_{\tilde{d}_1,\tilde{d}_2,\tilde{d}_3,\tilde{d}_4 \geq 0} (-1)^{\tilde{d}_3+\tilde{d}_4} a^{\tilde{d}_1+2\tilde{d}_2+\tilde{d}_3+\tilde{d}_4} q^{-\tilde{d}_1-2\tilde{d}_2-\frac{3\tilde{d}_3+\tilde{d}_4}{2}} q^{\frac{1}{2}\sum_{i,j=1}^4 \tilde{C}_{ij}\tilde{d}_i\tilde{d}_j} \times x^{\tilde{d}_1+\tilde{d}_2+\tilde{d}_4} \frac{(x;q^{-1})_{\tilde{d}_1+\tilde{d}_2+\tilde{d}_3+\tilde{d}_4}}{(q)_{\tilde{\mathbf{d}}}},$$

where

$$\tilde{C} = \begin{pmatrix} 0 & 0 & 0 & 0 \\ 0 & 2 & 1 & 1 \\ 0 & 1 & 1 & 1 \\ 0 & 1 & 1 & 1 \end{pmatrix}.$$

In order to obtain $F_K$ in a quiver form, we need to expand the $q$-Pochhammer $(x;q^{-1})_{\tilde{d}_1+\tilde{d}_2+\tilde{d}_3+\tilde{d}_4}$. Using the expansion (4.4.4), we get

$$(x;q^{-1})_{d_1+\ldots+d_4} = \sum_{i,j\geq 0} (-1)^i x^{i+j} q^{\frac{1}{2}i+j} q^{-i(d_1+d_2+d_3+d_4)} q^{\frac{1}{2}i^2} \frac{1}{(q)_i (q)_j},$$

which gives us a quiver form with six summation variables[10]:

$$(d_1,\ldots,d_6) = (\tilde{d}_1,\ldots,\tilde{d}_4,i,j)$$

[10] As opposed to 8 if we had used (4.4.3)

and with the quiver matrix $C$ and vector $\mathbf{x}$ given by,

$$C = \begin{pmatrix} 0 & 0 & 0 & 0 & -1 & 0 \\ 0 & 2 & 1 & 1 & -1 & 0 \\ 0 & 1 & 1 & 1 & -1 & 0 \\ 0 & 1 & 1 & 1 & -1 & 0 \\ -1 & -1 & -1 & -1 & 1 & 0 \\ 0 & 0 & 0 & 0 & 0 & 0 \end{pmatrix}, \quad \begin{pmatrix} x_1 \\ x_2 \\ x_3 \\ x_4 \\ x_5 \\ x_6 \end{pmatrix} = \begin{pmatrix} xaq^{-1} \\ xa^2q^{-2} \\ aq^{-\frac{3}{2}} \\ xaq^{-\frac{1}{2}} \\ xq^{\frac{1}{2}} \\ xq \end{pmatrix}. \tag{4.4.6}$$

Let us move to the abelian branch. In that case we cannot apply the reasoning from Section 4.4.1 since some entries of conormal quiver are negative. In particular, we have $C_{\min} = -2$, so framing 2 would be needed, as we saw in the paragraph above. However, for the abelian branch we can use a direct approach, matching the quiver adjacency matrix and the change of variables against order by order expansion of $F_{\mathbf{4}_1}$. This leads to

$$F_{\mathbf{4}_1}(x,a,q) = \sum_{d_1,\cdots,d_6\geq 0} (-q^{\frac{1}{2}})^{\sum_{i,j=1}^{6} C_{ij}d_id_j} \prod_{i=1}^{6} \frac{x_i^{d_i}}{(q)_{d_i}} \tag{4.4.7}$$

with

$$\begin{pmatrix} x_1 \\ x_2 \\ x_3 \\ x_4 \\ x_5 \\ x_6 \end{pmatrix} = \begin{pmatrix} qx \\ qx \\ qx \\ q^{-\frac{1}{2}}ax \\ q^{-\frac{1}{2}}ax \\ q^{-\frac{1}{2}}ax \end{pmatrix},$$

and $C$ given by any of the following matrices:

$$\begin{pmatrix} 0 & 0 & 0 & 0 & 0 & 0 \\ 0 & 0 & -1 & -1 & 0 & 0 \\ 0 & -1 & 0 & 0 & 1 & 0 \\ 0 & -1 & 0 & 1 & 1 & 0 \\ 0 & 0 & 1 & 1 & 1 & 0 \\ 0 & 0 & 0 & 0 & 0 & 1 \end{pmatrix}, \begin{pmatrix} 0 & 0 & 0 & 1 & 0 & 0 \\ 0 & 0 & -1 & -1 & 0 & 0 \\ 0 & -1 & 0 & 0 & 0 & 0 \\ 1 & -1 & 0 & 1 & 1 & 0 \\ 0 & 0 & 0 & 1 & 1 & 0 \\ 0 & 0 & 0 & 0 & 0 & 1 \end{pmatrix}, \begin{pmatrix} 0 & 0 & 0 & 0 & 0 & 0 \\ 0 & 0 & -1 & 0 & 0 & 0 \\ 0 & -1 & 0 & 0 & 1 & -1 \\ 0 & 0 & 0 & 1 & 1 & 0 \\ 0 & 0 & 1 & 1 & 1 & 0 \\ 0 & 0 & -1 & 0 & 0 & 1 \end{pmatrix}. \tag{4.4.8}$$

Note that all these quiver matrices are all equivalent in the sense of [JKLNS21].

An analogous approach applied to the non-abelian branch with slope $-\frac{1}{2}$ leads to

$$F_{\mathbf{4}_1}^{(-\frac{1}{2})}(x,a,q) = \sum_{d_1,\cdots,d_5\geq 0} (-q^{\frac{1}{2}})^{\sum_{1\leq i,j\leq 5} C_{ij}d_id_j} \prod_{i=1}^{5} \frac{x_i^{d_i}}{(q)_{d_i}} \tag{4.4.9}$$

with,

$$C = \begin{pmatrix} 0 & 1 & 0 & 0 & 0 \\ 1 & 0 & 1 & 0 & 0 \\ 0 & 1 & 1 & 1 & 0 \\ 0 & 0 & 1 & 1 & 0 \\ 0 & 0 & 0 & 0 & 1 \end{pmatrix}, \quad \begin{pmatrix} x_1 \\ x_2 \\ x_3 \\ x_4 \\ x_5 \end{pmatrix} = \begin{pmatrix} qx \\ ax \\ q^{\frac{3}{2}}x \\ q^{\frac{3}{2}}x \\ q^{-\frac{1}{2}}ax \end{pmatrix}. \tag{4.4.10}$$

We expect this quiver along with (4.4.6) are equivalent (up to a factor independent of $x$). Far more examples of this method can be found in [EGGKPSS22] but we have excluded them here for brevity.

### $(2, 2p+1)$ torus knots

In [Kuc20] it was shown that there is a recursion relating quivers corresponding to $(2, 2p+1)$ torus knot complements. Those quivers are obtained by expanding $q$-Pochhammer $(x; q^{-1})_d$ in the general formula from Theorem 4.1.3 using (4.4.3). Using expansion (4.4.4), we can obtain the corresponding quivers in a simpler form.

Using Theorem 4.1.3 we compute the following quiver for the trefoil:

$$F_{\mathbf{3}_1}(x, a, q) = \sum_{d_1, \cdots, d_4 \geq 0} (-q^{\frac{1}{2}})^{\mathbf{d} \cdot C \cdot \mathbf{d}} \frac{x^{\mathbf{n} \cdot \mathbf{d}} a^{\mathbf{a} \cdot \mathbf{d}} q^{\mathbf{q} \cdot \mathbf{d} - \frac{1}{2} \sum_i C_{ii} d_i}}{(q)_{\mathbf{d}}},$$

where $q_i - \frac{1}{2} C_{ii} = l_i$ and the vectors $\mathbf{n}, \mathbf{a}, \mathbf{q}$ and the matrix $C$ are given by

$$C = \begin{pmatrix} 1 & 0 & -1 & 0 \\ 0 & 0 & -1 & 0 \\ -1 & -1 & 1 & 0 \\ 0 & 0 & 0 & 0 \end{pmatrix}, \qquad \begin{aligned} \mathbf{n} &= (1, 1, 1, 1), \\ \mathbf{a} &= (1, 0, 0, 0), \\ \mathbf{q} &= (0, 1, 1, 1) = 1 - \mathbf{a}. \end{aligned}$$

The key idea is to keep in mind that the last two rows and columns originate from the expansion of the $q$-Pochhammer $(x, q^{-1})_k$. For more complicated torus knots, the upper-left part will grow, whereas the last two rows and columns remain unchanged. Let us see it in the example of $\mathbf{5}_1$ and $\mathbf{7}_1$ knots. For the $\mathbf{5}_1$ knot we can derive

$$F_{\mathbf{5}_1}(x, a, q) = \sum_{d_1, \cdots, d_6 \geq 0} \left(-q^{\frac{1}{2}}\right)^{\mathbf{d} \cdot C \cdot \mathbf{d}} \frac{x^{\mathbf{n} \cdot \mathbf{d}} a^{\mathbf{a} \cdot \mathbf{d}} q^{\mathbf{q} \cdot \mathbf{d} - \frac{1}{2} \sum_i C_{ii} d_i}}{(q)_{\mathbf{d}}},$$

$$C = \begin{pmatrix} 1 & 0 & 0 & 0 & -1 & 0 \\ 0 & 0 & -1 & -1 & -1 & 0 \\ 0 & -1 & -1 & -2 & -1 & 0 \\ 0 & -1 & -2 & -2 & -1 & 0 \\ -1 & -1 & -1 & -1 & 1 & 0 \\ 0 & 0 & 0 & 0 & 0 & 0 \end{pmatrix}, \qquad \begin{aligned} \mathbf{n} &= (1,1,3,3,1,1), \\ \mathbf{a} &= (1,0,1,0,0,0), \\ \mathbf{q} &= (0,1,0,1,1,1) = 1 - \mathbf{a}, \end{aligned} \tag{4.4.11}$$

whereas for $\mathbf{7}_1$ we have

$$F_{\mathbf{7}_1}(x,a,q) = \sum_{d_1,\cdots,d_8 \geq 0} \left(-q^{\frac{1}{2}}\right)^{\mathbf{d}\cdot C\cdot\mathbf{d}} \frac{x^{\mathbf{n}\cdot\mathbf{d}} a^{\mathbf{a}\cdot\mathbf{d}} q^{\mathbf{q}\cdot\mathbf{d} - \frac{1}{2}\sum_i C_{ii} d_i}}{(q)_{\mathbf{d}}}$$

$$C = \begin{pmatrix} 1 & 0 & 0 & 0 & 0 & 0 & -1 & 0 \\ 0 & 0 & -1 & -1 & -1 & -1 & -1 & 0 \\ 0 & -1 & -1 & -2 & -2 & -2 & -1 & 0 \\ 0 & -1 & -2 & -2 & -3 & -3 & -1 & 0 \\ 0 & -1 & -2 & -3 & -3 & -4 & -1 & 0 \\ 0 & -1 & -2 & -3 & -4 & -4 & -1 & 0 \\ -1 & -1 & -1 & -1 & -1 & -1 & 1 & 0 \\ 0 & 0 & 0 & 0 & 0 & 0 & 0 & 0 \end{pmatrix}, \qquad \begin{aligned} \mathbf{n} &= (1,1,3,3,5,5,1,1), \\ \mathbf{a} &= (1,0,1,0,1,0,0,0), \\ \mathbf{q} &= (0,1,0,1,0,1,1,1) \\ &= 1 - \mathbf{a}. \end{aligned}$$

Using the general formula from Theorem 4.1.3, we can show that the pattern continues and

$$F_{T_{2,2p+1}}(x,a,q) = \sum_{d_1,\cdots,d_{2p+2} \geq 0} \left(-q^{\frac{1}{2}}\right)^{\mathbf{d}\cdot C\cdot\mathbf{d}} \frac{x^{\mathbf{n}\cdot\mathbf{d}} a^{\mathbf{a}\cdot\mathbf{d}} q^{\mathbf{q}\cdot\mathbf{d} - \frac{1}{2}\sum_i C_{ii} d_i}}{(q)_{\mathbf{d}}}$$

$$C = \begin{pmatrix} \mathbf{I}_{2p} - \mathbf{D} & \mathbf{-1} & \mathbf{0} \\ \mathbf{-1} & 1 & 0 \\ \mathbf{0} & 0 & 0 \end{pmatrix}, \qquad \begin{aligned} \mathbf{n} &= (1,1,3,3,\cdots,2p-1,2p-1,1,1), \\ \mathbf{a} &= (1,0,1,0,\cdots,1,0,0,0), \\ \mathbf{q} &= (0,1,0,1,\cdots,0,1,1,1) = \mathbf{1} - \mathbf{a}, \end{aligned}$$

where $\mathbf{-1}, \mathbf{0}$ denote constant vectors of appropriate size, $\mathbf{I}_{2p}$ is the identity matrix and $\mathbf{D}$ is the matrix $\mathbf{D}_{ij} = \min(i,j) - 1$ with $1 \leq i, j \leq 2p$. Note that we always have a totally disconnected node, which we can remove and replace with a $q$-Pochhammer prefactor.

### 4.4.3 Quivers from $R$-matrices

Another method which allows us to find quiver forms is to get them directly from our $R$-matrix expressions.

**Theorem 4.4.12.** *For any positive braid knot $K$, there is an algorithm to produce a quiver form of $F_K^N(x,q)$ from the $R$-matrix state sum.*

*Proof.* The essential idea behind this proof is that the form of the ${}_{\mathfrak{sl}_N}R$ matrix given in (3.1.2) already closely resembles a quiver form thanks to the $(q)_{\mathbf{r}}$ in the denominator. All we will need to do is keep careful track of labels. Let $\beta_K$ denote a positive $n+1$-strand braid representative for a knot $K$. Following the construction in Chapter 3, we start by colouring the open strand by $\mathbf{0}$ and the remaining strands $\mathbf{a}_1, \cdots, \mathbf{a}_n$.

Assume that that $\beta_K$ has $m$ crossings which we label 1 to $m$. For each crossing $\alpha$, pick a non-negative vector $\mathbf{r}_\alpha = r^j_{\alpha,i}$ with $1 \leq i \leq j \leq N-1$. Additionally, let $\mathbf{c}_\alpha$, $\mathbf{d}_\alpha$ and $\mathbf{c}'_\alpha$, $\mathbf{d}'_\alpha$ respectively denote the labels on the incoming and outgoing strands for crossing $\alpha$. Note that $c'_{\alpha,i} = d_{\alpha,i} + |(r_\alpha)^{(i,N-1)}_{(1,i)}|$ and $d'_{\alpha,i} = c_{\alpha,i} - |(r_\alpha)^{(i,N-1)}_{(1,i)}|$. After passing through all crossings, let $\mathbf{b}_0, \mathbf{b}_1, \cdots, \mathbf{b}_n$ denote the final labellings on the strands. Each $\mathbf{b}_i$ is a sum of components of the $\mathbf{a}_i$'s and $\mathbf{r}_\alpha$'s depending on the precise braid $\beta$. Then we can re-write our state sum for $F_K$, (3.2.1), as

$$\sum_{\substack{\mathbf{a}_1,\cdots,\mathbf{a}_n \\ \mathbf{r}_\alpha}} \delta_{\mathbf{0},\mathbf{b}_0} \prod_{i=1}^{n} \delta_{\mathbf{a}_i,\mathbf{b}_i} x^{\frac{N-1}{2}} q^{-|\mathbf{a}_i|} \prod_{\alpha \in \text{crossings}} {}_{\mathfrak{sl}_N}R^{\mathbf{c}'_\alpha,\mathbf{d}'_\alpha}_{\mathbf{c}_\alpha,\mathbf{d}_\alpha}. \tag{4.4.13}$$

First we need to deal with the fact that the summation over $\mathbf{a}_i$ is not free as we require $a_{i,j} \geq a_{i,j+1}$. Hence, we instead sum over $\overline{a}_{i,j}$, defined by $\overline{a}_{i,j} = a_{i,j} - a_{i,j+1}$ so that $a_{i,j} = \sum_{k=k}^{N-1} \overline{a}_{i,k}$. Clearly, our delta functions can be rewritten as $\delta_{\mathbf{0},\overline{\mathbf{b}}_0}$, $\delta_{\overline{\mathbf{a}}_i,\overline{\mathbf{b}}_i}$.

Now to deal with the $\delta$ functions, we can apply a trick. Consider the following ratio of $q$-Pochhammers for $a, b \in \mathbb{N}$:

$$\frac{(q^{1+b-a},q)_a}{(q)_a}.$$

If $a > b$, then this is 0 and if $a = b$, then this is 1. As the $R$-matrix preserves the sum of labels we are guaranteed

$$\sum_{i=1}^{n} \overline{\mathbf{a}}_i = \sum_{i=0}^{n} \overline{\mathbf{b}}_i.$$

Hence if for some $i, j$ value $\overline{a}_{i,j} < \overline{b}_{i,j}$ there must be another $i'$ such that $\overline{a}_{i',j} > \overline{b}_{i',j}$. Additionally, if $\overline{b}_{i,j}$ is ever negative, then there will be an $R$-matrix element which

would evaluate to 0. Thus, the $\delta$ functions can be replaced by the following ratio of $q$-Pochhammers:

$$\prod_{i,j} \frac{(q^{1+\overline{b}_{i,j}-\overline{a}_{i,j}})_{\overline{a}_{i,j}}}{(q)_{\overline{a}_{i,j}}}.$$

Adding this into equation (4.4.13) we get[11]

$$\sum_{\substack{\overline{\mathbf{a}}_1,\cdots,\overline{\mathbf{a}}_n \\ \mathbf{r}_\alpha}} x^{\frac{N-1}{2}} \prod_{i,j,\alpha} q^{-\sum_j j\ \overline{a}_{i,j}} \frac{(q^{1+\overline{b}_{i,j}-\overline{a}_{i,j}}, q)_{\overline{a}_{i,j}}}{(q)_{\overline{a}_{i,j}}} \mathfrak{sl}_N R^{\mathbf{c}'_\alpha,\mathbf{d}'_\alpha}_{\mathbf{c}_\alpha,\mathbf{d}_\alpha}.$$

This expression is now 90% of the way towards a quiver form. Looking again at the equation for the $R$-matrix (3.1.2) we see that for each crossing $\alpha$ we have a quadratic power of $q$ and a linear power of $x$ depending on $\mathbf{c}_\alpha$, $\mathbf{d}_\alpha$ and $\mathbf{r}_\alpha$. We also see every summation variable appear in the denominator a single time as a $q$-Pochhammer. All we need to do it deal with the $q$-Pochhammers which appear in the numerator, this can be done easily by repeated application of Lemma 4.5 from [KRSS19]. □

This theorem can also be easily extended to homogeneous braid knots as well, using the inverted state sum discussed in Section 3.3.

**Theorem 4.4.14.** *For any homogeneous braid knot $K$, there is an algorithm to produce a quiver form of $F_K^N(x,q)$ from the inverted state sum.*

While this theorem is in principle constructive, in practise the quivers it produces are quite large and scale quadratically as $N$ increases. Indeed, given an $n+1$ strand braid with $c$ crossings, the size of the quiver produced will have size roughly[12] $2n(N-1)+2c(N-1)(N-2)$. For say a 3 strand, 10 crossing knot (E.g. $10_{139}$ or $10_{152}$) with $N=3$ this is already 48 and for $N=4$ it is 128. This scaling in $N$ also makes it essentially impossible to use this construction to generate a quiver for the $a$ deformed $F_K$. All you can do is generate the $\mathfrak{sl}_2$ or $\mathfrak{sl}_3$ quiver and see if it admits and easy $a$-deformation, for more information see [EGGKPSS22].

## 4.5 The $B$-Polynomial and Holomorphic Lagrangian

In [MM21], it was observed that the cyclotomic coefficients of the coloured HOMFLY-PT polynomials satisfy not only a $q$-difference equations in the colour, $k$, but also

[11] Note that as $a_{i,j} = \sum_{k=k}^{N-1} \overline{a}_{i,k}$ we have $|\mathbf{a}_i| = \sum_j j\ \overline{a}_{i,j}$.

[12] The factors of 2 come from applications of Lemma 4.5 from [KRSS19], each application doubles the number of nodes. It needs to be applied once for the incoming labels $\overline{a}_{i,j}$ for $i \in \{1,\cdots n\}$, $j \in \{1,\cdots,N-1\}$ and twice for crossing labels $r^j_{\alpha,i}$ with $1 \leq i \leq j \leq N-1$.

in the rank, $N$. This immediately implies that the quantum invariants $\mathcal{P}_k^N(K;q)$ are also $q$-holonomic in $N$.

In addition to $\hat{x}, \hat{y}$ which appear in the $A$-polynomial, define the operators $\hat{a}, \hat{b}$ by

$$\begin{aligned} \hat{x}\mathcal{P}_k^N(K;q) &= q^k\mathcal{P}_k^N(K;q), & \hat{a}\mathcal{P}_k^N(K;q) &= q^N\mathcal{P}_k^N(K;q), \\ \hat{y}\mathcal{P}_k^N(K;q) &= \mathcal{P}_{k+1}^N(K;q), & \hat{b}\mathcal{P}_k^N(K;q) &= \mathcal{P}_k^{N+1}(K;q). \end{aligned}$$

We see that $(\hat{a}, \hat{b})$ interact with the group rank $N$ in complete analogy with the action of $(\hat{x}, \hat{y})$ on the colour $k$ and satisfy the same commutation relation $\hat{b}\hat{a} = q\hat{a}\hat{b}$.

As indicated above, $\mathcal{P}_k^N(K;q)$ satisfies a recurrence relation in variable $N$. We will call the corresponding $q$-difference operator the *quantum B-polynomial* and denote it by $\hat{B}_K(\hat{a}, \hat{b}, \hat{x}, q)$. In other words, the recurrence relation in $N$ is given by

$$\hat{B}_K(\hat{a}, \hat{b}, \hat{x}, q)\mathcal{P}_k^N(K;q) = 0.$$

Similarly to $\hat{A}_K$, $\hat{B}_K$ also annihilates $F_K(x, a, q)$ associated to any branch:

$$\hat{B}_K(\hat{a}, \hat{b}, x, q)F_K^{(\alpha)}(x, a, q) = 0,$$

where

$$\hat{a}F_K(x, a, q) = aF_K(x, a, q) \qquad \hat{b}F_K(x, a, q) = F_K(x, qa, q).$$

Quantum $B$-polynomials for simple knots are given in Table 4.1.

| $K$ | $\hat{B}_K(\hat{a}, \hat{b}, x, q)$ |
|---|---|
| $0_1$ | $1 - \hat{b}$ |
| $3_1$ | $qx^2 - x(1 + q - (1 + qx)\hat{a} + qx^2\hat{a}^2)\hat{b} + (1 - \hat{a})(1 - qx\hat{a})\hat{b}^2$ |
| $4_1$ | $q^2x^2\hat{a}^2 + qx\hat{a}(1 + q - (1 + 3qx + q^2x^2)\hat{a} + qx^2(1 + q)\hat{a}^2)\hat{b}$ $+ (1 - \hat{a})(1 - qx\hat{a})(1 - 2qx(1 + qx)\hat{a} + q^3x^3\hat{a}^2)\hat{b}^2$ $- x(1 - \hat{a})(1 - q\hat{a})(1 - qx\hat{a})(1 - q^2x\hat{a})\hat{b}^3$ |
| $5_1$ | $-qx^4\big(1 + q + q^2 - (1 + q)(1 + qx)\hat{a} + qx(1 + x + qx)\hat{a}^2$ $- qx^2(1 + qx)\hat{a}^3 + q^2x^4\hat{a}^4\big)\hat{b}$ $+ x^2(1 - \hat{a})(1 - qx\hat{a})(1 + q + q^2 - q(1 + qx)\hat{a} + q^2x^2(1 + q)\hat{a}^2)\hat{b}^2$ $- (1 - \hat{a})(1 - q\hat{a})(1 - qx\hat{a})(1 - q^2x\hat{a})\hat{b}^3 + q^3x^6$ |

Table 4.1: Quantum $B$-polynomials for some simple knots.

### 4.5.1 Classical $B$-polynomial

Similarly to the case of $A$-polynomial, the $q \to 1$ limit of the quantum $B$-polynomial can be obtained directly from the effective twisted superpotential:

$$\lim_{q\to 1} \hat{B}_K(\hat{a}, \hat{b}, x, q) = B_K(a, b, x) = 0 \quad \Leftrightarrow \quad \log b = \frac{\partial \widetilde{\mathcal{W}}^{\text{eff}}_{T[M_K]}(x, a)}{\partial \log a}. \tag{4.5.1}$$

Recall that $\widetilde{\mathcal{W}}^{\text{eff}}_{T[M_K]}(x, a)$ comes from integrating out the dynamical fields in the twisted superpotential (see Section 2.5.2), which can be read from the double-scaling limit (2.5.3) with $N \to \infty$, $q^N = a$:

$$\mathcal{P}^N_k(K; q) \overset{\substack{k,N\to\infty \\ \hbar\to 0}}{\longrightarrow} \int \prod_i \frac{dz_i}{z_i} \exp\left[\frac{1}{\hbar}\widetilde{\mathcal{W}}(z_i, x, a) + O(\hbar^0)\right].$$

The construction of $A$- and $B$-polynomials via the effective twisted superpotential (2.5.5, 4.5.1) immediately leads to the constraint

$$\frac{\partial \log y}{\partial \log a} = \frac{\partial^2 \widetilde{\mathcal{W}}^{\text{eff}}_{T[M_K]}(x, a)}{\partial \log x \, \partial \log a} = \frac{\partial \log b}{\partial \log x}. \tag{4.5.2}$$

This relation allows us to derive $A(x, y, a)$ from $B(a, b, x)$ up to a function $f(x)$. Namely, we can solve $B(a, b, x) = 0$ for $b(a, x)$, integrate over $\log a$

$$\widetilde{\mathcal{W}}^{\text{eff}}_{T[M_K]}(x, a) = \int \log b(a, x) \; d(\log a) + f(x),$$

and differentiate with respect to $\log x$:

$$A_K(x, y, a) = 0 \quad \Leftrightarrow \quad \log y = \frac{\partial}{\partial \log x}\left(\int \log b(a, x) \; d(\log a) + f(x)\right).$$

We can apply the same reasoning to derive $B(a, b, x)$ from $A(x, y, a)$ up to a function $f(a)$. If we consider what happens when we fix a branch (A solution $y(x, a)$ to $A_K(x, y, a) = 0$), it follows from this that there is a canonical one-to-one correspondence between the branches of $b$ and the branches of $y$, as functions of $x$ and $a$.

Classical $B$-polynomials for simple knots in the reduced normalisation are given in Table 4.2. Observe that, if we set $x = 1$, we see that $B_K(a, b, x = 1)$ always has a factor of $b - 1$. This is analogous to the presence of the factor $y - 1$ in $A_K(x, y, a = 1)$. This condition lets us fix the integration constants coming from equation (4.5.2).

| $K$ | $B_K(a,b,x)$ |
|---|---|
| $0_1$ | $1-b$ |
| $3_1$ | $x^2-x(2-(1+x)a+x^2a^2)b+(1-a)(1-xa)b^2$ |
| $4_1$ | $x^2a^2+ax(2-(1+3x+x^2)a+2x^2a^2)b$ $+(1-a)(1-xa)(1-2x(1+x)a+x^3a^2)b^2$ $-x(1-a)(1-a)(1-xa)(1-xa)b^3$ |
| $5_1$ | $x^6-x^4\big(3-2(1+x)a+x(1+2x)a^2-x^2(1+x)a^3+x^4a^4\big)b$ $+x^2(1-a)(1-xa)(3-(1+x)a+2x^2a^2)b^2$ $-(1-a)(1-a)(1-xa)(1-xa)b^3$ |
| $5_2$ | $1-x^{-2}\left(2a^2x^3+a^2x^2-4ax^2-ax-a+3x+1\right)b$ $-x^{-3}(a-1)(ax-1)\left(a^3x^4-3a^2x^3-2a^2x^2\right.$ $\left.+5ax^2+ax+a-3x-3\right)b^2$ $-x^{-4}(a-1)^2(ax-1)^2\left(a^2x^3-2ax^2-ax+x+3\right)b^3$ $+x^{-5}(a-1)^3(ax-1)^3b^4$ |

Table 4.2: Classical $B$-polynomials for some simple knots.

### 4.5.2 The Holomorphic Lagrangian

Given the close relation between $A$ and $B$ explored in the previous section, it seems natural to expect a higher structure which unifies them. This should be a holomorphic Lagrangian[13] $\gamma_K \subset (\mathbb{C}^*)^4$ with symplectic form

$$\Omega = d\log x \wedge d\log y + d\log a \wedge d\log b$$

such that the projections to $(\mathbb{C}^*)^3_{x,y,a}$ and $(\mathbb{C}^*)^3_{x,a,b}$ are the $\mathcal{A}_K$ and $\mathcal{B}_K$ varieties. This variety, or more precisely its defining ideal, which we denote $\Gamma_K$, should also admit a quantization corresponding to the ideal of relations which annihilates $F_K$

$$\widehat{\Gamma}_K = \{\hat{T} \in \mathbb{C}[\hat{x}^{\pm 1}, \hat{a}^{\pm 1}, q^{\pm 1}, \hat{y}^{\pm 1}, \hat{b}^{\pm 1}] \mid \hat{T}F_k(x,a,q) = 0\}.$$

Somewhat surprisingly, even for the Trefoil, we can show that the $\widehat{\Gamma}_{3^1}$ is bigger than $\langle \widehat{A}_{3^1}, \widehat{B}_{3^1}\rangle$. Indeed, we find the relation

$$\widehat{D}_{\mathbf{3}_1} = 1 - x^{-1}(1-q^{-1}\hat{a})(1-q\hat{a}\hat{x}^2)\hat{b} - \hat{y}$$

in $\widehat{\Gamma}_{3^1}$ and it can be easily checked that $\widehat{D}_{\mathbf{3}_1}$ is not in $\langle \widehat{A}_{3^1}, \widehat{B}_{3^1}\rangle$. This example is the $p=1$ case of a more general $q$ difference relation for $(2, 2p+1)$ torus knots:

$$(1-q^{-1}\hat{a}\hat{x}) - x^p(1-q^{-1}\hat{a}\hat{x}^2)\hat{b}^{-1} + q^{-p-1}a^{p+1}\hat{x}^{2p+1}(1-x)\hat{y}^{-1}.$$

[13] This naturally appears in the physics setting as the Coloumb branch of a $3d-5d$ coupled system, see [EGGKPSS22], but we will not discuss that here.

This shows that for all these knots $\widehat{\Gamma}_{T^{2,2p+1}}$ is bigger than $\langle \widehat{A}_{T^{2,2p+1}}, \widehat{B}_{T^{2,2p+1}} \rangle$.

In general, computing the quantum ideal $\widehat{\Gamma}$ is difficult, but the classical ideal can be found using quiver forms. Starting with a quiver expression, simply eliminate variables from the quiver $A$-polynomials to get the ideal defining $\Gamma_K$.

*Chapter 5*

# RESURGENT ANALYSIS IN CHERN SIMONS THEORY

The main goal of this chapter is to investigate to what extent non-perturbative information can be extracted from a perturbative series. We will first describe the basic topological invariants of closed 3-manifolds $M^3$ that are expected to match with the position and strength of singularities on the Borel plane, and how to compute these for surgeries $M^3 == S^3_{\frac{p}{r}}$. We then put this to the test by exploring the Borel plane in a couple of simple cases, $S^3_{\frac{1}{2}}(4_1)$, $S^3_{\pm\frac{1}{2}}(5_2)$ to see how well these predictions line up. Finally, we will explore some surprising and previously unknown regularities in the surgery coefficient, $\frac{p}{r}$, which appears in the aforementioned analysis.

## 5.1 Borel Plane Predictions from Knot Polynomials

The computation of these invariants echoes the construction of $S^3_{\frac{p}{r}}(K)$ itself; namely, the relevant invariant of a closed 3-manifold is obtained via a suitable surgery formula from the corresponding invariant of the knot complement, $S^3 \setminus K$, and the surgery coefficient $\frac{p}{r}$. The invariant of a knot complement, in turn, can be expressed in terms of a suitable knot polynomial. For the position of singularities on the Borel plane and their associated Stokes coefficients, the relevant knot polynomials are respectively the A-polynomial and the twisted Alexander polynomial. While the former has already appeared in the study of complex Chern Simons theory, to the best of our knowledge the twisted Alexander polynomial so far did not play a noticeable role in this study, and it is our goal here to bring it into the spotlight.

### 5.1.1 Spectral curves for complex Chern Simons theory

Conceptually, the $A$-polynomial variety[1], $\mathcal{A}_K \subset (\mathbb{C}^*)^2$ should, be thought of as a holomorphic Lagrangian subvariety. That way, it naturally represents the classical limit of a state in $\mathcal{H}(T^2)$ associated with the knot complement. Indeed, one can explicitly verify that[2] $\omega = \frac{\partial y}{y} \wedge \frac{\partial x}{x}$ vanishes when restricted to the image of $\mathcal{M}_{\text{flat}}(M^3, G)$ in $\mathcal{M}_{\text{flat}}(\Sigma, G)$, for more general $M^3$ with boundary $\Sigma = \partial M^3$ and for $G$ of higher rank. Therefore, in the WKB approximation, the state associated to the knot complement is a function (more precisely, a half-density) on $\mathcal{A}_K \subset (\mathbb{C}^*)^2$

[1] As long as one remembers the $\mathbb{Z}_2$ quotient, and all the ingredients are properly invariant under the Weyl group action, it sometimes can be omitted at the intermediate stages to avoid clutter.

[2] Note $\omega$ is the natural holomorphic Atiyah-Bott symplectic form on the space of flat connections.

obtained by integrating the primitive 1-form $d^{-1}\omega|_{\mathcal{A}_K}$ along a path on $\mathcal{A}_K$ that connects the point of interest $(x, y)$ to some reference point. This has been discussed in great detail throughout the history of the subject; see [KK90, GM08, GMP16] and references therein.

In particular, for a general surgery as in (2.0.4), flat connections on $S^3 \setminus K$ that extend to $S^3_{\frac{p}{r}}(K)$ satisfy $y^r x^p = 1$ since the Dehn filling has the effect of annihilating the element $l^r m^p$ in homology. In practice, almost all points in the intersection of $A_K(x, y) = 0$ and $y^r x^p = 1$ correspond to true extendable flat connections, and the WKB integral along a path on the $A$-polynomial curve provides an easy method that allows to compute all Chern Simons invariants $CS(\alpha)$ for simple surgeries.

**Proposition 5.1.1.** *Let $\rho_1 : \pi_1(S^3\backslash K) \to \mathrm{SL}(2,\mathbb{C})$ be a non-parabolic representation which extends to a flat connection $\alpha$ on $S^3_{\frac{p}{r}}(K)$. Then there exists a path $\rho_t$ of non-parabolic representations with $\rho_0 = 1$ and*

$$2\pi^2 CS(\alpha) = \int_\gamma \frac{\log(y)}{x}\, dx + \frac{vp}{2}\log((\rho_1)_x)^2 + \frac{sr}{2}\log\big((\rho_1)_y\big)^2 - vr\log((\rho_1)_x)\log\big((\rho_1)_y\big), \tag{5.1.2}$$

*where $v, s$ is a pair of integers satisfying $ps - rv = 1$.*

Note that, due to branching, $\gamma$ should be thought of as a path in the Riemann surface associated to the map $(x, y) \mapsto (\log(x), \log(y))$. Specifically, for 0 surgeries this formula simplifies to

$$CS(\rho_1) = \frac{1}{2\pi^2}\left(\int_\gamma \frac{\log(y)}{x}\, dx + \log((\rho_1)_x)\log\big((\rho_1)_y\big)\right) \tag{5.1.3}$$

and for the so-called "small" $\frac{1}{r}$ surgeries it gives

$$CS(\rho_1) = \frac{1}{2\pi^2}\left(\int_\gamma \frac{\log(y)}{x}\, dx + \frac{j}{2}\log\big((\rho_1)_y\big)^2\right). \tag{5.1.4}$$

Using Lemma 5.1.1, if we are given a path in $\mathcal{A}_K$, provided a lift to a path in the representation variety of $S^3 \setminus K$ exists, we can apply equation (5.1.2) without ever having to explicitly construct the lift. For simple knots, these lifts usually exist, and so the problem of computing Chern Simons values boils down to finding appropriate paths in $\mathcal{A}_K$. One minor caveat is that different paths $\gamma$ between $\rho_0$ and $\rho_1$ may lead to $(\rho_1)_x$ and $(\rho_1)_y$ ending on different branches of log, and this can produce different CS values. Thus, this method requires a careful treatment of branches.

As a variety, $\mathcal{A}_K$ decomposes into the union of two subvarieties, $\mathcal{A}_K^{ab}$ and $\mathcal{A}_K^{irred}$, called the abelian and irreducible branches, respectively. the abelian branch is simply the plane $y = 1$ coming from abelian representations, which behave identically for all knots as $H_1(S^3 \setminus K) = \mathbb{Z}$. The irreducible branch corresponds to irreducible representations and is the closure of what remains after the abelian branch is removed, $\mathcal{A}_K^{irred} = \overline{\mathcal{A}_K \setminus \mathcal{A}_K^{ab}}$. Correspondingly, the $A$-polynomial factors into polynomials representing the two branches

$$A_K(x, y) = (y - 1)A_K^{irred}(x, y). \tag{5.1.5}$$

As we want to start all paths at the trivial flat connection $A = 0$, i.e. at $(x, y) = (1, 1)$, the first problem we encounter is how to travel off the abelian branch. While points connecting the abelian and irreducible branches in $\mathcal{A}_K$ are easy to find[3], we need to find a branch point which, when lifted to the representation variety of the knot complement, lifts to a path connecting the abelian and irreducible branches.

**Lemma 5.1.6** ([CCGLS94]: Section 6)**.** *In the representation variety of the knot complement, the abelian and irreducible branches meet along non-abelian reducible representations. In $\mathcal{A}_K$, these reducible representations map surjectively to points $(x, 1)$ where $x^2$ is a root of the Alexander polynomial of the knot $K$.*

We provide a brief sketch of the proof here. Up to conjugation, non-abelian reducible representations are representations $\rho$ landing in the upper triangular subgroup. Assume $\rho$ acts on an arbitrary element by

$$\rho(g) = \begin{bmatrix} x_g & z_g \\ 0 & x_g^{-1} \end{bmatrix}$$

then a path to the abelian branch is given by the family $\rho_t$ which act as

$$\rho_t(g) = \begin{bmatrix} x_g & tz_g \\ 0 & x_g^{-1} \end{bmatrix}.$$

It remains to understand when $\rho$ exists.

If we project $\rho$ onto $\mathcal{A}_K$, we find that the image is heavily constrained. As the longitude $l$ lies in the second commutator subgroup of $\pi_1(S^3 \setminus K)$ and all second commutators of $2 \times 2$ upper triangular matrices are trivial, $\rho$ projects onto a point

[3] They correspond to solutions of $A_K^{irred}(x, 1) = 0$.

$(x, 1)$. Then through careful analysis [DeR67] it can be shown that $\rho$ exists if and only if $x^2$ is a root of the Alexander polynomial.[4]

Altogether, this discussion guarantees that we can always move off the abelian branch and onto the irreducible branch. From here, we move along the irreducible branch until we reach our desired point, taking care when moving between different sheets of the irreducible branch.

### 5.1.2 Reidemeister torsion and the twisted Alexander polynomial

Based on the earlier work in complex Chern Simons theory summarized around equation (2.3.7), we expect the residues $\mathcal{S}_\alpha^\beta$ in (2.3.8) to be related to a 3-manifold invariant called torsion. (See also Conjecture 2.3.9.) This invariant has both an algebraic and analytic description. The analytic description is directly relevant to the way it appears in (2.3.7), as a ratio of one-loop determinants in complex Chern Simons theory. However, it is not as computationally friendly as the algebraic formulation [Fre92, Por15], which will be our main focus here.

Given two bases $\alpha, \beta$ of a vector space $V$ over a field $\mathbb{F}$, let $\eta$ be the unique change of basis matrix satisfying $\alpha_i = \sum_j \eta_{ij}\beta_j$. Define

$$[\alpha, \beta] = \det(\eta) \in \mathbb{F}^\times.$$

**Definition 5.1.7** (Reidemeister Torsion)**.** *Let*

$$C_* : 0 \to C_n \xrightarrow{\partial} C_{n-1} \xrightarrow{\partial} \cdots \xrightarrow{\partial} C_1 \xrightarrow{\partial} C_0 \to 0$$

*be a chain complex of finite-dimensional vector spaces over $\mathbb{F}$ with homology $H_*(C_*, \partial)$. Fix a pair of bases, $\boldsymbol{c}$ for the chain complex and $\boldsymbol{h}$ for the homology, such that $\boldsymbol{c}_i$ and $\boldsymbol{h}_i$ are bases of $C_i$ and $H_i$ respectively. Let $k_j$ be the rank of $\partial : C_j \to C_{j-1}$ and choose a collection of $k_j$ elements $\boldsymbol{s}_j = \{s_{j,i}\} \subset C_j$ such that $\partial \boldsymbol{s}_j = \{\partial s_{j,i}\}$ spans $\mathrm{Im}(\partial)$. For each homology basis $\boldsymbol{h}_j$, choose a lift $\hat{\boldsymbol{h}}_j \subset C_j$. Then the Reidemeister Torsion, $\tau_{C_*,\boldsymbol{c},\boldsymbol{h}}$ is given by:*

$$\tau_{C_*,\boldsymbol{c},\boldsymbol{h}} = \prod_{j=0}^{n} \left[ \left\{ \partial \boldsymbol{s}_{j+1}, \boldsymbol{s}_j, \hat{\boldsymbol{h}}_j \right\}, \boldsymbol{c}_j \right]^{(-1)^{j+1}} \in \mathbb{F}^\times$$

There are a couple of observations to make:

[4] This is a special case of a more general representation deformation problem which is solved by the twisted Alexander polynomial [Wad94].

- Despite appearances, the choices of $s_j$ and $\hat{h}_j$ do not affect the value of $\tau$.
- If we change our basis for $C_*$ and $H_*$, then $\tau$ changes as

$$\frac{\tau_{C_*,\mathbf{c}',\mathbf{h}'}}{\tau_{C_*,\mathbf{c},\mathbf{h}}} = \prod_i \left( \frac{[\mathbf{c}_i', \mathbf{c}_i]}{[\mathbf{h}_i', \mathbf{h}_i]} \right)^{(-1)^i} \tag{5.1.8}$$

Currently, this discussion is purely algebraic, but there is a natural link to geometry. Let $X$ be a CW space, $\tilde{X}$ its universal cover and $\rho : \pi_1(X) \to \mathrm{GL}(V_\rho)$ a linear representation. By construction, $\tilde{X}$ has an induced $CW$ structure upon which $\pi_1(X)$ acts freely. Hence, each term of the cellular chain complex $C(\tilde{X}, \mathbb{Z})$ is a free $\mathbb{Z}[\pi_1(X)]$ module, and so we can define the twisted chain complex

$$C_*(X; V_\rho) = C(\tilde{X}) \otimes_{\mathbb{Z}[\pi_1(X)]} V_\rho.$$

There is a canonical[5] basis for $C_j(X; V_\rho)$ of the form

$$\mathbf{c} = \{\sigma_1 \otimes v_1, \sigma_1 \otimes v_2, \cdots, \sigma_{k_q} \otimes v_n\},$$

where $\{v_1, \cdots, v_n\}$ is a basis of $V_\rho$ and $\sigma_1, \cdots \sigma_{k_q}$ are q-cells giving a basis (as a module) of $C(\tilde{X}, \mathbb{Z})$. Additionally, if there is homology, pick a basis $\mathbf{h}$.

**Definition 5.1.9.** *The Reidemeister torsion $\tau_{X,\boldsymbol{h}}(\rho)$ is*

$$\tau_{X,\boldsymbol{h}}(\rho) = |\tau_{C_*(X;V_\rho),\boldsymbol{c},\boldsymbol{h}}|.$$

Whilst there is a choice in the basis $\mathbf{c}$, the following theorem is well known [Joh, Mil66].

**Theorem 5.1.10.** *$\tau_{X,\boldsymbol{h}}(\rho)$ is a piecewise linear invariant of $X, \boldsymbol{h}$ and $\rho$.*

Observe that for a given group homomorphism $\rho : \pi_1(X) \to \mathrm{SL}(2, \mathbb{C})$, there is a family of Reidemeister torsions corresponding to the family of irreducible representations of $\mathrm{SL}(2, \mathbb{C})$. In the literature, the majority of attention has been on the studying the Reidemeister torsion corresponding to the standard representation, but it is essential here that we work with the adjoint one. To distinguish this choice, we will label $\tau$ as $\tau^{st}$ or $\tau^{adj}$ depending on the context.

[5] Naively, this basis is not canonical as it depends on the chosen cellular structure and a basis for the representation space, but the torsion is independent of both these choices.

Often[6], after quotienting by the conjugation action, the space of representations $\pi_1(X) \to \mathrm{SL}(2,\mathbb{C})$ is finite and, for each representation $\rho$, $C_*(X;V_\rho)$ is acyclic. In these cases, we get a finite collection of $\mathbb{C}$-valued torsion invariants for $X$ which are algebraic and so can be assembled into a rational polynomial called the torsion polynomial $\sigma_X(t)$ by[7]

$$\sigma_X(t) = \prod_{\rho:\pi_1(X)\to\mathrm{SL}(2,\mathbb{C})} (t - \tau_X(\rho)) \in \mathbb{Q}(t). \tag{5.1.11}$$

In the literature, $\sigma_X^{st}(t)$ has been computed for surgeries on torus knots and the $4_1$ knot [Joh, Kit16] but $\sigma_X^{adj}(t)$ has not appeared.

Given a surgery manifold $S^3_{\frac{p}{r}}(K)$, the particular Reidemeister torsion relevant to the residues $\mathcal{S}^{\beta}_{\alpha}$ is expected to be the adjoint torsion $\tau^{adj}_{S^3_{\frac{p}{r}}(K)}(\rho)$. Ideally we would like to find a method to compute this systematically for surgeries $\frac{p}{r}$ as opposed to attempting to proceed via first principals in each case. To do this, we need to study the torsion associated to knot complements. In the literature [Kit15, Tra15a], this problem has mainly been studied in the standard representation however there is a marked difference between the standard and adjoint representations in this case as the adjoint representations will not lead to acyclic complexes.

For knot complements, a general description of the twisted homology groups was given by Porti:

**Lemma 5.1.12** ([Por15], Appendix B)**.** *For a generic representation $\rho : \pi_1(S^3\backslash K) \to \mathrm{SL}(2,\mathbb{C})$, let $V$ denote the adjoint representation of $\mathrm{SL}(2,\mathbb{C})$ and $V_\rho$ the induced representation of $\pi_1(K)$. Then*

$$H_i(S^3\backslash K;V_\rho) = \begin{cases} \mathbb{C} & i = 1,2 \\ 0 & i = 0,3 \end{cases}.$$

*These groups can be realised as*

$$H_1(S^3\backslash K;V_\rho) = \langle i_*(a\otimes[\gamma])\rangle \quad \text{and} \quad H_2(S^3\backslash K;V_\rho) = \langle i_*(a\otimes[T^2])\rangle$$

*where $i_* : H_1(T^2,V_\rho) \to H_1(S^3 \setminus K, V_\rho)$ is the map induced from the boundary inclusion map, $[T^2]$ is a fundamental class, $[\gamma]$ is any non-zero element in $H^1(T^2)$, and $a$ is the unique invariant vector in $V_{\rho|_{T^2}}$.*

[6] In particular this is the case for manifolds which are surgeries on knot complements.

[7] It is conventional to remove denominators to get a non-monic polynomial in $\mathbb{Z}(t)$.

Thus, a choice of $[\gamma] \in H^1(T^2)$ determines the adjoint torsion, and so we define

$$\tau^{adj}_{S^3\backslash K,\ [\gamma]}(\rho) = \tau^{adj}_{S^3\backslash K,\ \{i^*(a\otimes[\gamma]),i^*(a\otimes[T^2])\}}(\rho).$$

For comparison, in the standard case, the twisted complex is acyclic so no choice of $[\gamma]$ is required. Choosing a meridian $m$ and longitude $l$ in $S^3\backslash K$, we can use $\tau^{adj}_{S^3\backslash K,[l]}(\rho)$ to compute $\tau^{adj}_{S^3_{\frac{p}{r}}(K)}(\rho)$.

**Lemma 5.1.13.** *Let $x$ and $y$ denote eigenvalues of $\rho(m)$ and $\rho(l)$ viewed in the standard representation corresponding to a common eigenvector. Then*[8]

$$\tau^{adj}_{S^3_{\frac{p}{r}}(K)}(\rho) = \frac{\left(p\frac{y}{x}\frac{dx}{dy} + r\right)\tau^{adj}_{S^3\backslash K,[l]}(\rho)}{2 - y^2 - y^{-2}}.$$

We will prove this Lemma, but first we compute the adjoint torsion in the simple cases, $S^1$ and $T^2$.

**Proposition 5.1.14.** *For a generic representation $\rho$, $H_*(S^1, V_\rho) \cong H_0 \oplus H_1 \cong \langle [a\otimes p], [a\otimes x]\rangle$ where $p, x$ are generators of $H_0(S^1), H_1(S^1)$ and $a \in V_\rho$ is an invariant vector. Then*

$$\tau^{adj}_{S^1}(\rho) = \tau^{adj}_{S^1,\ \{[a\otimes p],[a\otimes x]\}}(\rho) = \frac{1}{2 - y^2 - y^{-2}}$$

*where $y$ is an eigenvalue of $\rho(x) \in \mathrm{SL}(2,\mathbb{C})$ viewed in the standard representation. Similarly, for $T^2$, $H_*(T^2, V_\rho) \cong \langle [a\otimes p], [a\otimes m], [a\otimes l], [a\otimes T^2]\rangle$ and*

$$\tau^{adj}_{T^2}(\rho) = \tau^{adj}_{S^1,\ \{[a\otimes p],[a\otimes m],[a\otimes l],[a\otimes T^2]\}}(\rho) = 1.$$

*Proof.* We explicitly demonstrate the case of $S^1$. Choosing a basis which diagonalizes $\rho(x)$ we find

$$\rho(x) = \begin{pmatrix} y & 0 \\ 0 & y^{-1} \end{pmatrix}$$

and so, passing to the adjoint representation of $\mathrm{SL}(2,\mathbb{C})$, $\rho$ acts as

$$\rho^{adj}(x) = \begin{pmatrix} 1 & 0 & 0 \\ 0 & y^2 & 0 \\ 0 & 0 & y^{-2} \end{pmatrix}.$$

[8] It is interesting to compare this to the corresponding surgery formula for the standard torsion:

$$\tau^{st}_{S^3_{\frac{p}{r}}(K)}(\rho) = \frac{\tau^{st}_{S^3\backslash K}(\rho)}{2 - y - y^{-1}}.$$

The invariant vector is clearly $a = \begin{pmatrix} 1 \\ 0 \\ 0 \end{pmatrix}$ and so the induced map $\partial^* : C^1(S^1, V_\rho)/\langle a \otimes x \rangle \to C^0(S^1, V_\rho)/\langle a \otimes p \rangle$ is given by

$$\partial^* = I_2 - \rho^{adj}(x)|_{\{2,3\}} = \begin{pmatrix} 1 - y^2 & 0 \\ 0 & 1 - y^{-2} \end{pmatrix}.$$

Hence,

$$\tau^{adj}_{T^2}(\rho) = \frac{1}{\det(\partial^*)} = \frac{1}{2 - y^2 - y^{-2}}.$$

The proof for $\tau^{adj}_{T^2}(\rho)$ is identical. □

The main tool we need to prove Lemma 5.1.13 is the following Theorem.

**Theorem 5.1.15** ([Mil66]: Theorem 3.2)**.** *Suppose that*

$$0 \to C'_* \xrightarrow{i} C_* \xrightarrow{j} C''_* \to 0$$

*is a short exact sequence of chain complexes giving rise to the long exact sequence of homology*

$$H_* = \cdots \to H_1(C''_*) \xrightarrow{\partial} H_0(C'_*) \xrightarrow{i} H_0(C_*) \xrightarrow{j} H_0(C''_*) \to 0.$$

*For each $k$, choose compatible*[9] *volume elements in $C'_k, C_k, C''_k$ such that the torsion of the short exact sequence is* 1*. Then*

$$\tau_C = \tau_{C'} \tau_{C''} \tau_H.$$

Given a surgery $S^3_{\frac{p}{r}}(K) = (S^3 \setminus K) \cup_{T^2} (S^1 \times D^2)$ we have a corresponding Mayer-Vietoris-like sequence

$$0 \to C_*(T^2, V_\rho) \xrightarrow{i} C_*(S^3 \setminus K, V_\rho) \oplus C_*(S^1, V_\rho) \xrightarrow{j} C_*(S^3_{\frac{p}{r}}(K), V_\rho) \to 0$$

and the above theorem yields

$$\tau^{adj}_{S^3_{\frac{p}{r}}(K)}(V_\rho) = \frac{\tau^{adj}_{S^3 \setminus K, \mathbf{h}}(V_\rho) \tau^{adj}_{S^1, \mathbf{h}'}(V_\rho)}{\tau^{adj}_{T^2, \mathbf{h}''}(V_\rho) \tau^{adj}_H} = \frac{\tau^{adj}_{S^3 \setminus K, [\gamma]}(V_\rho) \tau^{adj}_{S^1}(V_\rho)}{\tau^{adj}_H}.$$

With a careful choice of $\gamma$, we can force $\tau_H = 1$ yielding

[9] Denoting the chosen elements as $\mathbf{c}'_k$, $\mathbf{c}_k$, $\mathbf{c}''_k$, compatible means that $\mathbf{c}_k = i(\mathbf{c}'_k) \wedge \mathbf{b}_k$ with $j(\mathbf{b}_k) = \mathbf{c}''_k$.

**Proposition 5.1.16** ([Por15]: Proposition 4.23)**.** *Fix a group homomorphism* $\rho : \pi_1(S^3_{\frac{p}{r}}(K)) \to \mathrm{SL}(2,\mathbb{C})$*. Then*

$$\tau^{adj}_{S^3_{\frac{p}{r}}(K)}(\rho) = \tau^{adj}_{S^3\setminus K,\ p[m]+r[l]}(\rho)\tau^{adj}_{S^1}(\rho)$$

As $H_1(S^3 \setminus K)$ is one-dimensional, equation (5.1.8) shows

$$\tau^{adj}_{S^3\setminus K,\ p[m]+r[l]}(\rho) = p\ \tau^{adj}_{S^3\setminus K,[m]}(\rho) + r\ \tau^{adj}_{S^3\setminus K,[l]}(\rho)$$

and we can express $\tau^{adj}_{S^3\setminus K,[m]}(\rho)$ in terms of $\tau^{adj}_{S^3\setminus K,[l]}(\rho)$ via the following lemma.

**Lemma 5.1.17** ([Por95])**.** *Let* $x$ *and* $y$ *denote eigenvalues of the meridian and longitude in the standard representation. Then*

$$\tau^{adj}_{S^3\setminus K,[m]}(\rho) = \pm\frac{y}{x}\frac{dx}{dy}\tau^{adj}_{S^3\setminus K,[l]}(\rho).$$

This $\pm$ disappears if we ensure that $x, y$ are eigenvalues of a common eigenvector. Combining this all with our previous computation of adjoint torsion for the circle completes the proof of Lemma 5.1.13.

Let us turn now to studying how to explicitly compute these torsions, illustrating the computations with examples of surgeries on hyperbolic knots $4_1$ and $5_2$. The main difficulty is in computing $\tau^{adj}_{S^3\setminus K,[l]}(\rho)$, for which we will need to take a brief detour to discuss twisted Alexander polynomials.

### Twisted Alexander Polynomials

Let $\alpha : \pi_1(S^3 \setminus K) \to \mathbb{Z} = \langle t \rangle$ denote the abelianization homomorphism. Then any linear representation $\rho : \pi_1(S^3 \setminus K) \to \mathrm{SL}(n,\mathbb{C})$ can be lifted to a representation $\rho \otimes \alpha : \pi_1(S^3 \setminus K) \to \mathrm{GL}(n,\mathbb{C}(t))$.

**Definition 5.1.18** ([Kit96])**.** *For generic* $t$*,* $C_*(S^3 \setminus K, V_{\rho\otimes\alpha})$ *is acyclic, letting us define*

$$\Delta_{K,\rho}(t) = \tau_{S^3\setminus K}(\rho \otimes \alpha).$$

*This family of invariants are known as the twisted Alexander polynomials.*

When $\rho(g) = 1$ is the trivial representation, $(1-t)\Delta_{K,1}(t)$ is the Alexander polynomial, justifying the name. These invariants were initially described in a different context in [Lin01, Wad94] before being related to the Reidemeister torsion in [Kit96]. Assuming that $\rho$ lands in a non-trivial irreducible representation $\mathbf{n}$ of $\mathrm{SL}(2,\mathbb{C})$, consider what happens in the limit as $t \to 1$.

**Theorem 5.1.19** ([Yam08]). *There are two possible cases*

- *If* $H_*(S^3 \setminus K, V_\rho) = 0$, *then*

$$\lim_{t\to 1} \Delta^{\boldsymbol{n}}_{K,\rho}(t) = \tau^{\boldsymbol{n}}_{S^3\setminus K}(\rho)$$

- *If* $H_*(S^3 \setminus K, V_\rho) \neq 0$, *then*

$$\lim_{t\to 1} \frac{\Delta^{\boldsymbol{n}}_{K,\rho}(t)}{t-1} = \tau^{\boldsymbol{n}}_{S^3\setminus K,[l]}(\rho) \tag{5.1.20}$$

Hence, we can compute $\tau^{adj}_{S^3\setminus K,[l]}(\rho)$ via the computation of $\Delta^{adj}_{K,\rho}(t)$. This is easier as the acyclic situation is far simpler to work with. Computations of $\Delta^{\mathbf{n}}_{K,\rho}(t)$ have been done for certain knots and representations in the literature [Tra13, Tra15b], and here we show explicitly how it works for the adjoint representation for our class of manifolds. First, recall the definition of the Fox derivative.

**Definition 5.1.21.** *Given a free group* $F$ *with generators* $g_i$ *the Fox derivative is the function* $\frac{\partial}{\partial g_i} : \mathbb{Z}[F] \to \mathbb{Z}[F]$ *defined by*

$$\begin{aligned}
\frac{\partial}{\partial g_i} g_j &= \delta_{ij} \\
\frac{\partial}{\partial g_i} e &= 0 \\
\frac{\partial}{\partial g_i}(uv) &= \frac{\partial}{\partial g_i}(u) + u\frac{\partial}{\partial g_i}(v)
\end{aligned}$$

Fix a Wirtinger presentation[10] of the knot group

$$\pi_1(S^3\setminus K) = \langle g_1, \cdots, g_n \mid r_1, \cdots, r_{n-1}\rangle,$$

where each $g_i$ is a meridian and, given a representation $\rho : \pi_1(S^3 \setminus K) \to \mathrm{SL}(2,\mathbb{C})$. Then it is well known that $S^3 \setminus K$ retracts onto a 2-complex with one 0-cell, $n$ 1-cells labelled $g_1, \cdots, g_n$ and $(n-1)$ 2-cells with attaching maps given by $r_1, \cdots, r_{n-1}$. From this we can compute the chain complex $C_*(S^3 \setminus K; V_\rho)$ to be

$$0 \to V^{\oplus(n-1)} \xrightarrow{\partial_2} V^{\oplus n} \xrightarrow{\partial_1} V \to 0,$$

[10] With a little care this definition can be extended to work with any deficiency 1 representation.

where[11]

$$\partial_2 = A = \begin{pmatrix} \rho(\frac{\partial r_1}{\partial g_1}) & \cdots & \rho(\frac{\partial r_1}{\partial g_n}) \\ \vdots & \ddots & \vdots \\ \rho(\frac{\partial r_{n-1}}{\partial g_1}) & \cdots & \rho(\frac{\partial r_{n-1}}{\partial g_n}) \end{pmatrix} \quad \text{and} \quad \partial_1 = \begin{pmatrix} \rho(g_1) - I \\ \vdots \\ \rho(g_n) - I \end{pmatrix}.$$

Let $A_i$ denote the square matrix where we have removed the $i$'th column from $A$. Then a careful computation shows[12]

**Theorem 5.1.22** (Johnson)**.** *Assuming $C_*(S^3 \setminus K; V_\rho)$ is acyclic, there exists an $i$ such that* $\det(\rho(g_i) - I)$ *and* $\det A_i$ *are both non-zero and, using this $i$, the Reidemeister torsion is given by*

$$\tau(S^3 \setminus K, V_\rho) = \frac{\det(A_i)}{\det(\rho(g_i) - I)}.$$

*This is independent of the choice of $i$, up to overall factors of $t$.*

This is easy to compute for any knot and is particularly simple when the knot group admits a presentation with 2 generators and 1 relation, as is the case for the $4_1$ and $5_2$ knots which we consider next.

### Riley polynomials

The $K_n$ twist knot has knot group

$$\langle g, h \mid h^{-1}\omega^n g \omega^{-n} \rangle \qquad \omega = hg^{-1}h^{-1}g,$$

where $h, g$ are two meridians and the longitude is

$$l = \overleftarrow{\omega}^n \omega^n \quad \text{with} \quad \overleftarrow{\omega} = gh^{-1}g^{-1}h.$$

Given a representation $\rho : \pi_1(S^3 \setminus K_n) \to \mathrm{SL}(2, \mathbb{C})$, as the generators are conjugate we can assume that, up to conjugation

$$\rho(g) = \begin{pmatrix} x & x^{-1} \\ 0 & x^{-1} \end{pmatrix} \text{ and } \rho(h) = \begin{pmatrix} x & 0 \\ -xu & x^{-1} \end{pmatrix}.$$

If we compute $\rho(\omega^n g) - \rho(h\omega^n)$ we find that

$$\rho(\omega^{-1}g) - \rho(h\omega^{-1}) = \begin{bmatrix} 0 & x^{-1}\phi_n(x,u) \\ ux\ \phi_n(x,u) & 0 \end{bmatrix}$$

[11] Note that $\rho(\frac{\partial r_i}{\partial g_j})$ means computing $\frac{\partial r_i}{\partial g_j}$ in $\mathbb{Z}[F]$ and then taking the natural quotient $\mathbb{Z}[F] \to \mathbb{Z}[G]$ before applying $\rho$.

[12] While this was initially proven in [Joh], a clearer proof was given in [Kit94], Theorem 2.1.

for a polynomial $\phi_n(x,u)$ known as the Riley polynomial [Ril84]. To simplify notation, let

$$\theta_m := x + x^{-1} \quad \text{and} \quad \theta_{m,j} := x^j + x^{-j}$$

denote the trace of the meridian and higher order functions of that trace. Then, for the knots $4_1$ and $5_2$ we have $n = -1$ and $n = 2$, respectively, so that

$$\begin{aligned}\phi_{-1}(x,u) &= u^2 - (u+1)(\theta_{m,2} - 3)\\ \phi_2(x,u) &= u^3 + (3 - 2\theta_{m,2})(u^2+1) + (6 - 3\theta_{m,2} + \theta_{m,4})u.\end{aligned}$$

Similarly, we can compute the longitude in each of these cases to get

$$\rho(l_{4_1}) = \begin{pmatrix} y_{4_1}(x,u) & -\frac{\theta_m(\theta_{m,2}-3-2u)}{x} \\ 0 & y_{4_1}(x^{-1},u)\end{pmatrix}$$
$$y_{4_1}(x,u) = \frac{1 - 2x^2 - ux^2 - x^4 + x^6 + ux^6}{x^4}$$

and

$$\rho(l_{5_2}) = \begin{pmatrix} y_{5_2}(x,u) & \frac{\theta_m(u\theta_{m,8} - (2+2u+u^2)\theta_{m,6} + (1+2u)\theta_{m,4} - \theta_{m,2} - 1)}{x} \\ 0 & y_{5_2}(x^{-1},u)\end{pmatrix}$$
$$y_{5_2}(x,u) = 1 - x^2(1+u)(2 - x^4 + x^6) + (1+u)^2x^4 - u^2x^8 + ux^{10}.$$

Using the corresponding Riley polynomial we can verify that $y(x^{-1},u) = y(x,u)^{-1}$. From this we can read off the torsion corresponding to the gluing torus (for $y \neq \pm 1$) to be

$$\tau^{adj}_{S^1,4_1} = \frac{1}{2 - y_{4_1}^2 - y_{4_1}^{-2}} = \frac{1}{(\theta_{m,2}+2)(\theta_{m,2}+1)(\theta_{m,2}-2)(\theta_{m,2}-3)}$$

and

$$\begin{aligned}\tau^{adj}_{S^1,5_2} &= \frac{1}{2 - y_{5_2}^2 - y_{5_2}^{-2}}\\ &= \Big( - u\theta_{m,20} + (2+3u+u^2)\theta_{m,18} - (3+3u+u^2)\theta_{m,16} - (3u+u^2)\theta_{m,14}\\ &\quad + (7+8u+3u^2)\theta_{m,12} - (4+u-u^2)\theta_{m,10} - 3(2+3u+u^2)\theta_{m,8}\\ &\quad + (6+3u-u^2)\theta_{m,6} + (2+5u+u^2)\theta_{m,4} - 2(2+u)\theta_{m,2}\Big)^{-1}.\end{aligned}$$

We can also compute the derivative $\frac{dx}{dy}$. In practice, it is easier to compute $\frac{dy}{dx}$, which can be done in the following two-step process. We first use the Riley polynomial to

compute $\frac{du}{dx}$ and then we can differentiate the expressions $y(x,u)$ given above. We get

$$\frac{du_{4_1}}{dx} = -\frac{2(x-x^{-1})\theta_m(1+u)}{x(\theta_{m,2}-3-2u)}$$
$$\frac{du_{5_2}}{dx} = -\frac{2(x-x^{-1})\theta_m(2u\theta_{m,2}-2-3u-2u^2)}{x(\theta_{m,4}-(3+4u)\theta_{m,2}+3(2+2u+u^2))}$$

and, using this we find[13]

$$\frac{y_{4_1}}{x}\frac{dx}{dy_{4_1}} = \frac{3+2u-\theta_{m,2}}{2(2\theta_{m,2}-1)}$$
$$\frac{y_{5_2}}{x}\frac{dx}{dy_{5_2}} = \frac{19+29u+5u^2-(19+11u+u^2)\theta_{m,2}-(2+u)\theta_{m,4}+2\theta_{m,6}}{2(39+105u+7u^2)-2(58+49u+21u^2)\theta_{m,2}+2(21u-4)\theta_{m,4}}.$$

Finally, we need to compute the twisted Alexander polynomial in both these cases. Passing to the adjoint representation, we find that our matrices become

$$\rho^{adj}(g) = \begin{pmatrix} 1 & 0 & x^{-2} \\ -2 & x^2 & x^{-2} \\ 0 & 0 & x^{-2} \end{pmatrix} \text{ and } \rho^{adj}(h) = \begin{pmatrix} 1 & ux^2 & 0 \\ 0 & x^2 & 0 \\ -2u & -u^2x^2 & x^{-2} \end{pmatrix}$$

in the basis $\{h,e,f\}$. For the generic twist knot $K_n$,

$$A_2 = \rho\left(\frac{\partial(h^{-1}\omega^n g\omega^{-n})}{\partial g}\right) = \rho\left(-h^{-1}+(h^{-1}-1)\frac{\partial\omega^n}{\partial\omega}(1-hg^{-1}h^{-1})\right),$$

where

$$\frac{\partial\omega^n}{\partial\omega} = \begin{cases} 1+\omega+\cdots+\omega^{n-1} & n\geq 0 \\ -\omega^{-1}-\cdots-\omega^{-n} & n<0. \end{cases}$$

For our two examples of $4_1$ and $5_2$ knots, this simplifies to

$$A_2^{4_1} = \rho\left(-h^{-1}+(h^{-1}-1)(g^{-1}-\omega^{-1})\right)$$
$$A_2^{5_2} = \rho\left(-h^{-1}+(h^{-1}-1)(1+\omega)(1-hg^{-1}h^{-1})\right)$$

and applying Theorem 5.1.22 we get

$$\Delta^{adj}_{4_1,\rho}(t) = (1-t)(2t(\theta_{m,2})-1+t-t^2)$$
$$\Delta^{adj}_{5_2,\rho}(t) = (1-t)\Big(2(1+t^2)(\theta_{m,2}^2u-\theta_{m,2}-(1+\theta_{m,2})(1+u+u^2))$$

[13] There are many equivalent expressions here, depending on different simplification procedures. This one is chosen for simplicity and to make the $x\to x^{-1}$ Weyl symmetry manifest.

$$+ (3 + (4 + \theta_{m,4})u + (1 - \theta_{m,2})(2 + 3u + u^2))t\Big).$$

Therefore, equation (5.1.20) gives

$$\tau^{adj}_{S^3\setminus 4_1,[l]}(\rho) = (2\theta_{m,2} - 1)$$
$$\tau^{adj}_{S^3\setminus 5_2,[l]}(\rho) = 1 - 10\theta_{m,2} + (11 - 7\theta_{m,2} + 5\theta_{m,4})u - (3 + 5\theta_{m,2})u^2.$$

Putting it all together we find

$$\tau^{adj}_{S^3_{\frac{p}{r}}(4_1)}(\rho) = \frac{\frac{p}{2}(3 + 2u - \theta_{m,2}) + r\ (2\theta_{m,2} - 1)}{(\theta_{m,2} + 2)(\theta_{m,2} + 1)(\theta_{m,2} - 2)(\theta_{m,2} - 3)} \tag{5.1.23}$$

$$\tau^{adj}_{S^3_{\frac{p}{r}}(5_2)}(\rho) = \frac{p\ \frac{y_{5_2}}{x}\frac{dx}{dy_{5_2}}\tau^{adj}_{S^3\setminus 5_2,[l]}(\rho) + r\ \tau^{adj}_{S^3\setminus 5_2,[l]}(\rho)}{\tau^{adj}_{S^1,5_2}}. \tag{5.1.24}$$

### 5.1.3 Examples: surgeries on small twist knots

Combining the previous two subsections, we end up with a simple algorithm to compute the Chern Simons values and torsions corresponding to each flat connection on a general surgery $S^3_{\frac{p}{r}}(K)$ and for surgeries on twist knots (2.0.4) in particular.

1. Find all intersections between the curves $A^{irred}_K(x, y) = 0$ and $y^r x^p = 1$ with $x, y \neq 0, 1, -1$. These come in pairs $(x, y), (x^{-1}, y^{-1})$. For the sake of consistency, pick solutions so that $\mathrm{Im}(x) > 0$ or $\mathrm{Im}(x) = 0$ and $|x| > 1$.

2. For each solution $(x^*, y^*)$, determine $u$ by solving $\phi(x^*, u) = 0, y(x^*, u) = y^*$ and use this to compute $\tau^{adj}_{S^3_{\frac{p}{r}}(K)}$.

3. Fix a root of $\Delta_{4_1}(x^2)$; the choice is irrelevant, but for simplicity and consistency we choose the root $\chi$ which minimises $|\log(\chi)|$.

4. For each solution $(x, y)$, find a path from $(\chi, 1)$, the intersection with the abelian branch to $(x, y)$. This will involve computing which sheet $(x, y)$ lies on, and may involve passing through intersection points. Additionally, determine the appropriate continuous extension of the log function.

5. Apply (5.1.2) to determine the Chern Simons value and normalise to get an answer in the interval $[-\frac{1}{2}, \frac{1}{2}]$.

After computing the complete set of invariants for a given knot, we additionally give normalisations, which are important for comparisons to numerical results in the Borel Plane.

- The normalized CS invariants are given by $\frac{\mathrm{CS}_\alpha}{\mathrm{CS}_{\text{leading}}}$, where $\mathrm{CS}_{\text{leading}}$ denotes the smallest invariant. These give a clearer picture of the relative magnitude of these invariants. This is important when identifying the CS invariants with Borel singularities, as their relative distance from the origin is an important physical consideration, the closest ones being related to more dominant non-perturbative effects.

- The residues corresponding to Borel singularities, (Stokes constants, $\mathcal{S}_\alpha := \mathcal{S}_0^\alpha$), are related to the adjoint Reidemeister torsion $\tau_\alpha$ via:

$$\mathcal{S}_0^\alpha = \frac{1}{\sqrt{4\pi\tau_\alpha\ (-4\pi^2\mathrm{CS}_{\text{leading}})^3}} \tag{5.1.25}$$

**Surgeries on the $4_1$ knot**

We start with the $4_1$ knot. The irreducible $A$-polynomial is

$$A_{4_1}^{irred}(x,y) = (-x^4 + (1 - x^2 - 2x^4 - x^6 + x^8)y - x^4y^2). \tag{5.1.26}$$

As this is quadratic in $y$, it forms a 2 sheeted branched covering space over $(\mathbb{C}^*)_x$ with local[14] sections $y_1(x)$ and $y_2(x)$. In this simple case, at each root of $\Delta_{4_1}(x^2)$, both irreducible branches meet the Abelian branch. This means we can always choose straight line paths from roots of $\Delta_{4_1}(x^2)$ to our desired points, and we will not have to move between different irreducible branches. From the $4_1$ Alexander polynomial,

$$\Delta_{4_1}(x^2) = -x^2 - x^{-2} + 3,$$

we set our intersection point with the abelian branch to be $(x,y) = \left(\frac{1+\sqrt{5}}{2}, 1\right)$.

Let us start by looking at the 0-surgery. Setting $y = 1$, we find

$$A_{4_1}^{irred}(x,1) = x^2(1+x^2)^2(x^2 + x^{-2} - 3) = -x^2(1+x^2)^2\Delta_{4_1}(x^2). \tag{5.1.27}$$

Hence there is a single interesting pair of roots located at $(\pm i, 1)$ with multiplicity 2. Visualising our branches $y_1(x), y_2(x)$ along the straight line from $x = \frac{1}{2}(1+\sqrt{5})$ to $x = i$ produces Figure 5.1. While the two branches of $\mathcal{A}_{4_1}^{iired}$ join at $(1,i)$, when lifted to the representation variety, these branches separate. Hence, the two possible CS values for the 0-surgery correspond to travelling to $(1,i)$ along each branch. As both of the loops in Figure 5.1 do not contain 0, we stay on the initial logarithm

[14] It is impossible to continuously extend $y_1(x)$ and $y_2(x)$ to all of $(\mathbb{C}^*)_x$ as the roots of a polynomial equation form an unordered set.

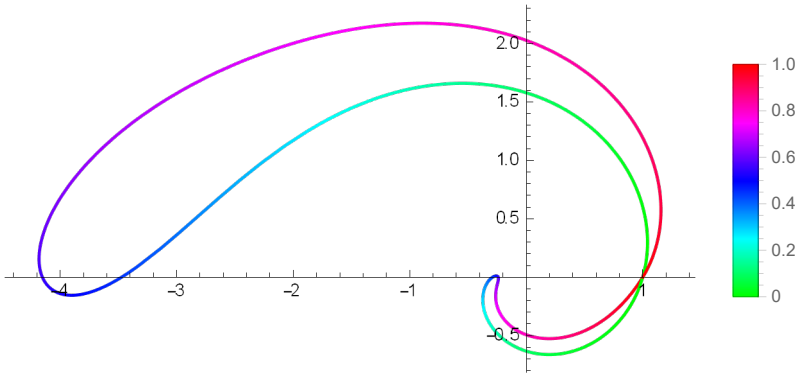


Figure 5.1: Branches of $\mathcal{A}_{4_1}$ along the line $x(t) = \frac{1-t}{2}(1+\sqrt{5}) + t\,i$. The colour indicates the $t$ value, and the position is the complex value of $y_1(x(t))$ or $y_2(x(t))$. Intersection points where the colours align correspond to sheet intersection points in $\mathcal{A}_{4_1}$, so this diagram shows two distinct paths from $(\frac{1-t}{2}(1+\sqrt{5}), 1)$ to $(i, 1)$.

branch and so the boundary term in (5.1.3) vanishes. Thus, we find[15] that the Chern Simons invariants of the upper and lower branches are $-\frac{1}{5}$ and $+\frac{1}{5}$ respectively, as previously shown in [KK90].

Let us now move to the more interesting case of $-\frac{1}{2}$ surgery. This surgery enforces $x = y^2$ and so flat connections correspond to roots of

$$A_{4_1}^{irred}(y^2, y) = y(1+y)^2\big(1 - 2y + 3y^2 - 4y^3 + 4y^4 - 4y^5 + 4y^6 - 5y^7 + 4y^8 \\ - 4y^9 + 4y^{10} - 4y^{11} + 3y^{12} - 2y^{13} + y^{14}\big).$$

The $x$ values of these roots are plotted in Figure 5.2. Note that several flat connections land almost directly on an intersection with the abelian branch. Modding out by the Weyl symmetry, there are 7 pairs of intersection points and a fixed point of multiplicity 2 at $(1, -1)$. From here, we simply apply the remainder of the algorithm described at the start of this section to compute all CS and torsion invariants. The results are shown in Table 5.1.

Let us illustrate the computational procedure using the example of the leading Chern Simons invariant, which corresponds to $x = 1.622$, as in the first row of Table 5.1. As in Section 5.1.2, define $\theta_{m,2}^{\text{leading}} \equiv (x^{\text{leading}})^2 + (x^{\text{leading}})^{-2} = 3.012$. Then the A-polynomial expression (5.1.4) for the Chern Simons invariant can be expressed[16] (after some simple integrations-by-parts) as

$$\text{CS}_{\text{leading}} = \frac{1}{8\pi^2}\left(\left[\log\left(x^{\text{leading}}\right)\right]^2\right.$$

[15] Up to a precision of $10^{-100}$.

[16] While in general the integration contour needs to stay on $\mathcal{A}_{4_1}$, for small contours like this one it doesn't matter.

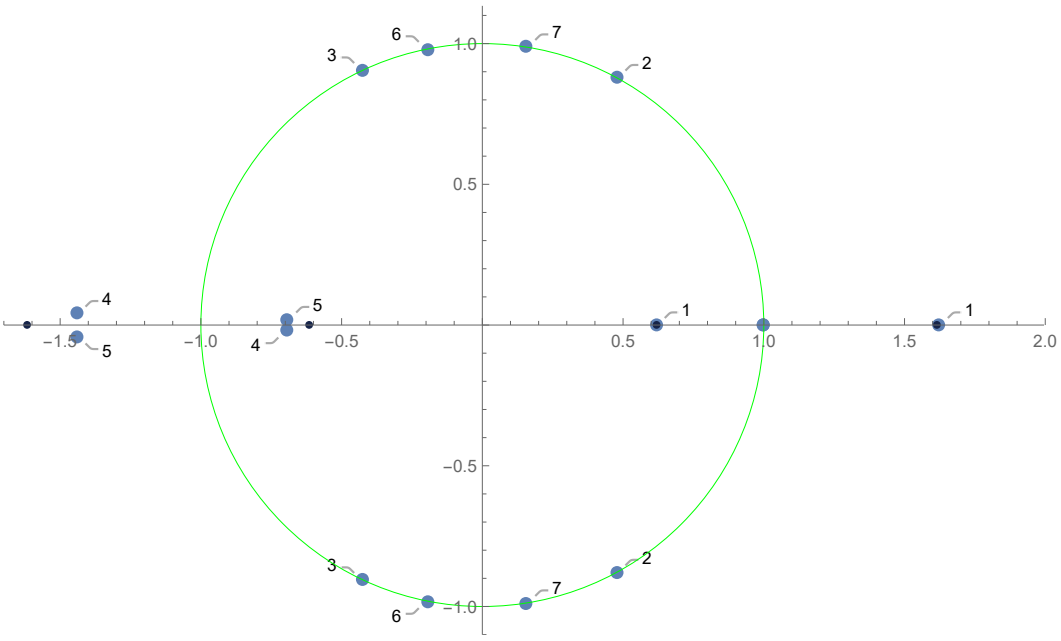


Figure 5.2: Intersections of the irreducible branch with $y^2 = x$ for the $4_1$ knot. Intersections with the abelian branch are in black.

$$
\begin{aligned}
& -\frac{1}{2}\int_3^{\theta_{m,2}^{\text{leading}}} d\theta \, \log\left(\frac{\theta+\sqrt{\theta^2-4}}{\theta-\sqrt{\theta^2-4}}\right)\frac{2(2\theta-1)}{\sqrt{(\theta+1)(\theta^2-4)(\theta-3)}}\Bigg) \\
= \;& -0.0029434014775824953....
\end{aligned}
$$

This is the $CS$ invariant value listed in the first row of Table 5.1. The lower limit on the $\theta$ integration comes from the chosen reference intersection point, $x^{\text{ref}} = \frac{1}{2}(1+\sqrt{5})$, for which $\theta_{m,2}^{\text{ref}} \equiv (x^{\text{ref}})^2 + (x^{\text{ref}})^{-2} = 3$.

Similarly, from the adjoint Reidemeister torsion analysis in Section 5.1.2, we use equation (5.1.23) with $p = -1$, $q = 2$, $u$ evaluated at the vanishing of the Riley polynomial (with thee branch fixed by the $y$ value), $\phi_{-1}(x,u) = 0$, all evaluated at $\theta_{m,2}^{\text{leading}}$:

$$
\begin{aligned}
\tau^{adj}_{S^3_{-\frac{1}{2}}(4_1)}(\text{leading}) &= \left[\frac{-\frac{1}{2}\sqrt{(\theta_{m,2}-3)\,(\theta_{m,2}+1)}+2(2\theta_{m,2}-1)}{(\theta_{m,2}+1)(\theta_{m,2}+2)(\theta_{m,2}-2)(\theta_{m,2}-3)}\right]_{\theta_{m,2}=\theta_{m,2}^{\text{leading}}} \\
&= 41.6374502692239...
\end{aligned}
$$

This is the Torsion value listed in the first row of Table 5.1. Note that both of these invariants can be evaluated to any desired precision, and the procedure is similar for the other intersection pairs in Table 5.1.

| $\alpha$ | $x$ | $y$ | CS | Torsion | NCS | Stokes |
|---|---|---|---|---|---|---|
| 1 | 1.622270086 | 1.273683668 | −0.0029434 | 41.6374 | 1 | 1.104 |
| 2 | $0.48+0.88i$ | $-0.86-0.51i$ | −0.4858743 | 5.78919 | 165.0 | 2.960 |
| 3 | $-0.42+0.91i$ | $-0.54-0.84i$ | 0.0539336 | 2.69687 | −18.3 | 4.337 |
| 4 | $-1.44+0.04i$ | $-0.02-1.20i$ | 0.1233036 | −1.9759 | −41.9 | −0.01 |
| 5 | $-0.69+0.02i$ | $-0.01-0.83i$ | $\pm 0.035425i$ | $\mp 0.0763i$ | $\mp 12.0i$ | $\pm 5.1i$ |
| 6 | $-0.19+0.98i$ | $0.64+0.77i$ | 0.2351598 | 3.51024 | −79.9 | 3.801 |
| 7 | $0.16+0.99i$ | $0.76+0.65i$ | −0.1718829 | 6.31797 | 58.4 | 2.833 |

Table 5.1: Chern Simons and adjoint Reidemeister torsion invariants for $-\frac{1}{2}$ surgery on the $4_1$ knot. The normalized CS invariants (NCS) are the CS invariants divided by the CS invariant of smallest magnitude, and the Stokes constants are related to the torsions via expression (5.1.25). These invariants can be evaluated to essentially any degree of precision.

Since the $4_1$ knot is an amphichiral, the Chern Simons and torsion invariants for $S^3_{\frac{1}{2}}(4_1)$ differ from $S^3_{-\frac{1}{2}}(4_1)$ only by minus signs.

As a brief cross-check, the intersections lying on the unit circle ($\alpha = 2, 3, 6, 7$ in Table 5.1) can be realised in SU(2) and in those cases our CS results match [KK90]. A discussion of observations from these computations can be found in Section 5.1.4.

### Surgeries on the $5_2$ knot

For the $5_2$ knot we have

$$A^{irred}_{5_2}(x,y) = x^{14} + (x^4 - x^6 + 2x^{10} + 2x^{12} - x^{14})y + (-1 + 2x^2 + 2x^4 - x^8 + x^{10})y^2 + y^3 \tag{5.1.28}$$

and so $\mathcal{A}^{irred}_{5_2}$ forms a three-sheeted branched covering space over $(\mathbb{C}^*)_x$ with local sections $y_1(x), y_2(x), y_3(x)$. There are now several types of intersection points in $\mathcal{A}_{5_2}$:

- Exactly two sheets of the irreducible branch intersect[17].
- A single sheet of the irreducible branch intersects the abelian branch.
- All three sheets of the irreducible branch intersect.
- All three sheets of the irreducible branch intersect the abelian branch.

[17] These also occur the $4_1$ case but were not important there.

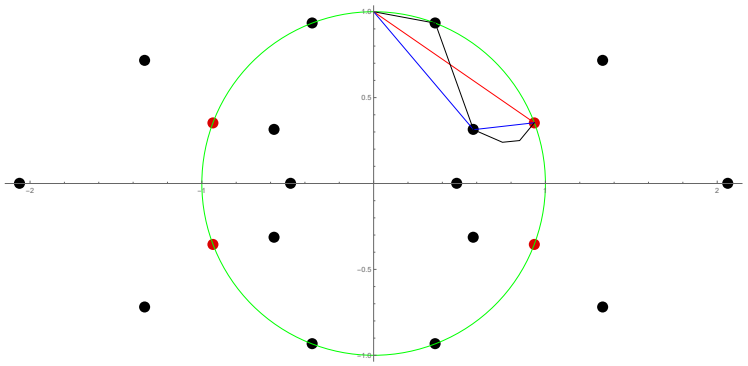

Figure 5.3: A plot of the $x$ values of branch points where exactly 2 sheets meet. Branch points involving the abelian branch are in red. The lines show three paths from the abelian branch to the point $(1, i)$, each arriving on a different sheet of the irreducible branch.

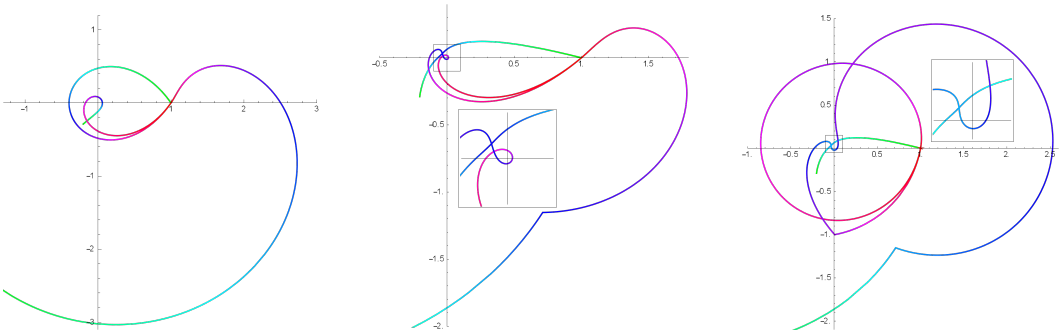

Figure 5.4: Plots of the three branches along respectively the red, blue and black paths in Figure 5.3. Intersection points where colours line up correspond to intersections of irreducible sheets. The shading is the same as in Figure 5.1, with green corresponding to $t$ close to 0, and red to $t$ close to 1.

We focus on the first two possibilities, as the last two are either all spurious or correspond to parabolic representations. This leaves us with a collection of points where exactly 2 sheets of $\mathcal{A}_{5_2}$ meet, as shown in Figure 5.3. As

$$\Delta_{5_2}(x^2) = 2x^2 + 2x^{-2} - 3$$

we set our intersection point with the abelian branch to be $\left(\frac{1}{2}\sqrt{3 + i\sqrt{7}}, 1\right) = \left(\frac{1}{2\sqrt{2}}(\sqrt{7} + i), 1\right)$.

We again start with analysing 0 surgeries, as this gives a simpler setting to explain the differences from the $4_1$ case. Setting $y = 1$, the polynomial for the irreducible branch factors as

$$A_{5_2}^{irred}(x, 1) = x^4(1 + x^2)^3\Delta_{5_2}(x^2) \tag{5.1.29}$$

and so we get three Chern Simons values corresponding to approaching the point $x = i$ along each of the three sheets. As only one of the irreducible sheets intersects the abelian branch, we need to use some intersection points to shift between the irreducible sheets. The simplest path for arriving on each sheet is shown in Figure 5.3, and the plot of what the three sheets look like along these paths is given in Figure 5.4.

Looking at Figure 5.4, we can clearly see that along the red and black paths, $y$ circles 0 once so $\log\big((\rho_1)_y\big) = 2\pi i$, and along the blue path it circles twice so $\log\big((\rho_1)_y\big) = 4\pi i$. Then, using Equation (5.1.3), we find that the three CS values are $-\frac{1}{7}, -\frac{2}{7}$ and $-\frac{4}{7}$, which agrees with the values given in [CGPS20].

Let us move on to the more interesting examples of $S^3_{\pm\frac{1}{2}}(5_2)$. Using the work in the preceding subsections, it is straightforward to extend our algorithm to the $\pm\frac{1}{2}$ surgeries. Intersection points of the irreducible branch with the curves $x = y^{\mp 2}$ correspond to roots of the polynomials,

$$\begin{aligned} A^{irred}_{5_2}(y^{-2}, y) =& y^{-28}(1+y)^3\Big(1 - 4y + 9y^2 - 16y^3 + 25y^4 - 34y^5 + 43y^6 \\ & -52y^7 + 61y^8 - 68y^9 + 74y^{10} - 79y^{11} + 83y^{12} - 86y^{13} + 87y^{14} \\ & -86y^{15} + 83y^{16} - 79y^{17} + 74y^{18} - 68y^{19} + 61y^{20} - 52y^{21} + 43y^{22} \\ & -34y^{23} + 25y^{24} - 16y^{25} + 9y^{26} - 4y^{27} + y^{28}\Big) \end{aligned} \tag{5.1.30}$$

$$\begin{aligned} A^{irred}_{5_2}(y^2, y) =& -y^2(1+y)^3(1 - y + y^2 - y^3 + y^4) \\ & (1 - 2y + y^2 - y^4 + y^6 - 2y^7 + y^8) \\ & (1 - y + 2y^2 - 2y^3 + 2y^4 - 3y^5 + 3y^6 - 3y^7 + 2y^8 - 2y^9 + 2y^{10} - y^{11} + y^{12}). \end{aligned} \tag{5.1.31}$$

These are shown[18] in Figure 5.5 along with the branch and sheet intersection points. From this we find that there are 12 and 14 pairs respectively. Using these intersection points and applying the general algorithm described above, we obtain the Chern Simons invariants and adjoint Reidemeister torsions, summarized in Tables 5.2 and 5.3. Note that these invariants can be computed to essentially any desired precision.

### 5.1.4 Curious observations

Looking at the complete set of geometric invariants for $\pm\frac{1}{2}$ surgery for the $4_1$ and $5_2$ knots, as shown in Tables 5.1, 5.2 and 5.3, some interesting structures emerge:

[18] Ignoring spurious points located at $x = 1$.

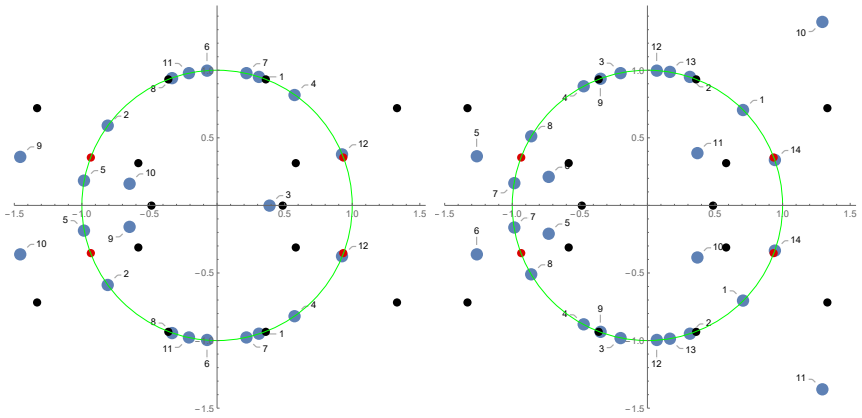

Figure 5.5: Intersections of the irreducible branch of the $5_2$ knot with $x = y^2$ and $x = y^{-2}$ respectively. Red and black points are sheet intersection points, as in Figure 5.3. Corresponding CS values and Torsions appear in Tables 5.2 and 5.3.

| $\alpha$ | $x$ | $y$ | CS | Torsion | NCS | Stokes |
|---|---|---|---|---|---|---|
| 1 | $0.71 + 0.70i$ | $-0.92 - 0.38i$ | $-0.414749$ | 34.6061 | $-266$ | 3.146 |
| 2 | $0.31 + 0.95i$ | $-0.81 - 0.59i$ | $-0.176788$ | 17.9748 | $-113$ | 4.366 |
| 3 | $-0.20 + 0.98i$ | $-0.63 - 0.77i$ | 0.3023154 | 16.0020 | 194.1 | 4.627 |
| 4 | $-0.47 + 0.88i$ | $-0.51 - 0.86i$ | 0.0340344 | 7.36201 | 21.86 | 6.822 |
| 5 | $-1.26 + 0.36i$ | $-0.16 - 1.14i$ | $-0.037604$ | $-1.8640$ | $-24.1$ | 3.820 |
| 6 | $-0.73 + 0.21i$ | $-0.12 - 0.86i$ | $\mp 0.06098i$ | $\mp 1.389i$ | $\mp 39i$ | $\pm 12i$ |
| 7 | $-0.99 + 0.17i$ | $-0.08 - 1.00i$ | $-0.146617$ | 9.50508 | $-94.1$ | 6.003 |
| 8 | $-0.86 + 0.51i$ | $0.27 + 0.96i$ | $-0.091864$ | 6.26070 | $-59.0$ | 7.397 |
| 9 | $-0.35 + 0.94i$ | $0.57 + 0.82i$ | 0.1012771 | 3.28448 | 65.04 | 10.21 |
| 10 | $1.29 + 1.36i$ | $1.26 + 0.54i$ | 0.1265890 | $-6.3007$ | 81.30 | 1.314 |
| 11 | $0.37 + 0.39i$ | $0.67 + 0.29i$ | $\pm 0.02553i$ | $\mp 2.453i$ | $\pm 16i$ | $\pm 7.0i$ |
| 12 | $0.07 + 1.00i$ | $0.73 + 0.68i$ | $-0.458462$ | 24.9297 | $-294$ | 3.707 |
| 13 | $0.17 + 0.99i$ | $0.76 + 0.65i$ | 0.2577722 | 14.3684 | 165.5 | 4.883 |
| 14 | $0.94 + 0.33i$ | $0.99 + 0.17i$ | $-0.001557$ | 267.536 | $-1$ | 1.132 |

Table 5.2: Chern Simons invariant and adjoint Reidemeister torsion for $\frac{1}{2}$ surgery on the $5_2$ knot.

| $\alpha$ | $x$ | $y$ | CS | Torsion | NCS | Stokes |
|---|---|---|---|---|---|---|
| 1 | $e^{\frac{2\pi i}{5}}$ | $e^{\frac{9\pi i}{5}}$ | $\frac{1}{6}$ | 5 | 94.43 | 6.856 |
| 2 | $e^{\frac{4\pi i}{5}}$ | $e^{\frac{3\pi i}{5}}$ | $\frac{1}{6}$ | 5 | 94.43 | 6.856 |
| 3 | 2.57746915 | 0.62287839 | $\frac{5}{48}$ | $2\left(7-\sqrt{8}\right)$ | 59.02 | 5.310 |
| 4 | $0.57+0.82i$ | $-0.89+0.46i$ | $-\frac{19}{48}$ | $2\left(7+\sqrt{8}\right)$ | $-224$ | 3.460 |
| 5 | $-0.98+0.19i$ | $0.09-1.00i$ | $\frac{5}{48}$ | $2\left(7-\sqrt{8}\right)$ | 59.02 | 5.310 |
| 6 | $-0.07+1.00i$ | $0.68-0.73i$ | $-\frac{19}{48}$ | $2\left(7+\sqrt{8}\right)$ | $-224$ | 3.460 |
| 7 | $0.22+0.98i$ | $-0.78+0.63i$ | $-0.134066$ | 21.5914 | $-76.0$ | 3.301 |
| 8 | $-0.33+0.94i$ | $-0.58+0.82i$ | 0.3884604 | 7.55810 | 220.1 | 5.580 |
| 9 | $-1.45+0.36i$ | $0.10-0.81i$ | $0.2113411$ | $-1.6733$ | 119.7 | 2.001 |
| 10 | $-0.65+0.16i$ | $0.15-1.22i$ | $\mp 0.05640i$ | $\mp 0.611i$ | $\mp 32i$ | $\pm 11i$ |
| 11 | $-0.21+0.98i$ | $0.63+0.78i$ | 0.3211581 | 7.76455 | 182.0 | 5.505 |
| 12 | $0.93+0.38i$ | $0.98-0.19i$ | 0.0017649 | 171.933 | 1 | 1.170 |

Table 5.3: Chern Simons invariant and adjoint Reidemeister torsion for $-\frac{1}{2}$ surgery on the $5_2$ knot.

- If we take the sum of all the Chern Simons values (for a given surgery) we get a rational number[19]

$$S^3_{-\frac{1}{2}}(4_1) \quad : \quad \sum_{\alpha=1}^{7} \mathrm{CS}(\alpha) = -\frac{1}{8}$$
$$S^3_{+\frac{1}{2}}(5_2) \quad : \quad \sum_{\alpha=1}^{14} \mathrm{CS}(\alpha) = -\frac{5}{12}$$
$$S^3_{-\frac{1}{2}}(5_2) \quad : \quad \sum_{\alpha=1}^{12} \mathrm{CS}(\alpha) = \frac{3}{4}$$

  This clearly hints at some form of integrability. From the standpoint of algebraic $K$-theory, Chern Simons values are realised as elements of the Bloch group, and so this condition translates to the sum of Chern Simons elements being trivial.

- It is clear from their definition that the torsions are algebraic numbers and so can be encoded as the roots of an integral polynomial, the torsion polynomial, (5.1.11):

$$\sigma^{adj}_{S^3_{-\frac{1}{2}}(4_1)}(t) = -7215127 + 2828784t^2 - 417832t^3 - 272624t^4$$

[19] To several hundred digits of precision.

$$+ 83296t^5 - 7168t^6 + 128t^7 \tag{5.1.32}$$

$$\begin{aligned}\sigma^{adj}_{S^3_{+\frac{1}{2}}(5_2)}(t) = {} & 5554214481270856813 - 833790268928570748t^2 \\ & - 163953024020455456t^3 + 128473842183215536t^4 \\ & - 11213038799872672t^5 - 2369935480771328t^6 \\ & + 398092105583488t^7 + 8781117136640t^8 \\ & - 6166471077376t^9 + 584070450176t^{10} - 26306131968t^{11} \\ & + 607559680t^{12} - 6316032t^{13} + 16384t^{14}\end{aligned} \tag{5.1.33}$$

$$\sigma^{adj}_{S^3_{-\frac{1}{2}}(5_2)}(t) = \big(-5+t\big)^2\big(164 - 28t + t^2\big)^2 \tag{5.1.34}$$

$$\begin{aligned}&\big(44241255 + 32803272t + 695124t^2 - 2966904t^3 \\ &\quad + 386592t^4 - 13152t^5 + 64t^6\big)\end{aligned}$$

Intriguingly, in each of these cases, the torsions are all algebraic half-integers. This follows immediately from observing that the leading term has the form $2^i t^j$ for $i \leq j$.

- Additionally, observe that, in all cases we consider, the sum of the inverse torsions vanishes. Writing the polynomial as $\sum_i a_i t^i$ we see that in all of these cases

$$\sum_{\alpha=1}^{\alpha_{\max}} \frac{1}{\tau(\alpha)} = \frac{a_1}{a_0} = 0 \tag{5.1.35}$$

  From the perspective of the Borel plane, this translates to a relation between the squares of the monodromies.

- In general, $\mathrm{SL}(2,\mathbb{C})$ flat connections naturally split in 3 categories, $\mathrm{SL}(2,\mathbb{R})$, $\mathrm{SU}(2)$ and full $\mathrm{SL}(2,\mathbb{C})$ connections. Given a point $(x, y) \in \mathcal{A}_K$, the flat connection lies in $\mathrm{SL}(2,\mathbb{R})$ if $x, y \in \mathbb{R}$ and in $\mathrm{SU}(2)$ if $x, y \in S^1$. We stress that the properties described above only hold when we consider all 3 categories together. In particular, for each knot surgery we find that

$$\sum_{SU(2)} \frac{1}{\text{torsion}} + \sum_{SL(2,\mathbb{R})} \frac{1}{\text{torsion}} = -\sum_{SL(2,\mathbb{C})} \frac{1}{\text{torsion}} \tag{5.1.36}$$

- For connections in $\mathrm{SL}(2,\mathbb{R})$ or $\mathrm{SU}(2)$, the corresponding torsions are positive real numbers. Hence, in order for the sum of the inverse torsions to be 0, the $\mathrm{SL}(2,\mathbb{C})$ contribution, needs to cancel the $\mathrm{SL}(2,\mathbb{R})$ and $\mathrm{SU}(2)$ contributions.

For some surgeries (such as $-1$ on the $4_1$ knot), all torsions lie in $\mathrm{SL}(2,\mathbb{R})$ or $\mathrm{SU}(2)$. Hence, for these surgeries, the sum of the inverse torsions must be non-zero. That being said, the sum appears to always be integral [CDGG23].

- In the case of the $-\frac{1}{2}$ surgery on $5_2$, half the CS invariants are simple rational numbers, with corresponding closed-form torsions. These simple values are associated with the factorization (for $-\frac{1}{2}$ surgery) of the irreducible A-polynomial $A_{5_2}(y^2, y)$ in (5.1.31), and of the torsion polynomial $\sigma^{adj}_{S^3_{-\frac{1}{2}}(5_2)}(t)$ in (5.1.34). This turns out to be the first indicator of a more general structure concerning the $-\frac{1}{n}$ surgery on the $K_n$ twist knots [CDGG23].

## 5.2 Resurgent Analysis for Surgeries

From the perspective of complex Chern Simons theory, the analysis in section 5.1 is essentially classical, or at best semi-classical, as it relies on the Gaussian approximation near each saddle point of the Feynman path integral (2.3.2). The goal of this section is to probe deeper into the structure of the full quantum theory by applying powerful techniques of the resurgent analysis to a very high loop order of the perturbative expansion (2.3.4). This should teach us about non-perturbative formulation of the theory, in particular allowing a direct comparison with the BPS $q$-series (1.0.2) that provides a candidate for the non-perturbative completion that behaves well under cutting-and-gluing operations.

For a given choice of the 3-manifold (2.0.4), the starting point of this analysis is the analytic continuation, $B_\alpha(\xi)$, of the Borel transform of the perturbative series (2.3.4). For a generic choice of $\mathrm{SL}(2,\mathbb{C})$ flat connection $\alpha$, the computation of (2.3.4) can be carried out by a variety of different methods (such as the explicit computation of Feynman diagrams, topological recursion, etc.), but for $\alpha = 0$ we can use a shortcut. At the perturbative level, the Feynman path integral (2.3.2) is analytic in $A$, and so all perturbative coefficients in (2.3.4) should be the same in theories with gauge groups $SU(2)$ and $\mathrm{SL}(2,\mathbb{C})$. This important feature was discussed in detail in [Guk05], where it was also used to explain the volume conjecture and to produce its various generalizations. In particular, one consequence of this is that the perturbative expansions in complex Chern Simons theory near the trivial flat

connection $\alpha = 0$ is given by the "Laplace transform" ([BBL05, GMP16]):

$$\mathcal{Z}^{\text{pert}}_{\alpha=0}(S^3_{\frac{p}{r}}(K);\hbar) \;\simeq\; \mathcal{L}^{(0)}_{\frac{p}{r}}\Big((x^{\frac{1}{2r}}-x^{-\frac{1}{2r}})\underbrace{(x^{\frac{1}{2}}-x^{-\frac{1}{2}})\sum_{m=0}^{\infty} C_m(K;q)(qx)_m(qx^{-1})_m}_{F(x,q)}\Big), \tag{5.2.1}$$

where the right-hand side should be expanded in $\hbar$ using $q = e^{\hbar}$, $C_m(K;q)$ are the cyclotomic coefficients for the knot $K$, and the operation $\mathcal{L}^{(a)}_{\frac{p}{r}}$ was defined earlier in (2.4.6). This formula should be highly reminiscent of the Dehn surgery formula for $F_K$, 2.4.5, indeed one can replace $F_K(x,q)$ by its non-perturbative counterpart [GM21], re-expanded in $\hbar$. Either way, for $\alpha = 0$ the computation of the perturbative series in complex Chern Simons theory drastically simplifies and can be expressed in terms of simpler objects familiar from the $SU(2)$ Chern Simons theory.[20] For general twist knots $K_n$, the cyclotomic coefficients can be written explicitly, [Mas03]:

$$C_m(K_n;q) = q^m \sum_{j=0}^{m}(-1)^j q^{j(j+1)n+j(j-1)/2}(1-q^{2j+1})\frac{(q;q)_m}{(q;q)_{m+j+1}(q;q)_{m-j}} \tag{5.2.2}$$

and in the special cases $p = -1$ and $p = 2$ reduce to rather compact expressions for the knots $4_1$ and $5_2$, which we use as our prime examples:

$$\begin{aligned} K_{-1} = 4_1 :&\qquad C_m(4_1;q) = (-1)^m q^{-\frac{m(m+1)}{2}} \\ K_2 = 5_2 :&\qquad C_m(5_2;q) = q^m \sum_{j=0}^{m}(-1)^j q^{j\frac{3+5j}{2}}(1-q^{2j+1})\frac{(q;q)_m}{(q;q)_{m+j+1}(q;q)_{m-j}} \end{aligned}$$

Substituting these into (5.2.1) gives an efficient way of computing the perturbative series to a very high loop order. Therefore, our next goal is to analyse the corresponding Borel plane for hyperbolic surgeries on twist knots.

### 5.2.1 Surgeries on $4_1$ knot

For $-\frac{1}{2}$ surgery on the figure-eight knot $K = 4_1$, using the procedure outlined above, we expand the perturbative partition function (5.2.1) to order $\hbar^{228}$. The first few terms are given here:

$$\begin{aligned} \mathcal{Z}^{\text{pert}}_{\alpha=0}(S^3_{-\frac{1}{2}}(4_1)) \;&=\; 1+\frac{97\hbar}{8}+\frac{33985\hbar^2}{128}+\frac{24726817\hbar^3}{3072}+\frac{30753823105\hbar^4}{98304}+\dots \\ &:=\; \sum_{n=0}^{\infty} a_n\,\hbar^n \end{aligned} \tag{5.2.3}$$

[20] Clearly, this can not be the case for more general $\alpha$; after all, even the notion of a complex flat connection itself may not be meaningful in a theory with $SU(2)$ gauge group.

The coefficients $a_n$ are all rational and positive. As mentioned above, the $4_1$ knot is amphichiral, and so the perturbative series for the $+\frac{1}{2}$ surgery can be obtained simply by replacing $\hbar \to -\hbar$. This has the effect of changing the sign of every other perturbative coefficient, i.e. corresponds to replacing $a_n \to (-1)^n a_n$.

### Leading Borel structure from the Perturbative Coefficients

Given this formal series (5.2.3), the first interesting physical observation is that it is factorially divergent. This can be seen clearly from a ratio test, which shows that

$$\frac{a_{n+1}}{a_n} \sim (8.6058\ldots) \times \left(n + \frac{3}{2}\right). \tag{5.2.4}$$

See Figure 5.6, which illustrates that the leading growth rate of this ratio is $\left(n + \frac{3}{2}\right)$,

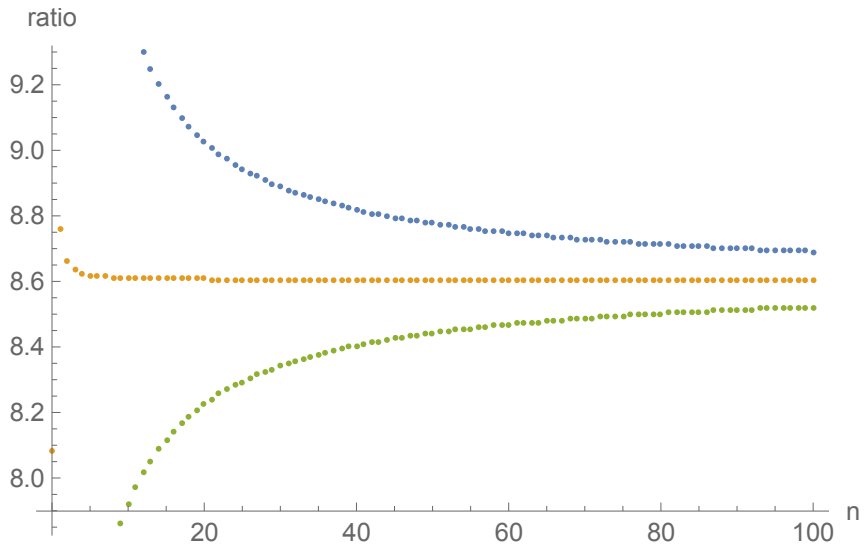


Figure 5.6: Ratio test for the coefficients $a_n$ of the perturbative series expansion of the Chern Simons partition function $\mathcal{Z}^{\text{pert}}_{\alpha=0}(S^3_{-\frac{1}{2}}(4_1))$ in (5.2.3). The curves plot the ratios $\frac{a_{n+1}}{a_n\left(n+\frac{1}{2}\right)}$ [blue dots], $\frac{a_{n+1}}{a_n\left(n+\frac{3}{2}\right)}$ [orange dots], and $\frac{a_{n+1}}{a_n\left(n+\frac{5}{2}\right)}$ [green dots], as a function of the perturbative order $n$. The $1/\left(n + \frac{3}{2}\right)$ factor is clearly preferred, as can be confirmed by further Richardson extrapolations.

rather than some other offset from $n$. The overall constant factor in (5.2.4) can be determined to extremely high precision using high order Richardson extrapolation of the ratio $\frac{a_{n+1}}{a_n\left(n+\frac{3}{2}\right)}$. The inverse of this overall constant gives the radius of convergence of the corresponding Borel transform:

$$\text{radius}_{4_1} = 0.116200832709284467265652483885021156937678 1\ldots \tag{5.2.5}$$

With our 228 coefficients $a_n$ as input, this radius of convergence can be computed to 140 stable digits. This determines to high precision the Chern Simons invariant (with conventional normalization) for the leading non-trivial saddle which agrees to all 140 stable digits with the theoretical value in Table 5.1:

$$\begin{aligned} CS(\alpha_1) &= -\frac{\text{radius}_{4_1}}{4\pi^2} \\ &= -0.00294340147758249530732138097249525292180 74\ldots \end{aligned} \tag{5.2.6}$$

The leading factorial divergence of the expansion coefficients is therefore of the form:

$$a_n \sim \mathcal{S}_{S^3_{-\frac{1}{2}}(4_1)} \frac{\Gamma\left(n+\frac{3}{2}\right)}{(\text{radius}_{4_1})^n}, \qquad n \to \infty \tag{5.2.7}$$

The Stokes constant $\mathcal{S}_{S^3_{-\frac{1}{2}}(4_1)}$, can also be determined to high precision using high order Richardson extrapolation. We find

$$\mathcal{S}_{S^3_{-\frac{1}{2}}(4_1)} = 1.10366976209388967154727717093434453161796588696\ldots \tag{5.2.8}$$

This Stokes constant agrees to all 140 stable digits with the Stokes constant associated with the leading Chern Simons invariant listed in Table 5.1. This is the first confirmation of the identifications (as shown in Table 5.1) of the geometric data, the Chern Simons invariant and the adjoint Reidemeister torsion, with the perturbative data derived directly from the formal perturbative expansion of the partition function. We see that while the perturbative expansion is an expansion about the trivial saddle point, it encodes in an easily accessible way both the location and the strength of the closest non-trivial Chern Simons saddle.

With 228 terms of the formal series, it is also straightforward to extract subleading power-law corrections to the leading large-order factorial growth in (5.2.7):

$$a_n \sim \mathcal{S}_{S^3_{-\frac{1}{2}}(4_1)} \frac{\Gamma\left(n+\frac{3}{2}\right)}{(\text{radius}_{4_1})^n} \left[1 - \frac{(0.0572609835...)}{\left(n+\frac{1}{2}\right)} + \ldots\right] + \ldots \quad , \quad n \to \infty \tag{5.2.9}$$

**Padé-Borel and Padé-Conformal-Borel Analysis**

We expect further exponentially suppressed corrections to the large order growth in (5.2.9) associated with more distant Borel singularities, which in turn are identified

with Chern Simons invariants of greater magnitude. These are difficult to resolve with ratio tests and root tests, because the exponentially suppressed corrections are swamped by the power-law corrections. However, some of these further Borel singularities can be resolved via Padé and conformal mapping methods in the Borel plane [CD20, CD22].

The first step is to regularize the divergent formal series (5.2.3) by transforming to the Borel plane via a normalized the Borel transform (Normalized, so the radius of convergence is 1):

$$\mathcal{B}_{S^3_{-\frac{1}{2}}(4_1)}(\xi) := \sum_{n=0}^{\infty} \frac{a_n}{\Gamma(n+1)} (\text{radius}_{4_1})^n \, \xi^n. \tag{5.2.10}$$

This is now a convergent series whose singularities are expected to encode information about non-perturbative features of the Chern Simons partition function. The formal perturbative series (5.2.3) can be reconstructed term-by-term using the Laplace-Borel integral

$$\mathcal{Z}^{\text{pert}}_{\alpha=0} = \frac{(\text{radius}_{4_1})^{3/2}}{\Gamma(3/2)\hbar^{3/2}} \int_0^{\infty} d\xi \sqrt{\xi} \, e^{-\text{radius}_{4_1}\xi/\hbar} \mathcal{B}_{S^3_{-\frac{1}{2}}(4_1)}(\xi). \tag{5.2.11}$$

Padé approximants [BGM96, BO99] provide an initial rough overview of the singularity structure in the Borel plane. Given our 228 term truncation of the Borel transform, we first construct a diagonal Padé approximant of order $[114, 114]$, and compute its poles in the Borel plane[21]. The Padé-Borel poles are shown in Figure 5.7, and a zoomed-in view of the neighbourhood of the leading singularity is shown in Figure 5.8.

This simple Padé analysis confirms that the leading Borel singularity is indeed at $\xi = 1$, consistent with our normalization convention in (5.2.10). Recall that since Padé is, by construction, an approximation by rational functions, its only possible singularities are poles. Padé represents branch points as the accumulation points of arcs of poles, according to the electrostatic interpretation of Padé as a minimizer of an associated capacitor [GS58, Sta97, Saf10, CD20, CD22].

Thus, this elementary Padé-Borel construction decodes the leading Chern Simons invariant, and by plotting the Padé-Borel transform as it approaches the leading singularity we can also extract a rough numerical estimate of the associated Stokes constant, which tells us the associated adjoint Reidemeister torsion. To obtain higher

[21] We also compute near-diagonal Padé approximants, to filter out spurious Padé poles.

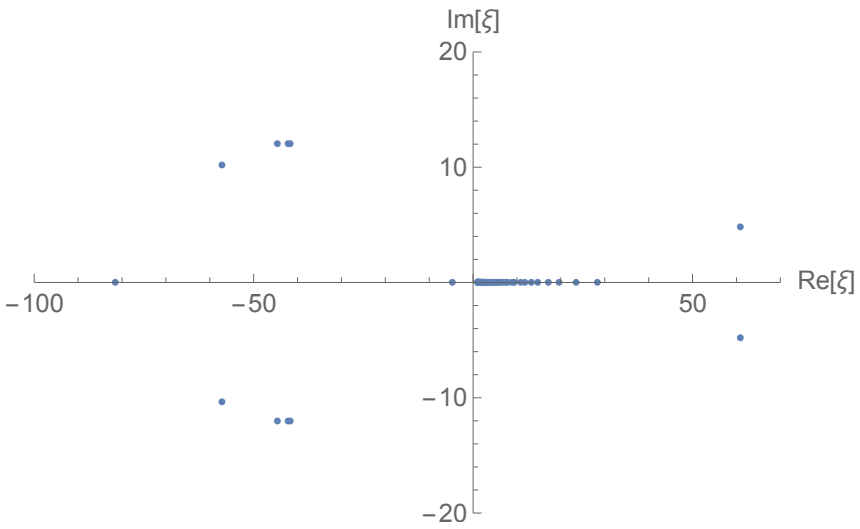


Figure 5.7: The Padé-Borel poles from an order [114, 114] diagonal Padé approximant to the 228 term truncated Borel transform in (5.2.10). The Borel variable $\xi$ is normalized so that the leading singularity is at +1. Figure 5.8 shows a zoomed-in view of the poles accumulating to $\xi = 1$ on the positive Borel axis.

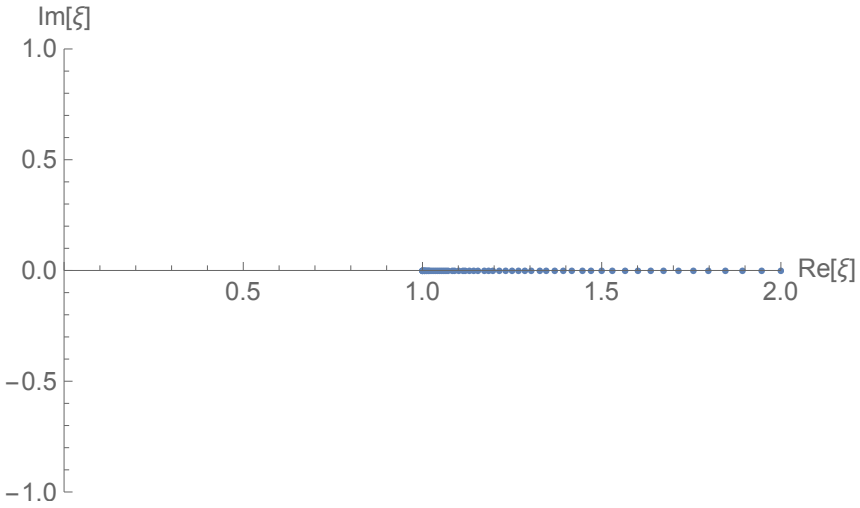


Figure 5.8: A zoomed-in view of the Padé-Borel poles accumulating on the positive Borel axis, from Figure 5.7. We see a line of poles accumulating to $\xi = 1$, which is how Padé attempts to represent a branch cut, with a branch point at the accumulation point.

precision, and more importantly to decode the other Chern Simons invariants, and their associated Reidemeister torsions, we need further tools. In this case, we can take advantage of the fact that the other Chern Simons invariants have much larger magnitude (see column 6 in Table 5.1). Hence, we expect the other Borel singularities to be far separated from the leading one. This means that the Borel branch cut

| Exact CS Invariant | Normalized CS Invariant | Padé-Borel | Padé-Conformal -Borel | Singularity Elimination |
|---|---|---|---|---|
| $-0.002943401$ | 1 | 1 | 1 | 1 |
| $-0.485874320$ | 165.072391 | not resolved | not resolved | 161.05 |
| 0.053933576 | $-18.323554$ | not resolved | absent | absent |
| $0.123303626$ $\pm 0.03542464i$ | $-41.891542$ $\mp 12.03527i$ | $-42 \mp 12i$ | $-41.8814$ $\mp 12.0371i$ | $-41.891542$ $\mp 12.03527i$ |
| 0.235159766 | $-79.893881$ | not resolved | not resolved | $-79.89$ |
| $-0.171882873$ | 58.3960000 | not resolved | 58.3754 | 58.3960000 |

Table 5.4: CS Invariants for $-\frac{1}{2}$ surgery on the $4_1$ knot, obtained from different analysis methods. The first column has the exact CS invariants, from Table 5.1. All subsequent columns list the normalized values, which are obtained from the exact ones by dividing by the minimal CS invariant $-0.002943401$. These subsequent columns show the CS invariants extracted using the Padé-Borel, Padé-Conformal-Borel, or singularity elimination methods to analyse the Borel transform based on the finite order perturbative expansion in (5.2.3). Note that the more precise methods exclude, with very high numerical precision, the existence of a Borel singularity near $-18.323554$. This illustrates the power of the singularity elimination method in resolving even very distant singularities.

starting at $\xi = 1$ is dominant, and we can therefore build an approximate conformal map based on it. This conformal map significantly improves the precision of the Padé analytic continuation of the truncated Borel transform (this improvement can be quantified [CD20]). This enables not only a more precise numerical probe of the leading singularity, but more importantly, it resolves more cleanly the more distant Borel singularities. Concentrating on this leading cut in the Borel plane, we map the cut plane into the unit disk via the invertible conformal map

$$\xi = \frac{4z}{(1+z)^2} \quad \longleftrightarrow \quad z = \frac{1-\sqrt{1-\xi}}{1+\sqrt{1-\xi}} \tag{5.2.12}$$

The Padé-Conformal-Borel procedure is to re-expand the mapped truncated Borel series $\mathcal{B}\left(\frac{4z}{(1+z)^2}\right)$ to the same order (this is optimal [CD22]) in $z$, and then make a Padé approximant in $z$, and finally to map back to the original Borel $\xi$ plane. The resulting landscape of singularities in the Borel plane is shown in Figure 5.9. The black dots show the Padé poles in the conformal $z$ plane when they are mapped back to the original Borel $\xi$ plane. The red dots show the Chern Simons invariants computed from the A-polynomial approach, as listed in Table 5.1. Compared to the Padé-Borel results in Figure 5.7, we now see much more clearly and precisely the complex conjugate pair of singularities at $\xi = -41.8814 \pm 12.0371i$, and we

also resolve a singularity around $\xi = 58.3754$. These values are shown in Table 5.4. We stress that these Padé-Conformal-Borel results are obtained from exactly the same perturbative input used for the Padé-Borel results shown in Figure 5.7, but just processed differently.

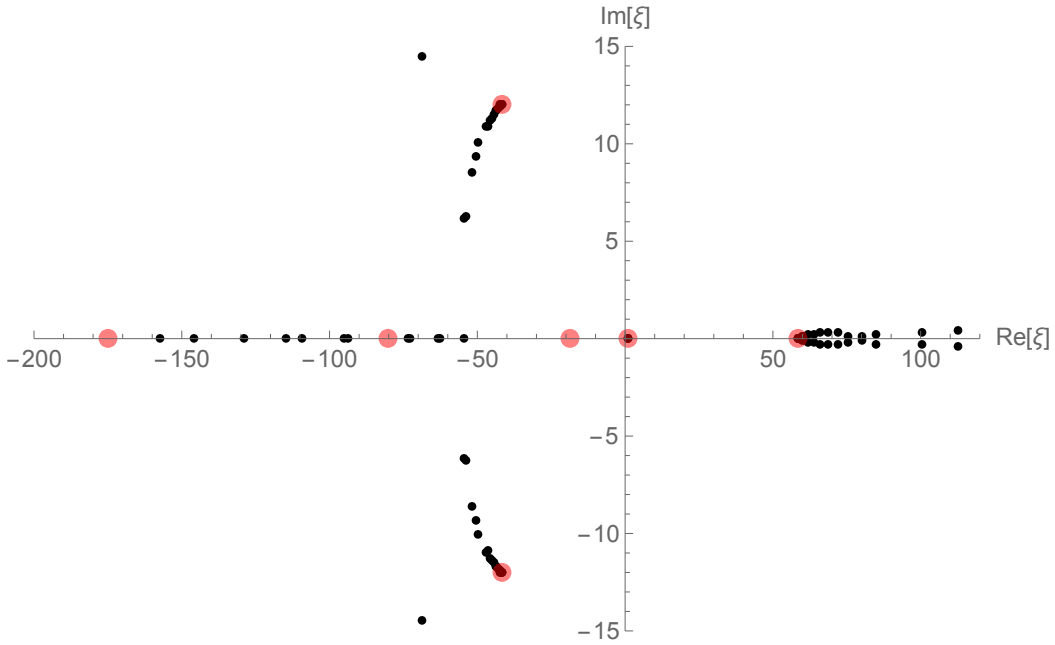


Figure 5.9: Padé-Conformal-Borel analysis of the Borel singularities. The black dots show the inverse conformal map images of the poles of the Padé approximant made in the conformal $z$ plane. The opaque red dots show the Chern Simons invariants (see Table 5.1) computed in Section 5.1.1. Notice that the Borel singularity near $\xi = 59$ is now resolved: compare with Figure 5.7 where this singularity is not resolved. The dot at $-175$ comes from the normalized CS invariant at 165, due to the mod 1 nature of these invariants.

However, this Padé-Conformal-Borel analysis is still not able to resolve the expected more distant singularities at $\xi = -79.893881$ and $\xi = 165.072391$. Nevertheless, it is interesting to note that this analysis does rule out the existence of a Borel singularity at $\xi = -18.3236$ to a high degree of precision. This analysis can be further improved by more singularity elimination techniques, [CD22, CDGG23] to remove the new leading singularity (after elimination of the closest singularity. With this tool, we resolve all the remaining (normalized) Chern Simons invariants, as shown in the last column of Table 5.1, except for the one at $-18.3236$ which we are able to rigorously rule out (to more than 100 digits of precision). This strongly suggests that this Chern Simons is a phantom saddle (as defined in 2.3.14) disconnected from the others.

### 5.2.2 Surgeries on $5_2$ Knot

We now apply the same numerical procedures to the $\pm\frac{1}{2}$ surgeries on the $5_2$ knot. The $5_2$ knot is interestingly different from the $4_1$ knot, so it is not clear in advance what to expect. In particular, since the $5_2$ knot is not amphichiral, the formal $\hbar$ series of the partition function for the $\pm\frac{1}{2}$ surgeries will be different. We show below that the Borel plane structure is also quite different for the $\pm\frac{1}{2}$ surgeries.

As before, we expand the partition function as a perturbative series in powers of $\hbar$. The first terms for the $\pm\frac{1}{2}$ surgery are:

$$\begin{aligned} Z_{S^3_{\frac{1}{2}}(5_2)}(\hbar) &= -1 - \frac{183\hbar}{8} - \frac{122577\hbar^2}{128} - \frac{56438733\hbar^3}{1024} - \frac{133022451595\hbar^4}{32768} - \dots \\ &:= \sum_{n=0}^{\infty} b_n^{\frac{1}{2}}\,\hbar^n \end{aligned} \tag{5.2.13}$$

$$\begin{aligned} Z_{S^3_{-\frac{1}{2}}(5_2)}(\hbar) &= 1 - \frac{191\hbar}{8} + \frac{107137\hbar^2}{128} - \frac{127522367\hbar^3}{3072} + \frac{261703390465\hbar^4}{98304} + \dots \\ &:= \sum_{n=0}^{\infty} b_n^{-\frac{1}{2}}\,\hbar^n \end{aligned} \tag{5.2.14}$$

For $-\frac{1}{2}$ surgery we generated 228 terms, while for $+\frac{1}{2}$ surgery we generated 188 terms. Note that the perturbative expansion for the $-\frac{1}{2}$ surgery case is alternating in sign, while for the $+\frac{1}{2}$ surgery case it is non-alternating.[22]

#### Leading Borel structure from the Perturbative Coefficients

We observe that the formal series (5.2.14) and (5.2.13) are factorially divergent. Ratio tests combined with Richardson extrapolation determine the leading growth as:

$$b_n^{\frac{1}{2}} \sim -\mathcal{S}_{S^3_{\frac{1}{2}}(5_2)}\,\frac{\Gamma\left(n+\frac{3}{2}\right)}{(\text{radius}_{S^3_{\frac{1}{2}}(5_2)})^n}, \quad n\to\infty \tag{5.2.15}$$

$$b_n^{-\frac{1}{2}} \sim (-1)^n\mathcal{S}_{S^3_{-\frac{1}{2}}(5_2)}\,\frac{\Gamma\left(n+\frac{3}{2}\right)}{(\text{radius}_{S^3_{-\frac{1}{2}}(5_2)})^n}, \quad n\to\infty \tag{5.2.16}$$

[22] This sign pattern correlates with the sign of the surgery in the opposite way compared to the $4_1$ case.

We see that the expansion coefficients $b_n^{\pm\frac{1}{2}}$ of both series have the same factorial divergence as, which is also the same as for, $S^3_{\pm\frac{1}{2}(4_1)}$ discussed in Section 5.2.1.

From (5.2.16) and (5.2.15) we can extract the radii of convergence of the associated Borel transforms:

$$\text{radius}_{S^3_{\frac{1}{2}}(5_2)} = 0.06147117938868975855184395044865487683233\ldots \quad (5.2.17)$$

$$\text{radius}_{S^3_{-\frac{1}{2}}(5_2)} = 0.06967508334205362331643137281436160974803\ldots \quad (5.2.18)$$

These Borel radii are somewhat surprisingly close in magnitude, this can be understood from the A-polynomial perspective: see Section 5.3.

This defines, for each surgery, the leading Chern Simons invariant:[23]

$$\begin{aligned} CS(\alpha_2)_{S^3_{\frac{1}{2}}(5_2)} &= -\frac{\text{radius}_{S^3_{\frac{1}{2}}(5_2)}}{4\pi^2} \\ &= -0.00155708316388813088325377802987280189096\ldots \\ CS(\alpha_2)_{S^3_{-\frac{1}{2}}(5_2)} &= \frac{\text{radius}_{S^3_{-\frac{1}{2}}(5_2)}}{4\pi^2} \\ &= 0.00176489047864885113073962589709477793304 9\ldots \end{aligned}$$

These leading Borel singularities match precisely the Chern Simons invariants of smallest magnitude, derived using the A-polynomial method: compare with the last row of Tables 5.2 and 5.3. The Stokes constants $\mathcal{S}_{S^3_{\pm\frac{1}{2}}(5_2)}$ in (5.2.16) and (5.2.15), can also be extracted with very high precision:

$$\mathcal{S}_{S^3_{\frac{1}{2}}(5_2)} = 1.131609358228288647823063995949199145039985372\ldots \quad (5.2.19)$$

$$\mathcal{S}_{S^3_{-\frac{1}{2}}(5_2)} = 1.169768176599218160480078065141126396593190545\ldots \quad (5.2.20)$$

The Stokes constants in (5.2.20) and (5.2.19) agree to more than 100 digits of precision with the corresponding Stokes constants in Tables 5.3 and 5.2, based on the identification of the Stokes constant with the adjoint Reidemeister torsion in (5.1.25). Note again that these Stokes constants and indeed also the Stokes constant for of the

[23] Recall the normalization convention that the Chern Simons invariant is equal to minus the Borel singularity.

leading singularity for the $4_1$ knot in (5.2.8) are quite close to one another. There is an explanation for this, analogous to the explanation for the similarity in Chern Simons values.

Overall we see that this elementary series analysis determines to high precision three important physical and geometric quantities: (i) the leading power factor in the growth rate, which determines the location of the leading Borel singularity, which in turn determines the leading non-trivial Chern Simons invariant; (ii) the offset of the factorial growth, which determines the nature of the leading Borel singularity; (iii) the overall Stokes constant which determines the adjoint Reidemeister torsion associated with the leading Chern Simons invariant. Thus, non-perturbative information about more distant Borel singularities (and therefore about other non-trivial flat connections) is indeed encoded in the formal asymptotic expansions about the trivial flat connection/Chern Simons saddle.

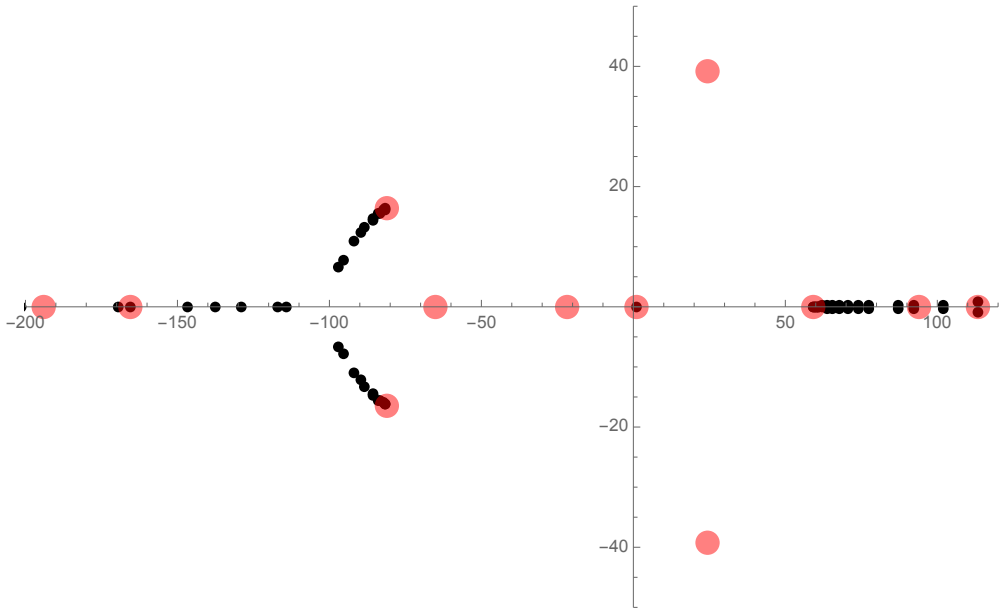


Figure 5.10: The Borel plane structure for the $+\frac{1}{2}$ surgery on the manifold $S^3\backslash N(5_2)$, resolved by the Padé-Conformal-Borel method. The black dots show the inverse conformal map images of the poles of the Padé approximant made in the conformal $z$ plane. The opaque red dots show the Chern Simons values computed using the A-polynomial method shown in Table 5.2.

### Padé-Conformal-Borel Analysis

To probe this more deeply, we turn again to the higher-precision methods of Borel analysis. We start again with the Borel transform where we normalized with the

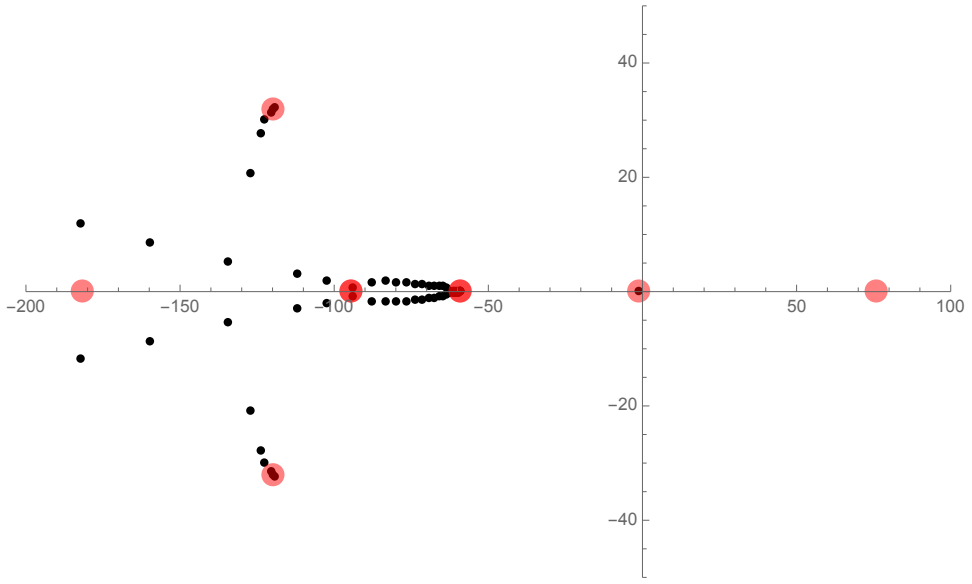


Figure 5.11: The Borel plane structure for the $-\frac{1}{2}$ surgery on the manifold $S^3\backslash N(5_2)$, resolved by the Padé-Conformal-Borel method. The black dots show the inverse conformal map images of the poles of the Padé approximant made in the conformal $z$ plane. The opaque red dots show the Chern Simons invariants computed using the A-polynomial method, shown in Table 5.3.

appropriate radius of convergence, so that the leading Borel singularity is at $\xi = \pm 1$:

$$\mathcal{B}_{S^3_{\pm\frac{1}{2}}(5_2)}(\xi) := \sum_{n=0}^{\infty} \frac{b_n^{\pm\frac{1}{2}}}{\Gamma(n+1)} \left|\text{radius}_{S^3_{\pm\frac{1}{2}}(5_2)}\right|^n \xi^n \tag{5.2.21}$$

from which the formal perturbative series (5.2.14) and (5.2.13) are reconstructed by the Laplace-Borel integral as in (5.2.11).

As described in Section 5.2.1, we use the Padé-Conformal-Borel procedure to extract information about the Borel plane singularities.[24] The results of this Padé-Conformal-Borel analysis are shown in Figures 5.11 and 5.10. In the plots, the black dots show the Padé poles in the conformal $z$ plane when they are mapped back to the original Borel $\xi$ plane. The red dots show the Chern Simons invariants computed from the A-polynomial approach, as listed in Tables 5.3 and 5.2.

In Figure 5.10 we see that for the $+\frac{1}{2}$ surgery, the Padé-Conformal-Borel procedure identifies with good precision the leading singularity, together with a more distant one near 59 on the positive Borel axis, in addition to another complex conjugate pair with negative real part. There are hints of singularities at $\xi \approx 94$ and $\xi \approx 113$, as

[24] We omit the lower-resolution Padé-Borel method for this example.

well as at $\xi \approx -165$. Furthermore, this analysis also finds several possible phantom saddles at $\xi \approx -22$, $\xi \approx -65$, and complex conjugate pair near $\xi \approx 24 \pm 39i$.

In Figure 5.11 we see that for the $-\frac{1}{2}$ surgery, the Padé-Conformal-Borel procedure identifies with good precision the leading singularity, together with two more distant ones on the negative Borel axis, in addition to another complex conjugate pair with negative real part. More distant Borel singularities at $\xi \approx -182$ and $\xi \approx -220$ are not resolved with the available data. However, this analysis rules out a singularity near $\xi \approx 76$, implying that we have found another phantom saddle.

It is interesting to note that the $+\frac{1}{2}$ surgery case has a more complicated Borel plane structure, consistent with the fact that the associated A-polynomials and torsion polynomials in (5.1.30) and (5.1.33) do not factorize like they do for the $-\frac{1}{2}$ surgery cases in (5.1.31) and (5.1.34). These differences, as well as the patterns of decoupled flat connections, deserve further study with more perturbative data and using more advanced analysis methods [CD22].

### 5.3 Generic Small Surgeries

One interesting observation from the above computations is that many of the invariants of $S^3_{\pm\frac{1}{2}}(5_2)$ are quite similar, see (5.2.17) and (5.2.18) or (5.2.19) and (5.2.20). This turns out to be an indicator of a more general structure linking invariants of different surgeries of a given knot $K$.

Recall that we can associate flat connections on the $\frac{p}{r}$ surgery to intersections between the affine varieties $\mathcal{A}$ and $\{y = x^{-\frac{p}{r}}\}$. The overarching idea is that for surgeries that are "close", in the sense that $|\frac{p}{r} - \frac{p'}{r'}| << 1$, we can estimate some CS invariants for the $\frac{p}{r}$ surgery from corresponding the CS invariants on the $\frac{p'}{r'}$ surgery. To illustrate this technique, we focus on the case where $\frac{p'}{r'} = 0$.

**Conjecture 5.3.1.** *Fix a knot $K$ and a root $x^*$ of $\Delta_K(x^2)$. Then for any $n \in \mathbb{Z}$, for small enough $\frac{p}{r} \in \mathbb{Q}$, the manifold $\mathcal{S}_{K^\theta}$ has a Chern Simons value approximately equal to*

$$\frac{(\log(x^*) + n\pi i)^2}{4\pi^2}\theta \qquad n \in \mathbb{Z}. \tag{5.3.2}$$

Assuming Conjecture 5.3.1, we get a simple prediction for the minimal Chern Simons value of $S^3_{\frac{p}{r}}(K)$ for $|r| >> |p|$. It should occur near $\frac{(\log(x^*))^2}{4\pi^2}\frac{p}{r}$ where $x^*$ is the root of $\Delta_K(x^2)$ which minimises $|\log(x^*)|$. There should also be an analogous conjecture for

the stokes constants[25] but it is more difficult to formulate as our method of computing stokes constants, Theorem 5.1.13, is entirely algebraic.

We present a partial proof for this conjecture. Given a root $x^*$ of $\Delta_K(x^2)$, we immediately know that $A(1, x^*) = 0$. Then for $\theta = \frac{p}{r} \in \mathbb{Q}$ close to 0 we expand

$$x(\theta) = x^* + c_1\theta + \cdots + c_n\theta^n + \cdots \tag{5.3.3}$$

Enforcing the surgery condition, $y(\theta) = x(\theta)^{-\theta}$, we find a collection of $y$'s

$$y_n(\theta) = x(\theta)^{-\theta} = 1-(\log(x^*)+2n\pi i)\theta+\left(\frac{2c_1}{x} + (\log(x^*) + 2n\pi i)^2\right)\frac{\theta^2}{2}+\cdots \tag{5.3.4}$$

labelled by choice of log branch (We can also impose $|n| < r$). As $\theta \to 0$, all branch choices should appear as intersection points and all such intersection points should be non-spurious[26]. Imposing $A(x(\theta), y(\theta)) = 0$, we can solve for $c_i$ by looking at the coefficient of $\theta^i$. Note that there can be multiple solutions along different branches if multiple irreducible branches of $\mathcal{A}$ meet at $(x^*, 1)$.

Next, recall the formula for the CS invariant given in Equation (5.1.2). Provided $\theta$ is small, we can ignore the branching of log and simplify this to

$$CS(\theta, n, x^*) = \frac{1}{2\pi^2}\left(\int_\gamma \frac{\log(y_n)}{x}\, dx + \frac{1}{2\theta}\log(y_n(\theta))^2\right) = a_0 + a_1\theta + a_2\theta^2 + \cdots \tag{5.3.5}$$

For $|\theta| << 1$, the integrand is analytic in a small region around $\gamma \subset \mathcal{A} \subset \mathbb{C}^2$ and so

$$\int_\gamma \frac{\log(y_n)}{x}\, dx = \int_0^\theta \theta\frac{\log(x(\theta)) + 2n\pi i}{x(\theta)}x'(\theta)d\theta = O(\theta^2). \tag{5.3.6}$$

Hence the integral does not contribute to the first 2 terms and so

$$\begin{aligned} CS(\theta, n, x^*) &= \frac{1}{4\pi^2\theta}\log(y_n(\theta))^2 + O(\theta^2) \\ &= \frac{(\log(x^*) + 2n\pi i)^2}{4\pi^2}\theta + O(\theta^2). \end{aligned}$$

Due to symmetries, if $x^*$ is a root, so are $\{-x^*, (x^*)^{-1}, -(x^*)^{-1}\}$ and as $\log(-x^*)) = \log(x^*) \pm \pi i$ we see why we should expect Conjecture 5.3.1. Additionally, for a

[25] Indeed this can be clearly seen if the perturbative expansion given in (5.2.1) is performed for generic $\frac{p}{r}$ giving a well-defined series in $\hbar, r$ and $\frac{1}{p}$. Working in the $|p| << |r|$ limit, we can compute the leading pole and residue as a series in $\frac{p}{r}$. See [CDGG23] for more details

[26] This is why this is given as a conjecture. While this seems intuitively clear that the intersections will be generically non-spurious, there is not currently a rigorous proof.

surgery $\frac{p}{r}$ with $|r| >> |p|$, we expect the appearance of the predicted Chern Simons values for with $|n| < |r|$ to appear.

One interesting implication from this conjecture is that if we normalize the smallest magnitude Borel singularity to be at $\pm 1$, then for small $\theta$ there is a family of poles which does not move much as $\theta$ changes. Explicitly these occur at

$$\frac{(\log(x^*) + n\pi i)^2}{\log(x^*)^2}$$

and will become a dominant family of subleading poles as $\theta \to 0$ as all other poles will go to $\infty$.

Let us test this conjecture on our two examples, the $4_1$ and the $5_2$ knots.

### 5.3.1 $4_1$ Knot

For the $4_1$ knot the universal small $\theta$ estimate (5.3.2) is already an excellent approximation as, due to the amphichirality of the $4_1$ knot, the $\theta^{2n}$ terms in the expansion vanish. Setting $x^* = \frac{1+\sqrt{5}}{2}$, we find that for the $\theta = -\frac{1}{2}$ surgery we get three predicted CS invariants,

$$\left(-\frac{1}{2}\right)\frac{(\log(x^*) + n\pi i)^2}{4\pi^2} = \begin{cases} -0.0029328 & , \quad n = 0 \\ 0.1220672 \mp 0.0382936i & , \quad n = \pm 1 \end{cases} \tag{5.3.7}$$

These Chern Simons invariants compare well to $\alpha = 1, 4, 5$ in Table 5.1 and we can improve the approximation by computing higher corrections. Letting $x_n = e^{n\pi i}x^*$ denote the solution on the branch $\log(x_n) = \log(x^*) + n\pi i$ we find

$$CS_{4_1}(n;\theta) = \frac{\log(x_n)^2}{4\pi^2}\theta + \frac{\sqrt{5}\log(x_n)^3}{300\pi^2}\theta^3 - O(\theta)^5. \tag{5.3.8}$$

Specialising to the $\theta = -\frac{1}{2}$ case, this improves our earlier predictions to

$$CS_{4_1}\left(n;-\frac{1}{2}\right) = \begin{cases} -0.0029433 & n = 0 \\ 0.1234017 \mp 0.0355726i & n = \mp 1. \end{cases}$$

### 5.3.2 $5_2$ Knot

Identical analysis applies to the roots of the Alexander polynomial for the $5_2$ knot. Since the $5_2$ knot is not amphichiral there will be $\theta^2$ corrections to the approximation in Equations (5.3.2) and (5.3.8) and we find

$$CS_{5_2}(n;\theta) = \frac{\log(x_n)^2}{4\pi^2}\theta - \frac{\log(x_n)^2}{32\pi^2}\theta^2 + \frac{\log(x_n)^2(21 - 2\sqrt{7}i\log(x_n))}{5376\pi^2}\theta^3 + O(\theta)^4. \tag{5.3.9}$$

Despite appearances, these are strictly real as $\log(x_n)$ is imaginary. Setting $\theta = \pm\frac{1}{2}$ we find

$$CS_{5_2}\left(n; -\frac{1}{2}\right) = \begin{cases} 0.0017643 & n = 0 \\ 0.1662666 & n = 1 \\ 0.1041303 & n = -1 \end{cases}$$

$$CS_{5_2}\left(n; \frac{1}{2}\right) = \begin{cases} -0.0015575 & n = 0 \\ -0.1468403 & n = 1 \\ -0.0918932 & n = -1. \end{cases}$$

Noting that $\frac{1}{6} \approx 0.166666...$, and $\frac{5}{48} \approx 0.104167...$, we see that for $\theta = \mp\frac{1}{2}$ surgery these simple estimates closely reproduce the three smallest magnitude exact Chern Simons invariants in Tables 5.2 and 5.3. This answers the question about why the smallest Chern Simons values of $S^3_{\pm\frac{1}{2}}(5_2)$ are so similar.

## Bibliography


[AENV14] Mina Aganagic, Tobias Ekholm, Lenhard Ng, and Cumrun Vafa. Topological strings, D-model, and knot contact homology. *Advances in Theoretical and Mathematical Physics*, 18(4):827–956, 2014. DOI: 10.4310/ATMP.2014.v18.n4.a3.

[AV12] Mina Aganagic and Cumrun Vafa. Large N duality, mirror symmetry, and a Q-deformed A-polynomial for knots, 2012. arXiv:1204.4709.

[BBL05] Anna Beliakova, Christian Blanchet, and Thang T. Q. Lê. Laplace transform and universal sl(2) invariants, 2005. arXiv:0509394.

[BGM96] George A. Baker and Peter Graves-Morris. *Padé Approximants*. Encyclopedia of Mathematics and its Applications. Cambridge University Press, 2 edition, 1996. DOI: 10.1017/CBO9780511530074.

[BH90] M. V. Berry and C. J. Howls. Hyperasymptotics. *Proceedings: Mathematical and Physical Sciences*, 430:653–668, 1990. DOI: 10.1098/rspa.1990.0111.

[BH91] M. V. Berry and C. J. Howls. Hyperasymptotics for integrals with saddles. *Proceedings: Mathematical and Physical Sciences*, 434:657–675, 1991. DOI: 10.1098/rspa.1991.0119.

[BMM20a] Kathrin Bringmann, Karl Mahlburg, and Antun Milas. Higher depth quantum modular forms and plumbed 3-manifolds. *Letters in Mathematical Physics*, 110, 10 2020. DOI: 10.1007/s11005-020-01310-z.

[BMM20b] Kathrin Bringmann, Karl Mahlburg, and Antun Milas. Quantum modular forms and plumbing graphs of 3-manifolds. *Journal of Combinatorial Theory, Series A*, 170:105145, 02 2020. DOI: 10.1016/j.jcta.2019.105145.

[BNG96] Dror Bar-Natan and Stavros Garoufalidis. On the Melvin-Morton-Rozansky conjecture. *Invent. Math.*, 125(1):103–133, 1996. DOI: 10.1007/s002220050070.

[BO99] C. M. Bender and S. A. Orszag. *Advanced Mathematical Methods for Scientists and Engineers*. Springer, 1999. DOI: 10.1007/978-1-4757-3069-2.

[Bur90] Nigel Burroughs. The universal R-matrix for Uqsl(3) and beyond! *Communications in Mathematical Physics*, 127(1):109–128, 1990. DOI: 10.1007/BF02096496.

[CCFGH19] Miranda C. N. Cheng, Sungbong Chun, Francesca Ferrari, Sergei Gukov, and Sarah M. Harrison. 3d Modularity. *JHEP*, 10:010, 2019. DOI: 10.1007/JHEP10(2019)010.

[CCGLS94] D. Cooper, M. Culler, H. Gillet, D. D. Long, and P. B. Shalen. Plane curves associated to character varieties of 3-manifolds. *Invent. Math.*, 118(1):47–84, 1994. DOI: 10.1007/BF01231526.

[CD20] Ovidiu Costin and Gerald V. Dunne. Physical Resurgent Extrapolation. *Phys. Lett. B*, 808:135627, 2020. DOI: 10.1016/j.physletb.2020.135627.

[CD22] Ovidiu Costin and Gerald Dunne. Uniformization and constructive analytic continuation of Taylor series. *Communications in Mathematical Physics*, 392:1–44, 03 2022. DOI: 10.1007/s00220-022-04361-6.

[CDGG23] Ovidiu Costin, Gerald Dunne, Angus Gruen, and Sergei Gukov. Going to the Other Side via the Resurgent Bridge, 2023. To Appear.

[CFS20] Miranda Cheng, Francesca Ferrari, and Gabriele Sgroi. Three-manifold quantum invariants and mock theta functions. *Philosophical Transactions of the Royal Society A: Mathematical, Physical and Engineering Sciences*, 378:20180439, 01 2020. DOI: 10.1098/rsta.2018.0439.

[CGPS20] Sungbong Chun, Sergei Gukov, Sunghyuk Park, and Nikita Sopenko. 3d-3d correspondence for mapping tori. *Journal of High Energy Physics*, 2020, 09 2020. DOI: 10.1007/JHEP09(2020)152.

[CS74] Shiin-Shen Chern and James Simons. Characteristic forms and geometric invariants. *Annals Math.*, 99:48–69, 1974. DOI: 10.2307/1971013.

[DE20] Luis Diogo and Tobias Ekholm. Augmentations, annuli, and Alexander polynomials, 2020. arXiv:2005.09733.

[DGLZ09] Tudor Dimofte, Sergei Gukov, Jonatan Lenells, and Don Zagier. Exact results for perturbative Chern-Simons theory with complex gauge group. *Communications in Number Theory and Physics*, 3, 03 2009. DOI: 10.4310/CNTP.2009.v3.n2.a4.

[DGR05] Nathan Dunfield, Sergei Gukov, and Jacob Rasmussen. The superpolynomial for knot homologies. *Experimental Mathematics*, 15, 06 2005. DOI: 10.1080/10586458.2006.10128956.

[DeR67] de Rham Georges. Introduction aux polynômes d'uneoud. *Enseignement Math*, 13(2):187–194, 1967. DOI: 10.5169/seals-41542.

[EGGKPS22] Tobias Ekholm, Angus Gruen, Sergei Gukov, Piotr Kucharski, Sunghyuk Park, and Piotr Sułkowski. $\widehat{Z}$ at large $n$: from curve counts to quantum modularity. *Communications in Mathematical Physics*, 396, 08 2022. DOI: 10.1007/s00220-022-04469-9.

[EGGKPSS22] Tobias Ekholm, Angus Gruen, Sergei Gukov, Piotr Kucharski, Sunghyuk Park, Marko Stošić, and Piotr Sułkowski. Branches, quivers, and ideals for knot complements. *Journal of Geometry and Physics*, 177:104520, 2022. DOI: 10.1016/j.geomphys.2022.104520.

[EKL20a] Tobias Ekholm, Piotr Kucharski, and Pietro Longhi. Physics and geometry of knots-quivers correspondence. *Communications in Mathematical Physics*, 379:361–415, 2020. DOI: 10.1007/s00220-020-03840-y.

[EKL20b] Tobias Ekholm, Piotr Kucharski, and Pietro Longhi. Multi-cover skeins, quivers, and 3d $\mathcal{N} = 2$ dualities. *Journal of High Energy Physics*, 2020, 02 2020. DOI: 10.1007/JHEP02(2020)018.

[EKL21] Tobias Ekholm, Piotr Kucharski, and Pietro Longhi. Knot homologies and generalized quiver partition functions, 2021. arXiv:2108.12645.

[EN20] Tobias Ekholm and Lenhard Ng. Higher genus knot contact homology and recursion for colored HOMFLY-PT polynomials. *Adv. Theor. Math. Phys.*, 24(8):2067–2145, 2020. DOI: 10.4310/ATMP.2020.v24.n8.a3.

[ES19] Tobias Ekholm and Vivek Shende. Skeins on branes, 2019. arXiv:1901.08027.

[Efi11] Alexander Efimov. Cohomological hall algebra of a symmetric quiver. *Compositio Mathematica*, 148, 03 2011. DOI: 10.1112/S0010437X12000152.

[FGS13] Hiroyuki Fuji, Sergei Gukov, and Piotr Sulkowski. Super-$A$-polynomial for knots and BPS states. *Nucl. Phys. B*, 867:506, 2013. arXiv:1205.1515.

[FGSA12] Hidetoshi Awata, Sergei Gukov, Piotr Sulkowski, and Hiroyuki Fuji. Volume conjecture: Refined and categorified. *Adv. Theor. Math. Phys.*, 16(6):1669–1777, 2012. DOI: 10.4310/ATMP.2012.v16.n6.a3.

[FGSS12] Hiroyuki Fuji, Sergei Gukov, Marko Stosic, and Piotr Sułkowski. 3d analogs of argyres-douglas theories and knot homologies. *Journal of High Energy Physics*, 2013, 09 2012. DOI: 10.1007/JHEP01(2013)175.

[FR18] Hans Franzen and Markus Reineke. Semi-stable Chow-Hall algebras of quivers and quantized Donaldson-Thomas invariants. *Alg. Number Th.*, 12(5):1001–1025, 2018. DOI: 10.2140/ant.2018.12.1001.

[Fre92] Daniel S. Freed. Reidemeister torsion, spectral sequences, and Brieskorn spheres. *Journal für die reine und angewandte Mathematik (Crelles Journal)*, 1992:75 – 90, 1992. DOI: 10.1515/crll.1992.429.75.

[GGP14] Abhijit Gadde, Sergei Gukov, and Pavel Putrov. Walls, Lines, and Spectral Dualities in 3d Gauge Theories. *JHEP*, 05:047, 2014. DOI: 10.1007/JHEP05(2014)047.

[GHNPPS21] Sergei Gukov, Po-Shen Hsin, Hiraku Nakajima, Sunghyuk Park, Du Pei, and Nikita Sopenko. Rozansky-Witten geometry of Coulomb branches and logarithmic knot invariants. *J. Geom. Phys.*, 168:104311, 2021. DOI: 10.1016/j.geomphys.2021.104311.

[GL05] Stavros Garoufalidis and Thang T Q Le. The colored Jones function is q-holonomic. *Geometry & Topology*, 9(3):1253 – 1293, 2005. DOI: 10.2140/gt.2005.9.1253.

[GM08] Sergei Gukov and Hitoshi Murakami. SL(2,C) Chern-Simons theory and the asymptotic behavior of the colored Jones polynomial. *Letters in Mathematical Physics*, 86:79–98, 2008. DOI: 10.1007/s11005-008-0282-3.

[GM21] Sergei Gukov and Ciprian Manolescu. A two-variable series for knot complements. *Quantum Topol.*, 12(1):1–109, 2021. DOI: 10.4171/qt/145.

[GMP16] Sergei Gukov, Marcos Marino, and Pavel Putrov. Resurgence in complex Chern-Simons theory, 5 2016. arXiv:1605.07615.

[GPPV20] Sergei Gukov, Du Pei, Pavel Putrov, and Cumrun Vafa. BPS spectra and 3-manifold invariants. *J. Knot Theor. Ramifications*, 29(02):2040003, 2020. DOI: 10.1142/S0218216520400039.

[GPV17] Sergei Gukov, Pavel Putrov, and Cumrun Vafa. Fivebranes and 3-manifold homology. *JHEP*, 07:071, 2017. DOI: 10.1007/JHEP07(2017)071.

[GS12] Sergei Gukov and Piotr Sulkowski. A-polynomial, B-model, and quantization. *JHEP*, 02:070, 2012. DOI: 10.1007/JHEP02(2012)070.

[GS58] U. Grenander and G. Szegö. *Toeplitz forms and their applications*. Univ. California Press, Berkeley, 1958. DOI: 10.1063/1.3062237.

[Gar04] Stavros Garoufalidis. On the charactersitic and deformation varieties of a knot. *Geometry and Topology Monographs*, 7:291–304, 2004. arXiv:math/0306230.

[Gru22] Angus Gruen. The $\mathfrak{sl}_N$ Symmetrically Large Coloured $R$ Matrix, 12 2022. arXiv:2212.05222.

[Guk05] Sergei Gukov. Three-dimensional quantum gravity, Chern-Simons theory, and the A-polynomial. *Commun. Math. Phys.*, 255:577–627, 2005. DOI: 10.1007/s00220-005-1312-y.

[HOMFLY85] Jim Hoste, Adrian Ocneanu, Kenneth Millett, Peter J. Freyd, W. B. R. Lickorish, and David N. Yetter. A new polynomial invariant of knots and links. *Bull. Am. Math. Soc.*, 12(2):239–246, 1985. DOI: 10.1090/S0273-0979-1985-15361-3.

[Hik04] Kazuhiro Hikami. On the quantum invariant for the Brieskorn homology spheres. *International Journal of Mathematics*, 16, 06 2004. DOI: 10.1142/S0129167X05003004.

[JKLNS21] Jakub Jankowski, Piotr Kucharski, Hélder Larraguível, Dmitry Noshchenko, and Piotr Sułkowski. Permutohedra for knots and quivers. *Physical Review D*, 104, 10 2021. DOI: 10.1103/PhysRevD.104.086017.

[Joh] Dennis Johnson. A geometric form of Casson's invariant and its connection to Reidemeister torsion. Unpublished lecture notes.

[Jon85] Vaughan Jones. A polynomial invariant for knots via von Neumann algebras. *Bull. Am. Math. Soc.*, 12:103–111, 1985. DOI: 10.1090/S0273-0979-1985-15304-2.

[KK90] Paul Kirk and Eric Klassen. Chern-Simons invariants of 3-manifolds and representation spaces of knot groups. *Mathematische Annalen*, 287:343–367, 03 1990. DOI: 10.1007/BF01446898.

[KRSS17] Piotr Kucharski, Markus Reineke, Marko Stosic, and Piotr Sulkowski. BPS states, knots and quivers. *Phys. Rev.*, D96(12):121902, 2017. DOI: 10.1103/PhysRevD.96.121902.

[KRSS19] Piotr Kucharski, Markus Reineke, Marko Stosic, and Piotr Sułkowski. Knots-quivers correspondence. *Adv. Theor. Math. Phys.*, 23(7):1849–1902, 2019. DOI: 10.4310/ATMP.2019.v23.n7.a4.

[KS08] Maxim Kontsevich and Yan Soibelman. Stability structures, motivic Donaldson-Thomas invariants and cluster transformations, 2008. arXiv:0811.2435.

[KS10] Maxim Kontsevich and Yan Soibelman. Cohomological hall algebra, exponential Hodge structures and motivic Donaldson-Thomas invariants. *Communications in Number Theory and Physics*, 5, 06 2010. DOI: 10.4310/CNTP.2011.v5.n2.a1.

[Kho00] Mikhail Khovanov. A categorification of the Jones polynomial. *Duke Mathematical Journal*, 101(3):359 – 426, 2000. DOI: 10.1215/S0012-7094-00-10131-7.

[Kit15] Teruaki Kitano. Reidemeister torsion of a 3-manifold obtained by a Dehn-surgery along the figure-eight knot. *Kodai Mathematical Journal*, 39, 06 2015. DOI: 10.2996/kmj/1467830138.

[Kit16] Teruaki Kitano. Some numerical computations on Reidemeister torsion for homology 3-spheres obtained by Dehn surgeries along the figure-eight knot. *arXiv: Geometric Topology*, 2016. arXiv:1603.03728.

[Kit94] Teruaki Kitano. Reidemeister torsion of the figure eight knot exterior for SL(2, C) representations. *Osaka Journal of Mathematics*, 31(3):523–532, 1994. DOI: 10.18910/11558.

[Kit96] Teruaki Kitano. Twisted Alexander polynomial and Reidemeister torsion. *Pacific Journal of Mathematics*, 174(2):431 – 442, 1996. DOI: 10.2140/pjm.1996.174.431.

[Kuc20] Piotr Kucharski. Quivers for 3-manifolds: the correspondence, BPS states, and 3d $\mathcal{N} = 2$ theories. *JHEP*, 09:075, 2020. DOI: 10.1007/JHEP09(2020)075.

[LM22] Charles Livingston and Allison H. Moore. Knotinfo: Table of knot invariants, 3 2022. https://knotinfo.math.indiana.edu/.

[LZ99] Ruth Lawrence and Don Zagier. Modular forms and quantum invariants of 3-manifolds. *Asian Journal of Mathematics*, 3:93–107, 1999. DOI: 10.4310/AJM.1999.v3.n1.a5.

[Lin01] XS Lin. Representations of knot groups and twisted Alexander polynomials. *Acta Mathematica Sinica English Series*, 17:361–380, 07 2001. DOI: 10.1007/PL00011612.

[MM21] Andrei Mironov and Alexei Morozov. Algebra of quantum $C$-polynomials. *JHEP*, 02:142, 2021. DOI: 10.1007/jhep02(2021)142.

[MM95] P. M. Melvin and H. R. Morton. The coloured Jones function. *Comm. Math. Phys.*, 169(3):501–520, 1995. DOI: 10.1007/BF02099310.

[MR14] Sven Meinhardt and Markus Reineke. Donaldson-Thomas invariants versus intersection cohomology of quiver moduli. *Journal für die reine und angewandte Mathematik (Crelles Journal)*, 2019, 11 2014. DOI: 10.1515/crelle-2017-0010.

[Mas03] Gregor Masbaum. Skein-theoretical derivation of some formulas of Habiro. *Algebraic & Geometric Topology*, 3(1):537–556, Jun 2003. DOI: 10.2140/agt.2003.3.537.

[Mil66] J. Milnor. Whitehead torsion. *Bulletin of the American Mathematical Society*, 72(3):358 – 426, 1966. DOI: 10.1090/S0002-9904-1966-11484-2.

[NRZS12] Satoshi Nawata, P. Ramadevi, Zodinmawia, and Xinyu Sun. Super-A-polynomials for twist knots. *JHEP*, 11:157, 2012. DOI: 10.1007/JHEP11(2012)157.

[OV00] Hirosi Ooguri and Cumrun Vafa. Knot invariants and topological strings. *Nuclear Physics B*, 577:419–438, 04 2000. DOI: 10.1016/S0550-3213(00)00118-8.

[PT87] Jozef Przytycki and Pawel Traczyk. Invariants of links of Conway type. *Kobe J. Math.*, 4:115–139, 1987. arXiv:1610.06679.

[Par20a] Sunghyuk Park. Higher rank $\hat{Z}$ and $F_K$. *SIGMA*, 16(044), 2020. DOI: 10.3842/SIGMA.2020.044.

[Par20b] Sunghyuk Park. Large color R-matrix for knot complements and strange identities. *Journal of Knot Theory and Its Ramifications*, 29(14):2050097, Dec 2020. DOI: 10.1142/s0218216520500972.

[Par21] Sunghyuk Park. Inverted state sums, inverted Habiro series, and indefinite theta functions, 6 2021. arXiv:2106.03942.

[Por15] Joan Porti. Reidemeister torsion, hyperbolic three-manifolds, and character varieties, 11 2015. arXiv:1511.00400.

[Por95] J.A. Porti. Torsion de Reidemeister pour les variétés hyperboliques. *Memoirs of the American Mathematical Society*, 128, 1995. DOI: 10.1090/memo/0612.

[RT90] Nicolai Reshetikhin and Vladimir Turaev. Ribbon graphs and their invaraints derived from quantum groups. *Communications in Mathematical Physics*, 127:1–26, 03 1990. DOI: 10.1007/BF02096491.

[Ril84] Robert Riley. Nonabelian representations of 2-bridge knot groups. *The Quarterly Journal of Mathematics*, 35(2):191–208, 06 1984. DOI: 10.1093/qmath/35.2.191.

[Roz96] Lev Rozansky. A contribution of the trivial connection to the Jones polynomial and Witten's invariant of 3d manifolds, I. *Communications in Mathematical Physics*, 175:275–296, 01 1996. DOI: 10.1007/BF02102409.

[Roz98] Lev Rozansky. The universal R-matrix, Burau representation, and the Melvin-Morton expansion of the colored Jones polynomial. *Adv. Math.*, 134(1):1–31, 1998. DOI: 10.1006/aima.1997.1661.

[SW17] Marko Stosic and Paul Wedrich. Rational links and DT invariants of quivers. *International Mathematics Research Notices*, 2021(6):4169–4210, 11 2017. DOI: 10.1093/imrn/rny289.

[SW21] Marko Stosic and Paul Wedrich. Tangle addition and the knots-quivers correspondence. *Journal of the London Mathematical Society*, 2021. DOI: 10.1112/jlms.12433.

[Saf10] E. Saff. Logarithmic potential theory with applications to approximation theory. *Surv. Approx. Theory*, 5, 10 2010. arXiv:1010.3760.

[Sta97] H. Stahl. The convergence of Padé approximants to functions with branch points. *Journal of Approximation Theory*, 91:139–204, 1997. DOI: 10.1006/jath.1997.3141.

[Tra13] Anh Tran. Twisted Alexander polynomials with the adjoint action for some classes of knots. *Journal of Knot Theory and Its Ramifications*, 23, 02 2013. DOI: 10.1142/S0218216514500515.

[Tra15a] Anh T. Tran. Reidemeister torsion and Dehn surgery on twist knots. *Tokyo Journal of Mathematics*, 39, 06 2015. DOI: 10.3836/tjm/1484903134.

[Tra15b] Anh Tran. Twisted Alexander polynomials of genus one two-bridge knots. *Kodai Mathematical Journal*, 41, 06 2015. DOI: 10.2996/kmj/1521424825.

[Tur88] V. G. Turaev. The Yang-Baxter equation and invariants of links. *Inventiones mathematicae*, 92:527 – 553, 1988. DOI: 10.1007/BF01393746.

[Wad94] Masaaki Wada. Twisted Alexander polynomial for finitely presentable groups. *Topology*, 33(2):241–256, 1994. DOI: 10.1016/0040-9383(94)90013-2.

[Wit89] Edward Witten. Quantum field theory and the Jones polynomial. *Comm. Math. Phys.*, 121(3):351–399, 1989. DOI: 10.1007/BF01217730.

[Yam08] Yoshikazu Yamaguchi. A relationship between the non-acyclic Reidemeister torsion and a zero of the acyclic Reidemeister torsion. *Annales de l'Institut Fourier*, 58(1):337–362, 2008. DOI: 10.5802/aif.2352.